NASA TM-83232

NASA Technical Memorandum 83232

Spectroscopic Requirements for HALOE: An Analysis of the HCℓ and HF Channels

C. P. Rinsland
College of William and Mary
Williamsburg, Virginia 23185

M. A. H. Smith, J. H. Park, Gale A. Harvey, J. M. Russell III
NASA Langley Research Center
Hampton, Virginia 23665

D. J. Richardson
Systems and Applied Sciences Corporation
Hampton, Virginia 23665

March 1982

National Aeronautics and
Space Administration

Langley Research Center
Hampton, Virginia 23665

Summary

The spectroscopic requirements for the HF and HCℓ channels of the Halogen Occultation Experiment (HALOE) have been studied. Recommendations for future spectroscopic research in support of HALOE have been made on the basis of a review of the literature and an analysis of high resolution stratospheric spectra. The most important recommendations are (1) more accurate HF and HCℓ strengths and N_2-broadened and self-broadened widths need to be determined, (2) parameters are required for the numerous weak CH_4 lines within the HF channel, (3) polymer formation within the HALOE HF gas cells must be studied, and (4) precise CH_4 air-broadened halfwidths are needed for the HCℓ channel region.

1.0 Introduction

The Halogen Occultation Experiment (HALOE) is a solar occultation experiment designed to measure the vertical profiles of important chemical species involved in stratospheric ozone chemistry, using a combination of gas filter and broad-band radiometers (Russell et al., 1977). The fundamental goal is to provide measurements of key species in the $C\ell O_x$, NO_x, and HO_x chemical cycles on a global scale with sufficient accuracy to resolve spatial and temporal variations.

This report presents results of a study of the spectroscopic requirements for the HALOE HF and HCℓ channels. Gas filter radiometry is used for both channels since it provides the required sensitivity and specificity. The measured HALOE signal is the correlation function of absorption lines in the atmosphere and a gas correlation cell. A positive correlation is obtained from atmospheric absorption lines overlapping with those of the gas cell both near the line center and in the wings of the lines. An anticorrelation is obtained from non-overlapping lines.

We have reviewed and evaluated the current state of knowledge of the spectral line parameters of the stratospheric gases that have absorption features within the HCℓ and HF channels. The parameters of interest are defined to be: (1) position (2) absolute strength, (3) energy of the lower level of the transition, (4) air-broadened collisional halfwidth, and (5) temperature dependence of the air-broadened collisional halfwidth. These quantities are required for the HCℓ and HF lines and the interfering species in each channel in order to interpret the gas-correlation signals from HALOE. In addition, since the HALOE instrument and calibration cells contain mixtures of HF in N_2 and

HCℓ in N_2, it is important to have accurate knowledge of the N_2-broadened and self-broadened HF and HCℓ collisional halfwidths. The accuracy of the state of knowledge of these parameters is also assessed in this report.

In section 2, we present line positions and identifications of atmospheric and solar absorption features within the HF and HCℓ channels. The identifications have been made through careful examination of stratospheric balloon-borne, solar-occultation spectra kindly provided to us by Dr. C. B. Farmer of the Jet Propulsion Laboratory. In section 3 the accuracy of the line parameters of the target and interfering species is assessed for both channels. Since the correlation signals depend on the interference near each of the HCℓ and HF lines within the HALOE filters, these spectral regions are discussed in detail in section 4 on the basis of the JPL spectra and other published data. In section 5, recommendations are presented for future spectroscopic investigations in support of HALOE.

The authors wish to thank R. Earl Thompson and Gloria Liu of Systems and Applied Sciences Corporation for many useful discussions on the results of their analysis of the HALOE gas cell spectra for HCℓ and HF, and Dr. Richard Tipping of the University of Nebraska at Omaha for helpful discussions of hydrogen halide line parameters.

2.0 Identification of Stratospheric Absorption Features Within the HCℓ and HF Channels

2.1 Description of the Atlas

In this section we present solar absorption spectra obtained during sunset with a high-resolution (0.18 cm^{-1}) Michelson

interferometer by C. B. Farmer and his associates at the Jet Propulsion Laboratory (JPL). Details of the balloon flights and trace gas mixing ratios derived from the spectra are described in the work of Farmer et al. (1980).

The regions analyzed in this report are 2890-2990 cm^{-1} for the HCℓ channel and 4000-4160 cm^{-1} for the HF channel. The HF channel has 50-percent transmittance points at 4047±6 cm^{-1} and 4109±6 cm^{-1} and a 5-percent transmittance width of 117 cm^{-1}. The HCℓ channel has 50-percent transmittance points of 2910±6 cm^{-1} and a 2970±6 cm^{-1} with a width of 108 cm^{-1} at the 5-percent transmittance points. For the HCℓ region, we have studied the spectra recorded from a float altitude of 37 km on May 18, 1976, near Palestine, Texas. The HF region was covered during a flight from Broken Hill, Australia, on March 23, 1977. The balloon altitude at sunset was 39 km.

In figures 1 to 26, signal amplitude is plotted as a function of wavenumber for a 10 cm^{-1} interval for a series of different solar zenith angles. The amplitudes have been normalized to the highest point within the HALOE channel. The positions of the observed spectral lines are indicated by vertical tick marks beneath the scan in which they were marked. At the bottom of each frame, the mean observed position of each line is indicated. The lines have been assigned sequence numbers in order of increasing wavenumber for each channel. The HCℓ region is covered in figures 1 to 10. Figures 11 to 26 span the HALOE HF channel.

The sequence numbers, observed wavenumbers and gas identifications are listed in Table 1 for the HCℓ channel and in Table 2 for

the HF channel. Calibration of the wavenumber scale of the Texas spectra was performed by comparing observed wavenumbers of isolated features with accurately known line positions of N_2O, CH_4, and H_2O (Amiot and Guelachvili, 1976; Toth, et al., 1977; Flaud and Camy-Peyret, 1975). The difference between observed and standard positions is plotted against wavenumber in figure 27. The dashed line is a linear least-squares fit to the data. This fit has been used to calibrate the wavenumber scale in the HCℓ region. The scatter suggests that the calibrated positions of unblended lines are accurate to about 0.01 cm^{-1}. A similar calibration procedure was adopted in the HF region. Accurate laboratory line positions of isolated CH_4 lines (Husson et al., 1972) and the R(1) line of HF (Guelachvili, 1976) were compared to the measured values in the stratospheric spectra.

In each line of Tables 1 and 2, the sequence in which the atmospheric molecular identifications are listed represents the relative importance of each species as observed in the scan corresponding to the lowest tangent altitude. Solar absorption features are listed last. In the case of multiple identifications, we include all species within a resolution element that could be detected in the JPL spectra if only that species were present. Identifications that are uncertain are marked with question marks, while features that seem to be too strong or too broad to be due to only the assigned species are indicated by "+?" or "?+." Minor contributors to features are enclosed in parentheses. Unidentified lines are marked with a question mark. In a few cases, weak

features adjacent to intense absorption lines may be sidelobes of the interferometric instrument line shape rather than real lines. No effort was made to distinguish between the two.

2.2 Method of Identification

The majority of the assignments were made on the basis of comparisons between the observational data and simulations produced with the 1980 Air Force Geophysical Laboratory (AFGL) line data (Rothman, 1981; Rothman et al., 1981) and the constituent profiles derived from the JPL spectra by Farmer et al. (1980). A simulation in the HCℓ region is shown in figure 28.

First-overtone solar CO lines were identified in the HF channel with the aid of a simulation of a high-temperature carbon monoxide spectrum. The carbon monoxide line positions were calculated with the constants of Dale et al. (1979) for ^{12}CO and ^{13}CO. The $Y_{0,3}$ and $Y_{1,3}$ Dunham coefficients of ^{12}CO have been changed on the basis of the measured positions of high-J lines reported in the atlas of Goldman et al. (1982). Strengths were calculated with the dipole moment function of Kirschner et al. (1977) following Tipping (1976). Although a temperature of 6000 K was used in the simulations, recent results indicate that a better fit to the data can be obtained with a 4500 K layer. A number of other lines did not change in strength with air mass and are listed as atomic solar lines. A few have been identified in the HF region using the Hall (1970) solar atlas.

Assignments for ozone within both channels were made using the high resolution laboratory atlas of Damon et al. (1981). Methane

features in the HF channel were identified with the aid of laboratory spectra recorded at 100 K and room temperature, using the high resolution (0.06 cm^{-1}) interferometer at NASA Langley Research Center. The room-temperature laboratory spectrum of CH_4 covering the entire HF channel is shown in figure 29. In figures 30 to 45, the CH_4 laboratory spectra at room temperature and ≈100 K are shown in 10-cm^{-1} segments along with the stratospheric solar absorption spectrum recorded at a 94.7-degree solar zenith angle by the JPL interferometer on the balloon flight from Broken Hill, Australia, in 1977. These laboratory spectra were recorded at 0.12 cm^{-1} resolution using a HALOE test cell (10 cm path length) filled with 0.8 atm of pure CH_4.

3.0 Evaluation of Spectroscopic Parameters

3.1 $H^{35}Cl$ and $H^{37}Cl$

Positions of (1-0) band lines of both isotopes have been recently measured to an absolute precision of about 0.001 cm^{-1} (Guelachvili et al., 1981). This French group has combined these measurements with experimental wavenumbers of the (2-0) and (3-0) band lines (Guelachvili, 1976; Guelachvili et al., 1981) to obtain a set of Dunham coefficients which can be used to calculate very accurate lower level excitation energies ($\pm 3 \times 10^{-3}$ cm^{-1}).

Intensities of the (1-0) band have been measured by Penner and Weber (1953), Benedict et al. (1956), Babrov et al. (1959), Toth et al. (1970), Varanasi et al. (1972), and Lin et al. (1978). In Table 3, experimental R-branch line intensities from several of these papers are compared with the values on the 1980 AFGL trace gas tape

(Rothman et al., 1981). It can be seen in the table that the 1980 AFGL line strengths appear to be consistently higher than the measured values of Benedict et al. (1956), Toth et al. (1970), and Varanasi et al. (1972) for the R0 through R8 lines, while the values of Lin et al. (1978) are 5 to 15 percent lower than those measured by the other three groups. The systematic low values of Lin et al. (1978) have been attributed to the loss of HCℓ to the walls of their absorption cell. The strengths on the new AFGL tapes were calculated by Ogilvie et al. (1980) using a dipole moment function derived from the line intensity measurements of Toth et al. (1970) and other investigators in the (1-0) and (2-0) bands, the intensity measurements in the higher overtone bands by Gelfand et al. (1981), and molecular beam electric resonance data (Kaiser, 1970; Smith, 1973). The apparent systematic difference between the AFGL intensities and the majority of measured values in the (1-0) band arises from the fact that the fundamental dipole matrix element derived from the complete set of available data (Smith, 1973) is 5 to 8 percent larger than that derived from the Toth et al. (1970) and Benedict et al. (1956) data. The estimated uncertainty of the AFGL line strengths is given as 10 percent. Varanasi et al. (1972) have noted differences of similar magnitude between the intensity measurements of various laboratories. Their own values are in good agreement (5 percent) with the measurements of Benedict et al. (1956) and Toth et al. (1970) in the R-branch, but in the P-branch their intensities agree very closely with the measurements of Babrov et al. (1959) and are about 10 percent higher than the Benedict et al. and Toth et al. measurements.

Air-broadened halfwidths have not been measured for HCℓ lines. Values on the 1980 trace gas tape are the N_2-broadened halfwidths of Toth and Darnton (1974) and have an estimated uncertainty of ±20 percent. Recently Houdeau et al. (1980) have measured N_2-broadened halfwidths at 298 K and 163 K with an uncertainty of less than 5 percent. Benedict et al. (1956), Babrov et al. (1959), Rank et al. (1963), Miziolek (1977), and Lin et al. (1978) have also measured N_2 broadening of HCℓ in the (1-0) band at room temperature with similar or larger uncertainty. These results are summarized in Table 4. Toth and Darnton (1974) and Benedict et al. (1956) have assumed that the J-dependent pattern of N_2-broadened halfwidths is symmetrical about the band center and have published only mean values as a function of $|m|$.

Although direct measurements of air-broadened HCℓ linewidths have not been reported, effective air-broadened widths may be calculated from existing data on N_2-broadened and O_2-broadened widths. Room temperature measurements of O_2-broadened halfwidths in the (1-0) band have been reported for the P1 - P8 lines by Babrov et al. (1960), for the P7 - P9 lines by Miziolek (1977), and for lines of both branches by Houdeau et al. (1980). O_2-broadened halfwidths were also measured by Houdeau et al. (1980) at 163 K. These results, along with a measurement of the O_2-broadened widths of the R10 line in the (2-0) band by Rank et al. (1960), indicate that the O_2-broadened widths have a different J-dependence than the N_2-broadened values, and are as much as 50 percent smaller than the corresponding N_2-broadened widths. Based on the Houdeau et al.

(1980) data, we calculate n = 0.69 and 0.84 for the average value of the temperature-dependence of the N_2-broadened and O_2-broadened halfwidths, respectively, where $(\gamma/\gamma_0) = (T/T_0)^{-n}$ and the halfwidths are in cm^{-1} atm^{-1} units.

Since the HALOE HCℓ instrument cell is filled with a gas mixture containing 10 percent HCℓ by volume and 90 percent N_2, self-broadened HCℓ halfwidths cannot be neglected in the spectroscopic determinations of total pressure within the cell and, consequently, the modulation (or the correlation function). The self-broadened halfwidths are also 2 to 4 times larger than the corresponding N_2-broadened halfwidths. The only known measurements of self-broadened widths in the (1-0) band were made at relatively low resolution and high pressures (Benedict et al., 1956; Babrov et al., 1960) and have typical uncertainties of 7 to 14 percent.

An interesting result occurs in the retrievals of HCℓ mixing ratios and total pressures in the HALOE gas cells from high-resolution spectra which cover the whole (1-0) band. While the mixing ratios derived from weak lines ($J \geq 9$) differs by 2 percent or less from the P- to the R-branch, the pressure values retrieved from stronger lines ($5 \leq J \leq 8$) are consistently 14 percent higher in the P-branch than in the R-branch. Since retrievals with the stronger lines are more sensitive to halfwidth, it is very likely that this consistent difference in retrieved pressures is related to an asymmetric J-dependent pattern of the self-broadened halfwidths which indicates somewhat larger halfwidths in the P-branch than in the R-branch. This type of asymmetry in the P- and R-branches for

self-broadened halfwidths has been calculated for the HF (1-0) and (3-0) bands by Boulet et al. (1976), whose results agree very well with the measurements of Lovell and Herget (1962) and Spellicy et al. (1972). Asymmetries in the distribution of the self-broadened halfwidths have also been measured in the HCℓ (4-0) through (7-0) bands by Zughul et al. (1980) and have been discussed by DePristo et al. (1981). It is unfortunate that the existing measurements of HCℓ self-broadened halfwidths in the (1-0) band were not made with sufficient accuracy to detect this asymmetry. To our knowledge, the temperature dependence of HCℓ self-broadened halfwidths has not been measured in the (1-0) band.

3.2 HF

The most precise wavenumbers available for the (1-0) band of HF are the positions measured by Guelachvili (1976) with an absolute accuracy of ± 0.00025 cm^{-1}. The rotational constants obtained from the (1-0) and (2-0) bands can be used to obtain very accurate lower state energies.

The HF line strengths on the 1980 AFGL trace gas tape (Rothman et al., 1981) are based on the calculations of Ogilvie et al. (1980) and are estimated to be accurate to about 10 percent. It should be noted that these strengths are primarily based on the experimental results of Lovell and Herget (1962) and other investigators at elevated temperatures (usually 100°C) where polymer formation is small. Experimental values are compared to the 1980 AFGL values in Table 5. Polymer formation occurs at lower temperature and is strongly pressure and temperature dependent (Smith, 1958a). The low

concentration of HF in the stratosphere assures that HF polymerization is negligible. However, polymer formation has been observed in laboratory spectra at room temperature in the HALOE HF cells (0.2 atm, 50 percent mixing ratio, N_2 broadened) and is stronger at the lowest expected operating temperature of the HALOE instrument (260 K).

No measurements of air-broadened HF halfwidths have been reported in the literature. Broadening efficiencies of five N_2-broadened lines were measured by Smith (1958b) at 25°C and 100°C. These measurements have been used to determine the halfwidth values listed on the current AFGL trace gas tape (Rothman et al., 1981). The accuracy estimated for these halfwidths is ±20 percent, and their temperature dependence is unknown.

Since the HALOE instrument HF cells are filled with a 50-50 mixture of HF in N_2, accurate knowledge of self-broadened halfwidths in the (1-0) band is essential for the spectroscopic analysis of these cells and calculation of the modulation signal. Self-broadened halfwidths in both branches of the band have been measured in the laboratory at 373 K by Lovell and Herget (1962) and are in good agreement with the theoretical calculations of Boulet et al. (1976). Hinchen and Hobbs (1979) have measured halfwidths for the P4 through P13 lines at room temperature (296 K) in conjunction with a detailed study of the influence of polymer formation on absorption in this region. Their values are in "good agreement" with the earlier high-temperature results when scaled by the $1/\sqrt{T}$ relation, although precise error estimates are not given for either

set of measurements. Room-temperature measurements of self-broadened halfwidths for the R1 through R5 lines have also been published by Beigang et al. (1979). However, these values are consistently about 30 percent higher than those reported by the investigators mentioned above. This discrepancy may be due to experimental problems such as polymer formation or wall absorption, which were not addressed in the Beigang et al. paper. Preliminary results from HALOE HF gas cell analyses indicate that values of self-broadened halfwidths are less than those of Lovell and Herget (1962) by about 30 percent.

Collisional narrowing of HF fundamental band lines has been observed by Pine (1980). Net narrowing of the Doppler distribution was produced by Ne and Ar with Ne providing the larger effect. However, no narrowing was observed for N_2 and O_2, the most important atmospheric gases.

3.3 Line Parameters of Interference Gas Transitions in the HCℓ Channel

As can be seen from identifications in Table 1, by far the dominant interference gas in the HCℓ channel is CH_4. Absorption lines of H_2O, O_3, and NO_2, and a number of solar features have been identified in the JPL balloon spectra, but they contribute only a small fraction of the total absorption. In this section, the accuracy of current state of the knowledge of the line parameters of each of these interfering gases is discussed. We also briefly consider the absorption line data for a number of other gases which may contribute a small amount of absorption in the HCℓ channel.

(1) $\underline{CH_4}$

Methane line parameters have been extensively updated for 2385-3200 cm^{-1} in the 1980 AFGL compilation (Rothman, 1981; Toth et al., 1981). This range covers the HCℓ filter region. The accuracy of the positions and strengths depends primarily on the degree of blending, but ranges from 0.001-0.006 cm^{-1} and 2 to 20 percent, respectively. The current AFGL line strength cutoff value is 3.3×10^{-24} cm/molecule, which should be low enough to evaluate the effect of weak methane absorption on the HCℓ modulation signal at all stratospheric tangent altitudes.

Air-broadened halfwidths on the 1980 tape were taken from the calculations of Tejwani and Fox (1974) and are in generally good agreement with laboratory measurements. These values, however, depend significantly on the magnitude of the octopole moment of methane, a quantity not accurately known at present.

(2) $\underline{H_2O}$

Quite reliable positions and intensities are now available for the $2\nu_2$, ν_1, and ν_3 bands of water vapor. Line parameters for all of the isotopic species are presented in the recent extensive compilation of Flaud et al. (1981) along with a list of references of their work. It is expected that these data will be included in the next update of the AFGL compilation. Air-broadened halfwidths on the 1980 AFGL tape were calculated from the theory of Davies and Oli (1978).

(3) $\underline{O_3}$

Weak absorption by the $3\nu_3$ band of ozone occurs near the high frequency edge of the HCℓ channel. The positions on the AFGL

tape are accurate only within ±5 cm^{-1} and do not correlate with absorption features observed at high resolution in the JPL balloon data or the Damon et al. (1981) ozone atlas. Assignments and intensity measurements in the $\nu_1 + \nu_2 + \nu_3$ band (center at 2779 cm^{-1}) are currently being made by Barbe (private communication, 1981), and he has additional unanalyzed laboratory spectra which cover the entire HCl filter region at a resolution of 0.025 cm^{-1}.

Until very recently, air-broadened halfwidths of O_3 were known with no better than 60 percent accuracy. Hoell et al. (1982) have measured air-broadening coefficients with much higher accuracy (±5 percent) in the 9μm region, and other American and French research groups are currently making similar measurements in the 5 to 10 μm and submillimeter regions. To our knowledge, air-broadened O_3 halfwidths have not been measured in the 2.5 μm and 3.3 μm regions, and their temperature dependence has not been studied.

(4) NO_2

The $\nu_1 + \nu_3$ band (ν_0 = 2906 cm^{-1}) occurs near the low frequency edge of the HCℓ channel. This band is quite intense, but simulations by one of us (Park) indicate it does not produce significant interference on the HCℓ modulation signal. We tentatively assign a number of weak absorption features to this gas in Table 1.

Dana and Maillard (1978) have studied this band at 0.0033 cm^{-1} resolution with a Fourier transform spectrometer. Recently, strengths have been measured by Toth and Hunt (1980) at

0.02 cm^{-1} resolution. These improvements were not included in the 1980 AFGL trace gas compilation (Rothman et al., 1981), but will be made in future updates of the compilation (Rothman, private communication, 1981).

(5) Other Gases

For the HALOE HCℓ channel, in addition to parameters for the gases discussed above, the 1980 AFGL trace-gas compilation lists spectroscopic parameters for a number of bands of formaldehyde (H_2CO). Our simulations of the expected stratospheric H_2CO signal, based on these line data and on the concentration profile of Ehhalt and Tönnissen (1980), as well as our examination of the stratospheric spectra, indicate that absorption by H_2CO is negligible above 22 km.

A number of small halocarbon and hydrocarbon species, which have been detected in the lower stratosphere by gas chromatographic techniques, also have absorption features which lie in the HCℓ channel but which are not detectable in the JPL spectra. These species include methyl chloride ($CH_3C\ell$), methyl chloroform ($CH_3CC\ell_3$), ethylene (C_2H_4), ethane (C_2H_6), and propane (C_3H_8). As was the case for H_2CO, examination of the JPL spectra and estimates of signal strength for the various gases based on the model concentration profiles of Crutzen et al. (1978) indicate negligible absorption by the small halocarbons and hydrocarbons above 22 km. However, since the concentrations of these gases are increasing with depth in the atmosphere, additional studies and spectroscopic data are needed to determine their expected absorption in the lower

stratosphere (12 to 22 km). High-resolution reference spectra between 2 and 5μm for these species and other halocarbons and hydrocarbons of stratospheric interest will be scanned at the Langley Research Center in the near future.

3.4 Line Parameters of Interference Gas Transitions in the HF Channels

In our analysis of the JPL Mark I spectra, we are able to identify absorption lines from the stratospheric gases CH_4, H_2O, and O_3, as well as HF. Interference in the HF channel is much weaker than in the HCℓ channel at all stratospheric altitudes, and the strongest absorbers are CH_4 and H_2O. Numerous solar absorption lines are prominent in the high-Sun spectra. Most are from the first-overtone sequence ($\Delta v=2$) of CO with a smaller number of solar atomic lines. A discussion of the line parameter data for these transitions follows.

(1) CH_4

The strongest lines of methane in the HF channel belong to the $\nu_1 + \nu_4$ band of $^{12}CH_4$. The center of this band (ν_0 = 4223 cm^{-1}) lies outside of the HF channel. Assignments and molecular constants have been obtained for the region 4136-4288 cm^{-1} by Husson et al. (1972) and Bobin (1974). The $^{13}CH_4$ $\nu_1 + \nu_4$ band has been analyzed by Pierre et al. (1978). Extended assignments for the $\nu_3 + \nu_4$ band of $^{12}CH_4$ have recently been published by Hunt et al. (1981). Although the band center is at 4313 cm^{-1}, transitions were assigned in the HALOE channel region to the P15 (--) manifold near 4070 cm^{-1}. The majority of the CH_4 lines in the HF channel have not yet been assigned,and no

high-resolution strength measurements are available at this time. Many of the lines are probably from the $\nu_2 + 2\nu_4$ band (center near 4123 cm^{-1}). The upper level of this band is strongly perturbed because of the close proximity of the $\nu_1 + \nu_4$ and $\nu_3 + \nu_4$ levels. Assignments and strengths are being determined in this spectral region by the French group at Dijon (L. Brown, private communication, 1981).

(2) H_2O

The strongest lines of water vapor in the HF channel are from $2\nu_2$, ν_1, and ν_3 bands. The parameters for these transitions were discussed in the last section.

(3) O_3

Relatively strong ozone absorption occurs in the HF channel at wavenumbers less than 4033 cm^{-1}. The identification of O_3 in the JPL spectra is based on the laboratory spectra of Damon et al. (1981) which were recorded at room temperature with a resolution of 0.04 cm^{-1}. Their data indicate that the O_3 absorption forms a band head and that the HF channel is free of O_3 lines for $\nu > 4033$ cm^{-1}. We are unaware of any research group that is planning to obtain assignments or strengths of O_3 in this spectral region.

(4) Other Gases

In the HALOE HF channel, the 1980 AFGL compilations also list line parameters for CO_2, N_2O, CO, and HI. For the first three of these gases, our examination of the JPL spectra for tangent altitudes down to 17 km, in addition to simulation studies,

indicates nearly negligible absorption by these gases above that altitude. For HI, no detectable absorption is expected anywhere in the stratosphere since the expected concentration of this gas is, at most, a few parts per trillion.

4.0 Evaluation of Interference at the HCℓ and HF Wavelengths

4.1 HCℓ

The spectral region near each of the HCℓ lines in the HALOE channel may be summarized as follows:

(1) RO $H^{37}Cℓ$ $\nu_0 = 2904.1113\ cm^{-1}$

The laboratory spectra of Toth et al. (1977) (0.02 cm^{-1} resolution) indicate that this line occurs at a wavelength nearly free of methane absorption. In the JPL balloon spectra (0.18 cm^{-1} resolution), this line is clearly visible at the lower tangent altitudes, but our simulations of these interferometric data indicate that the HCℓ line is slightly blended with the sidelobes of two adjacent, relatively strong CH_4 lines.

(2) RO $H^{35}Cℓ$ $\nu_0 = 2906.2474\ cm^{-1}$

This line is masked by the very strong F1(1) component of the P11 line of the $^{12}CH_4$ ν_3 band. The position of this methane line is 2906.2838 cm^{-1} (Ghérissi et al., 1981).

(3) R1 $H^{37}Cℓ$ $\nu_0 = 2923.7330\ cm^{-1}$

The lab spectra of Toth et al. (1977) show a relatively strong methane feature at 2923.738 cm^{-1}. Our simulations indicate that the CH_4 line is stronger than

this HCℓ line in the lower stratosphere. Dana and Maillard (1978) list six relatively strong NO_2 features within 0.04 cm^{-1} of this HCℓ line.

(4) R1 $H^{35}C\ell$ $\nu_0 = 2925.8973\ cm^{-1}$

This line can be seen at all tangent altitudes in the JPL data and is in a region free of methane and water vapor absorption. Two relatively weak NO_2 lines have been recorded at nearly the same wavelength by Dana and Maillard (1978), but simulations indicate that interference from these lines is negligible for the JPL spectra.

(5) R2 $H^{37}C\ell$ $\nu_0 = 2942.7226\ cm^{-1}$

This line is blended with a CH_4 line at 2942.676 cm^{-1}. This blend is partially resolved in a stratospheric spectrum recorded by Zander (1981) at 0.04 cm^{-1} resolution.

(6) R2 $H^{35}C\ell$ $\nu_0 = 2944.9157\ cm^{-1}$

This line is free of interference throughout most of the stratosphere. A weak H_2O line occurs at 2944.886 cm^{-1} and would have to be considered at tangent altitudes less than about 15 km (Zander, 1981).

(7) R3 $H^{37}C\ell$ $\nu_0 = 2961.0688\ cm^{-1}$

In the JPL spectra this line is blended with a methane feature at 2960.948 cm^{-1}. The two lines are resolved in the 0.02 cm^{-1} resolution spectra of Kendall and Buijs (1979), but their analysis suggests that this HCℓ line is overlapped by a weak, unidentified feature.

(8) R3 $H^{35}Cl$ $\nu_0 = 2963.2857\ cm^{-1}$

In the JPL balloon spectra this line is blended with a methane feature, but at 0.02 cm^{-1} resolution these lines appear to be fully resolved and the HCl line is free of interference (Kendall and Buijs, 1979).

(9) R4 $H^{37}Cl$ $\nu_0 = 2978.7593\ cm^{-1}$

This line is overlapped by the intense P4 line of the $^{12}CH_4$ ν_3 band. The E(0) component occurs at 2978.8482 cm^{-1} (Ghérissi et al., 1981). This HCl line is partially resolved at higher tangent altitudes in the Kendall and Buijs (1979) spectra.

(10) R4 $H^{35}Cl$ $\nu_0 = 2981.0009\ cm^{-1}$

This line is blended with methane lines at 2980.841 and 2981.083 cm^{-1} in the JPL spectra, but is well separated from the CH_4 lines in the Kendall and Buijs (1979) spectra.

4.2 HF

In this section we present a discussion of the interference near each of the HF lines in the HALOE channel.

(1) R0 HF $\nu_0 = 4000.9894\ cm^{-1}$

This line is nearly coincident with the solar ^{12}CO R77 line of the (8-6) band at 4001.010 cm^{-1}. The Damon et al. (1981) atlas of laboratory O_3 spectra shows a weak ozone line at 4000.812 cm^{-1} and a slightly stronger feature at 4001.089 cm^{-1}. However, the HF/solar CO feature appears to be well separated from the surrounding

O_3 features in the spectra of Kendall and Buijs. No CH_4 interference in this region is indicated by our laboratory spectra.

(2) R1 HF $\nu_0 = 4038.9625\ cm^{-1}$

This line is free of blending by solar and telluric features (Zander, 1981; Zander et al., 1977; Farmer and Raper, 1977). An excellent 0.04 cm^{-1} resolution stratospheric spectrum has been presented in this region by Zander (1981).

(3) R2 HF $\nu_0 = 4075.2936\ cm^{-1}$

This feature is blended with the solar ^{12}CO R30 line of the (7-5) band at 4075.292 cm^{-1} and a moderately strong $H_2{}^{16}O$ line at 4075.316 cm^{-1} (Flaud and Camy-Peyret, 1975). No CH_4 absorption was observed in our laboratory spectra at this frequency. High-Sun JPL spectra indicate that there is also a solar atomic line blended with this feature on the long wavelength side.

(4) R3 HF $\nu_0 = 4109.9363\ cm^{-1}$

Our laboratory spectra indicate that this feature is blended with a CH_4 absorption line.

(5) R4 HF $\nu_0 = 4142.8460\ cm^{-1}$

At the resolution of the JPL balloon data, this line is blended with the F1(0) and F2(0) components of the P11 line of the $\nu_1 + \nu_4$ $^{12}CH_4$ band at 4142.636 cm^{-1} (Husson et al., 1972) and the P15 (3-1) and P3 (4-2) band lines of solar ^{12}CO at 4142.749 and 4142.873 cm^{-1}, respectively.

5.0 Requirements and Recommendations

In this section the spectroscopic requirements are presented for the HF and HCℓ channels. Since a major objective of HALOE is to derive the HF/HCℓ ratio, the line parameter accuracy requirements reflect the need for an accurate absolute determination of the HF and HCℓ gas mixing ratio profiles. Requirements for interpretation of the spectra of the instrument and calibration cells, as well as parameters for the atmospheric gases, are discussed. The accuracy requirements for most parameters have been determined by varying each parameter in simulations of the modulation signal as a function of tangent altitude. This approach was used in the initial design of the HALOE instrument (Russell et al., 1977). The values are based on an instrument noise of 1 NEM (noise equivalent modulation) and accuracies of the HALOE CH_4 and H_2O mixing ratio profiles of 15 percent. A 1-NEM error would result in an error of approximately 5 percent in the retrieved stratospheric gas mixing ratio for each channel. Unfortunately, gaps in the existing spectroscopic data set prevented study of some effects (e.g. absorption by CH_4 in the HF channel) so that a few accuracy requirements are estimates. Based on the requirements defined here, recommendations have been made for future spectroscopic research that would enhance the accuracy of HALOE results.

5.1 Hydrogen Halides

Accurate knowledge of line parameters in the fundamental bands of HCℓ and HF is essential not only for the analysis of the instrument cells and calibration cells, but also for calculation of

the modulation signal in these two channels. The nominal fill conditions for the cells and requirements for pressure and mixing ratio stability over a 2-year lifetime are listed in Table 6, along with a summary of the line-parameter accuracy requirements which are discussed in detail later in this section. The cell stability requirements are based on the uncertainty in pressure or mixing ratio which would produce an error of 1 NEM (noise equivalent modulation) in the correlation signal.

We believe that the highest priority should be given to the accurate determination of line strengths and widths in the HCℓ and HF fundamental bands. Existing positions and assignments (Guelachvili, 1976; Guelachvili et al., 1981) are sufficiently accurate (± 0.001 cm^{-1} or better) to meet the needs of the HALOE experiment. As has already been discussed in sections 3.1 and 3.2, absolute line strengths in these two bands are currently known with an accuracy of 10 percent at best. However, the recent measurements of Gelfand et al. (1981) and Piollet-Mariel et al. (1981) in the overtone bands of HCℓ indicate that it is currently possible to measure hydrogen halide line strengths with uncertainties of 3 to 4 percent. We recommend that line strength measurements of similar accuracy (at least ±3 percent) be carried out for the (1-0) bands of both HF and HCℓ. For the purpose of quantitative analysis of the HALOE gas cells, the measurements should cover both branches of each band, out to $J = 11$ for HCℓ and $J = 10$ for HF.

The analysis of the stability of the HALOE gas cells also requires very accurate (±3 percent) knowledge of the self-broadened

and N_2-broadened halfwidths in the fundamental bands of HCℓ (to J = 8) and HF (to J = 9). Measurements of these halfwidths should be performed at a range of temperatures from room temperature (296 K) down to the lowest expected temperature of the HALOE instrument in orbit (about 260 K). It is known that absorption from the wings of HCl (1,0) band lines is greater than predicted by a Lorentz profile (Benedict et al., 1956; Varanasi et al., 1972). Rather large deviations from the Lorentz shape were observed for self-broadened lines by Benedict et al. (1956) when $|\nu-\nu_0| > 2\ cm^{-1}$. Further work is needed to define the far-wing line shape for HCℓ and HF self- and N_2-broadened lines so that the proper line shape can be used for the calculation of the HALOE modulation signal.

For accurate simulation of the atmospheric absorption signal due to HCℓ and HF, air-broadened halfwidths should be measured in the (1-0) bands of both gases. This is especially important since both the magnitude and J-dependence of the air-broadened halfwidths may be significantly different from the corresponding N_2-broadened values. For the purposes of the HALOE experiment, only the low J-lines (J < 5) in the R-branch of each band need to be measured with the desired accuracy of ±5 percent. However, measurements covering the entire (1-0) band for each gas would be of great value for analysis of data from other remote sensing experiments. These measurements should be made not only at room temperature, but also over the range of typical stratospheric temperatures (200 to 270 K).

We strongly recommend that the HCℓ and HF line width and strength measurements be carried out by two or more independent

research groups using different spectroscopic techniques (e.g., high-resolution grating spectrometers, Fourier-transform interferometers, laser techniques). Intercomparison of the results obtained by various groups should lead to a very reliable determination of the line parameters required for HALOE.

The effect of HF polymerization is important for HALOE and needs further study. For calculation of the gas cell spectrum (and then the modulation signal), it is very important to determine the fraction of HF molecules in the form of polymers at the operating temperature of the HALOE instrument. Any overlap of the polymer spectrum into the HF filter region must be known accurately so that its effect on the modulation signal can be evaluated. Although a laboratory study of polymer formation within the HALOE gas cells in this low temperature range (260 to 300K) is currently under way at the NASA Langley Research Center, an independent study by another group is desirable.

5.2 Interfering Species

Since the modulation signal results from a correlation between the atmospheric and gas cell absorption spectra, the spectroscopic parameters are required to be known very accurately within the spectral intervals overlapped by the profiles of the gas cell lines. For the conditions used to fill the instrument cells, this interval is about 2 cm^{-1} on both sides of the HF and HCℓ lines. The accuracies listed in Table 6 refer to these spectral intervals. Parameters of the atmospheric lines in the entire channel are still needed in the HALOE analysis, but the accuracy requirements are much

lower outside the spectral regions overlapped by the gas cell lines. For the two primary interfering gases, CH_4 and H_2O, line parameters are needed for all lines with strengths greater than 1 X 10^{-23} cm^{-1}/molecule and 4 X 10^{-24} cm^{-1}/molecule, respectively. This cutoff was selected so as to include all important interference lines for tangent altitudes above 12 km. The line position accuracy requirement is based on the Doppler halfwidth for CH_4, the most important interfering species. This accuracy will allow the effect of overlapping lines to be computed properly. Most groups can now derive line positions to this accuracy. Specific discussions of each channel follow.

HF Channel. As noted in previous sections, most of the interfering absorption lines are due to CH_4 and H_2O. Since line parameters are unavailable for almost all of the CH_4 lines, lab studies are needed to obtain quantum assignments and accurate positions, strengths, and halfwidths for these lines. Laboratory groups should coordinate their efforts with the analysis in progress at Dijon.

Water vapor causes a small but not insignificant contamination within the HF channel. The H_2O interference can be evaluated to the accuracy required by HALOE from the 6 μm band inversion results and the line parameters of Flaud et al. (1981).

Although no parameters are available for the strong O_3 absorption lines observed at $\nu < 4033$ cm^{-1} in the JPL balloon spectra, these data are not essential for HALOE because the ozone absorption occurs only near the long wavelength edge of the filter

for the HF channel. Only the R0 line of HF is in the region of O_3 absorption, and a negligible effect is expected on the modulation signal.

In the JPL spectra, a number of relatively strong solar lines were identified near the HF lines. Since the T vs. τ relation changes across the solar disk, the strength of these lines will vary from the limb to the center of the disk. This effect occurs in addition to the variation of the brightness of the solar continuum known as limb darkening. Most of the solar lines have been identified as transitions from the first-overtone sequence of carbon monoxide (CO). For these features, the absorption is strongest at the solar limb where cooler, higher layers of the solar atmosphere are viewed and formation of CO molecules from carbon and oxygen atoms is more complete. This effect should be considered for HALOE since atmospheric refraction changes the instrumental field-of-view on the solar disk as a function of tangent altitude.

Lines of HF have also been observed in sunspot umbra (Hall, 1970). Since sunspots cover only a very small fraction of the solar disk, their effect should be negligible for HALOE.

HCl Channel. The HCl gas correlation signal is significantly affected by strong, overlapping absorption by CH_4. Fortunately, as noted in section 3, parameters for the numerous methane bands in this region have been compiled for the 1980 AFGL tape by Toth et al. (1981). These positions, strengths, and lower state energies should be adequate for computing the effect of methane interference at all tangent altitudes. Measurements of CH_4 air-broadened half-

widths with an accuracy of 10 percent or better are needed to check the accuracy of the Tejwani and Fox (1974) halfwidths currently on the 1980 AFGL tape.

Absorption by H_2O has a small, but not negligible effect on the modulation signal. As for the HF channel, the line parameters of Flaud et al. (1981) should be accurate enough to correct for the water vapor contamination. Interference from NO_2 and O_3 is negligible.

REFERENCES

Amiot, C., and Guelachvili, G., Extension of the 10^6 samples Fourier spectrometry to the indium antimonide region: Vibration-rotation bands of $^{14}N_2{}^{16}O$: 3.3 - 5.5 μm. J. Mol. Spectrosc. 59, 171 (1976).

Babrov, H., Ameer, G., and Benesch, W. Line strengths and widths in the HCℓ fundamental band. J. Mol. Spectrosc. 3, 185 (1959).

Babrov, H., Ameer, G., and Benesch, W., Molecular collision cross sections from infrared absorption measurements. J. Chem. Phys. 33, 145 (1960).

Beigang, R., Litfin, G., and Schneider R., Line shapes and halfwidths of pure- and foreign-gas-broadened 2.5 μm HF absorption spectra. Phys. Rev. A 20, 229 (1979).

Benedict, W. S., Herman, R., Moore G. E. and Silverman, S. The strengths, widths, and shapes of infrared lines II. The HCℓ fundamental. Can. J. Phys. 31, 850 (1956).

Bobin, B., Sur la bande de vibration-rotation ($\nu_1+\nu_4$) du méthane $^{12}CH_4$, J. Physique 35, L121 (1974).

Boulet, C., Robert, D., and Galatry, L., Shifts of the vibration-rotation absorption lines of diatomic molecules perturbed by diatomic polar molecules. A theoretical analysis. J. Chem. Phys. 65, 5302 (1976).

Crutzen, P. J., Isaksen, I. S. A., and McAfee, J. R., The impact of the chlorocarbon industry on the ozone layer. J. Geophys. Res. 83, 345 (1978).

Dale, R. M., Herman, M., Johns, J. W. C., McKellar, A. R. W., Nagler, S., and Strathy, I. K. M., Improved laser frequencies and Dunham coefficients for isotopically substituted carbon monoxide. Can. J. Phys. 57, 677 (1979).

Damon, E., Hawkins, R. L., and Shaw, J. H., A Spectrum of ozone from 760 to 5800 cm^{-1}. RF Project 761420/711626 interim technical report, Ohio State University Research Foundation, Columbus, Ohio 43210 (Feb. 1981).

Dana, V., and Maillard, J. P., Analysis of the $\nu_1 + \nu_3$ band of $^{14}N^{16}O_2$. J. Mol. Spectrosc. 71, 1 (1978).

Davies, R. W. and Oli, B. A., Theoretical calculations of H_2O linewidths and pressure shifts: Comparisons of the Anderson theory with quantum many-body theory for N_2 and air-broadened lines. J. Quant. Spectrosc. Radiat. Transfer, 20, 95 (1978).

DePristo, A. E., BelBruno, J. J., Gelfand, J. and Rabitz, H., Direct inversion of high overtone collision broadened linewidths in the HCℓ-HCℓ system: Rotationally inelastic rates for highly vibrationally excited molecules. J. Chem. Phys. 74, 5031 (1981).

Ehhalt, D. H., and Tonnissen, A., Hydrogen and carbon compounds in the stratosphere. Proceedings of the NATO Advanced Study Institute on Atmospheric Ozone: Its Variation and Human Influences (A. C. Aiken, ed.), U.S. Federal Aviation Administration Report No. FAA-EE-80-20, 129-151 (1980).

Farmer, C. B., and Raper, O. F., The HF:HCℓ ratio in the 14-38 km region of the stratosphere. Geophys. Res. Lett. 4, 527 (1977).

Farmer, C. B., Raper, O. F., Robbins, B. D., Toth, R. A., and Muller, C., Simultaneous spectroscopic measurements of stratospheric species: O_3, CH_4, CO, CO_2, N_2O, H_2O, HCℓ, and HF at northern and southern mid-latitudes. J Geophys. Res. 85, 1621 (1980).

Flaud, J.-M., and Camy-Peyret, C., Vibration-rotation intensities in H_2O-type molecules application to the $2\nu_2$, ν_1, and ν_3 bands of $H_2{}^{16}O$. J. Mol. Spectrosc. 55, 278 (1975).

Flaud, J.-M., Camy-Peyret, C., and Toth, R. A., Water Vapor Line Parameters from Microwave to Medium Infrared, Pergamon Press, Inc., Elmsford, N.Y., 1981.

Gelfand, J., Zughul, M., Rabitz, H., and Han, C. J., Absorption intensities for the 4-0 through 7-0 overtone bands of HCℓ. J. Quant. Spectrosc. Radiat. Transfer 26, 303 (1981).

Ghérissi, S., Henry, A., Loete, M., and Valentin, A., Transition moment and line strengths of the ν_3 band of $^{12}CH_4$. J. Mol. Spectrosc. 86, 344 (1981).

Goldman, A., Blatherwick, F. J., Murcray, F. J., Van Allen, J. W., Murcray, F. H., and Murcray, D. G., New atlas of high resolution stratospheric infrared absorption spectra, preliminary edition. Department of Physics, U. of Denver, prepared under NSF grant ATM-79-27312 (August 1980).

Guelachvili, G., Absolute wavenumber measurements of 1-0, 2-0, HF and 2-0, $H^{35}C\ell$, $H^{37}C\ell$ absorption bands. Opt. Comm. 19, 150 (1976).

Guelachvili, G., Niay, P., and Bernage, P., Infrared bands of HCℓ and DCl by Fourier transform spectroscopy. J. Mol. Spectrosc. 85, 271 (1981).

Hall, D. N. B., An atlas of infrared spectra of the solar photosphere and sunspot umbrae, in the spectral intervals 4040 cm^{-1} - 5095 cm^{-1}, 5550 cm^{-1} - 6700 cm^{-1}, 7400 cm^{-1} - 8790 cm^{-1}, published by Kitt Peak National Observatory, Tucson, Ariz. (1970).

Hinchen, J. J., and Hobbs, R. H., Pressure-broadeded line widths in the 2.5-μ band of HF and the influence of polymer formation. J. Opt. Soc. Am. 69, 1546 (1979).

Hoell, J. M., Harward, C. N., Bair, C. H., and Williams, B. S., Ozone air broadening coefficients in the 9 μm region. Optical Engineering, in press (1982).

Houdeau, J. P., Larvor, M., and Haeusler, C., Etude à basse témperature des largeurs et des déplacements des rovibrationnelles de la bande fondamentale de $H^{35}C\ell$ comprimé par N_2, O_2, D_2 et H_2. Can. J. Phys. 58, 318 (1980).

Hunt, R. H., Brown, L. R., Toth, R. A., and Brault, J. W., Extended assignments for the $\nu_3 + \nu_4$ band of $^{12}CH_4$. J. Mol. Spectrosc. 86, 159-169 (1981).

Husson, N., Poussigue, G., Valentin, A., and Amiot, C., Étude de la bande $\nu_1 + \nu_4$ de $^{12}CH_4$ de 4136 a 4288 cm^{-1}. Rev. Phys. Appl. 7, 267 (1972).

Kaiser, E. W., Dipole moment and hyperfine parameters of $H^{35}C\ell$ and $D^{35}Cl$. J. Chem. Phys. 53, 1686 (1970).

Kendall, D. J. W., and Buijs, H. L., Stratospheric measurements of HCℓ and HF. Results of a balloon flight from Holloman AFB, October 27, 1978, Bomen, Inc. report for MCA contract No. 77-156 Bomen, Inc., Ville de Vanier, Quebec, Canada (1979).

Kirschner, S. M., LeRoy, R. J., Ogilvie J. F., and Tipping, R. H., Radial matrix elements and dipole moment function for CO. J. Mol. Spectrosc. 65, 306 (1977).

Lin, C. L., Niple E., Shaw, J. H., Uselman, W. M., and Calvert, J. G., Line parameters of HCl obtained by simultaneous analysis of spectra. J. Quant. Spectrosc. Radiat. Transfer 20, 581 (1978).

Lovell, R. J., and Herget, W. F., Lorentz parameters and vibration-rotation interaction constants for the fundamental band of HF. J. Opt. Soc. Am. 52, 1374 (1962).

Miziolek, A. W., Temperature dependence of foreign gas broadening of HCℓ fundamental lines. J. Mol. Spectrosc. 65, 134 (1977).

Ogilvie, J. F., Rodwell, W. R., and Tipping, R. H., Dipole moment functions of the hydrogen halides. J. Chem. Phys. 73, 5221 (1980).

Penner, S. S., and Weber, D., Infrared intensity measurements on nitric oxide, hydrogen chloride, and hydrogen bromide. J. Chem. Phys. 21, 649 (1953).

Pierre, C., Hilico, J. C., and Guelachvili, G., Étude préliminaire de la bande de vibration-rotation $\nu_1 + \nu_4$ de $^{13}CH_4$. J. Phys. 39, 1177 (1978).

Piollet-Mariel, E., Boulet, C. and Levy, A., An experimental investigation of rare gases pressure effects on the rovibrational line intensities of HCℓ. J. Chem. Phys. 74, 900 (1981).

Pine, A. S., Collisional narrowing of HF fundamental band spectral lines by neon and argon. J. Mol. Spectrosc. 82, 435 (1980).

Rank, D. H., Birtley, W. B., Eastman, D. P., and Wiggins, T. A., Pressure-induced shifts of HCℓ lines due to foreign gases. J. Chem. Phys. 32, 296-297 (1960).

Rank, D. H., Eastman, D. P., Rao, B. S., and Wiggins, T. A., Breadths and shifts of molecular band lines due to perturbation by foreign gases. J. Mol. Spectrosc. 10, 34 (1963).

Rothman, L. S., AFGL atmospheric absorption line parameters: 1980 version. Appl. Opt. 20, 791 (1981).

Rothman, L. S., Goldman, A., Gillis, J. R., Tipping, R. H., Brown, L. R., Margolis, J. S., Maki, A. G., and Young, L. D. G., AFGL trace gas compilation: 1980 version. Appl. Opt. 20, 1323 (1981).

Russell, J. M., Park, J. H., and Drayson, S. R., Global monitoring of stratospheric halogen compounds from a satellite using a gas filter spectroscopy in the solar occultation mode, Appl. Opt. 16, 607 (1977).

Smith, D. F., Infrared spectra analysis for hydrogen fluoride. Spectrochim. Acta 12, 224 (1958a).

Smith, D. F., Hydrogen fluoride polymer spectrum, hexameter and tetramer. J. Chem. Phys. 28, 1040 (1958b).

Smith, F. G., Dipole moment function and vibration-rotation matrix elements of $HC\ell^{35}$ and $DC\ell^{35}$. J. Quant. Spectrosc. Radiat. Transfer 13, 717 (1973).

Spellicy, R. L., Meredith, R. E., and Smith, F. G., Strengths and collision broadened widths in the second overtone band of hydrogen fluoride. J. Chem. Phys. 57, 5119 (1972).

Tejwani, G. D. T., and Fox, K., Calculated line widths for CH_4 broadened by N_2 and O_2. J. Chem. Phys. 60, 2021 (1974).

Tipping, R. H., Vibration-rotation intensities for "hot" bands. J. Mol. Spectrosc. 61, 272 (1976).

Toth, R. A., and Darnton, L. A., Linewidths of HCℓ;broadened by CO_2 and N_2 and CO broadened by CO_2. J. Mol. Spectrosc. 49, 100 (1974).

Toth, R. A., and Hunt, R. H., Line strengths, spin-splittings, and forbidden transitions in the (101) band of $^{14}N^{16}O_2$. J. Mol. Spectrosc. 79, 182 (1980).

Toth, R. A., Hunt, R. H., and Plyler, E. K., Line strengths, line widths, and dipole moment function for HCℓ. J. Mol. Spectrosc. 35, 110 (1970).

Toth, R. A., Brown, L. R., Hunt, R. H., Line positions and strengths of methane in the 2862 to 3000 cm^{-1} region. J. Mol. Spectrosc. 67, 1 (1977).

Toth, R. A, Brown, L. R., Hunt, R. H., and Rothman, L. S., Line parameters of methane from 2385 to 3200 cm^{-1}. Appl. Opt. 20, 932 (1981).

Varanasi, P., Sarangi, S. K., and Tejwani, G. D. T., Line shape parameters for HCℓ and HF in a CO_2 atmosphere. J. Quant. Spectrosc. Radiat. Transfer 12, 857 (1972).

Zander, R., Recent observations of HF and HCℓ in the upper stratosphere. Geophys. Res. Lett. 8, 413 (1981).

Zander, R., Roland, G., and Delbouille, L., Confirming the presence of hydrofluoric acid in the upper stratosphere. Geophys. Res. Lett. 4, 117 (1977).

Zughul, M., Gelfand, J., Rabitz, H., and DePristo, A.E., Pressure broadening in the 0-4 through 0-7 overtone bands of $H^{35}Cℓ$ and $H^{37}Cℓ$. J. Quant. Spectrosc. Radiat. Transfer 24, 371 (1980).

Table 1

Line Positions and Identifications within the HCℓ Channel

CODE NO.	ν(OBSERVED) (CM^{-1})	IDENTIFICATION
1	2890.087	CH4 + NO2 (?)
2	2890.684	CH4 + NO2 (?)
3	2890.982	NO2 (?) + SOLAR
4	2891.371	CH4 + NO2 (?) + SOLAR
5	2891.984	CH4 + NO2 (?)
6	2892.309	CH4 + NO2 (?)
7	2892.631	CH4 + NO2 (?)
8	2892.978	NO2 (?)
9	2893.296	NO2 (?)
10	2893.561	CH4 + NO2 (?) + SOLAR
11	2893.877	CH4 + (H2O)
12	2894.213	CH4 + NO2 (?)
13	2894.453	CH4 + NO2 (?)
14	2894.681	CH4 + NO2 (?)
15	2895.064	CH4
16	2895.804	CH4
17	2896.248	CH4
18	2896.628	(CH4) + SOLAR (?)
19	2896.984	CH4
20	2897.393	CH4
21	2897.784	CH4
22	2898.094	CH4 + NO2 (?)
23	2898.384	CH4 + NO2 (?)
24	2898.703	CH4
25	2899.021	CH4 + NO2 (?)
26	2899.323	CH4
27	2899.580	CH4 (?)
28	2899.914	CH4
29	2900.096	CH4
30	2900.448	CH4
31	2901.548	CH4
32	2901.883	CH4
33	2902.414	CH4 + ?
34	2903.103	CH4
35	2903.308	?
36	2903.549	CH4
37	2903.875	CH4
38	2904.167	CH4 + HCL
39	2904.523	CH4

Table 1 (continued)

CODE NO.	ν(OBSERVED) (CM^{-1})	IDENTIFICATION
40	2905.040	?
41	2905.297	CH4
42	2905.715	CH4
43	2906.279	CH4 + (HCL)
44	2906.661	CH4
45	2906.972	CH4
46	2907.330	CH4
47	2907.646	CH4
48	2908.328	CH4
49	2908.652	CH4
50	2908.909	?
51	2909.266	CH4
52	2909.580	CH4
53	2909.890	CH4
54	2910.201	CH4 + NO2 (?)
55	2910.557	CH4
56	2910.829	CH4
57	2911.140	CH4 + NO2 (?)
58	2911.342	CH4
59	2911.628	CH4 + NO2 (?)
60	2911.881	NO2 (?) + H2O
61	2912.250	CH4 (?) + NO2 (?)
62	2912.642	CH4 + NO2 (?)
63	2912.906	CH4 + NO2 (?)
64	2913.186	CH4 + NO2 (?)
65	2913.757	CH4
66	2914.073	CH4
67	2914.402	CH4
68	2914.613	CH4 + NO2 (?)
69	2914.906	CH4
70	2915.175	NO2 (?)
71	2915.461	NO2 (?)
72	2915.642	CH4 + NO2 (?)
73	2915.986	CH4
74	2916.302	CH4
75	2916.789	CH4
76	2917.026	CH4
77	2917.349	CH4
78	2917.637	CH4
79	2918.184	SOLAR

Table 1 (continued)

CODE NO.	ν(OBSERVED) (CM^{-1})	IDENTIFICATION
80	2918.481	CH4
81	2918.763	CH4
82	2919.126	CH4
83	2919.525	NO2 (?)
84	2919.918	CH4
85	2920.186	CH4 + NO2 (?)
86	2920.654	CH4
87	2920.961	CH4 + NO2 (?)
88	2921.329	CH4
89	2921.963	CH4
90	2922.445	CH4 + ?
91	2922.922	CH4
92	2923.242	CH4
93	2923.691	CH4 + HCL
94	2923.937	CH4
95	2924.683	CH4
96	2925.356	CH4 + ?
97	2925.569	CH4
98	2925.884	HCL
99	2926.784	CH4
100	2927.043	CH4 + SOLAR
101	2927.393	CH4
102	2927.637	CH4
103	2927.953	CH4
104	2928.484	CH4 + ?
105	2928.733	?
106	2929.150	CH4
107	2929.472	?
108	2929.701	?
109	2930.040	CH4
110	2930.403	?
111	2930.661	?
112	2930.921	?
113	2931.189	?
114	2931.428	CH4 + ?
115	2931.730	CH4
116	2932.022	CH4
117	2932.245	CH4
118	2932.571	CH4 (?)
119	2933.018	CH4

Table 1 (continued)

CODE NO.	ν(OBSERVED) (CM^{-1})	IDENTIFICATION
120	2933.371	CH4 + H2O
121	2933.705	H2O + SOLAR
122	2934.070	CH4
123	2934.407	CH4
124	2934.682	SOLAR
125	2935.193	H2O + CH4
126	2935.495	CH4
127	2935.860	CH4
128	2936.222	CH4
129	2936.666	CH4
130	2936.946	CH4 + H2O
131	2937.276	CH4
132	2937.474	CH4
133	2937.776	CH4
134	2938.228	CH4
135	2938.563	CH4 + ?
136	2938.803	?
137	2939.052	? + SOLAR
138	2939.547	CH4
139	2940.025	SOLAR
140	2940.414	SOLAR
141	2940.618	CH4
142	2940.986	CH4
143	2941.468	CH4
144	2941.822	SOLAR
145	2942.096	CH4
146	2942.412	(CH4) + SOLAR
147	2942.696	HCL + CH4
148	2943.275	CH4
149	2943.698	(CH4) + SOLAR
150	2944.069	CH4
151	2944.502	CH4 + (SOLAR)
152	2944.904	HCL
153	2945.351	CH4 + ?
154	2945.629	CH4
155	2945.949	CH4
156	2946.268	CH4
157	2946.555	?
158	2946.801	SOLAR
159	2947.095	CH4

Table 1 (continued)

CODE NO.	ν(OBSERVED) (CM^{-1})	IDENTIFICATION
160	2947.416	CH4
161	2947.815	CH4
162	2948.116	CH4
163	2948.450	CH4
164	2948.787	CH4
165	2949.120	CH4
166	2949.416	CH4
167	2949.691	?
168	2949.961	?
169	2950.351	CH4
170	2950.592	CH4
171	2950.931	?
172	2951.210	CH4
173	2951.609	CH4
174	2952.110	CH4
175	2952.417	?
176	2952.647	?
177	2952.888	CH4 + ?
178	2953.192	CH4
179	2953.594	CH4
180	2954.109	CH4 + H2O
181	2954.428	CH4 + (H2O)
182	2954.942	CH4
183	2956.074	CH4
184	2956.964	(CH4) + SOLAR
185	2957.689	CH4
186	2958.116	CH4
187	2958.601	CH4
188	2959.002	CH4
189	2959.974	SOLAR (?)
190	2960.967	CH4 + (HCL)
191	2961.732	H2O
192	2961.977	H2O (?)
193	2962.218	CH4
194	2962.501	CH4
195	2962.985	CH4
196	2963.260	HCL + (CH4)
197	2963.496	CH4
198	2963.914	CH4 + SOLAR
199	2964.915	CH4

Table 1 (continued)

CODE NO.	ν(OBSERVED) (CM⁻¹)	IDENTIFICATION
200	2965.490	CH4
201	2965.818	CH4
202	2966.087	CH4 + H2O
203	2966.407	CH4
204	2967.132	? + SOLAR
205	2967.370	?
206	2968.116	H2O + (CH4) + SOLAR
207	2968.440	CH4
208	2968.783	CH4
209	2970.229	O3 + (CH4)
210	2970.723	SOLAR
211	2971.069	CH4
212	2971.278	CH4
213	2971.611	CH4
214	2972.067	CH4 + SOLAR
215	2972.427	CH4
216	2972.900	CH4
217	2973.249	H2O + CH4
218	2973.794	CH4
219	2974.066	?
220	2974.610	H2O
221	2974.754	CH4
222	2975.109	H2O + CH4
223	2975.423	CH4 + ?
224	2975.788	CH4
225	2976.408	CH4
226	2976.701	CH4
227	2977.054	?
228	2977.336	CH4 + O3 (?)
229	2977.631	?
230	2977.947	H2O
231	2978.284	CH4
232	2978.727	CH4 + (HCL)
233	2978.944	CH4
234	2979.700	CH4 + ?
235	2979.951	(CH4) + SOLAR (?)
236	2980.309	H2O + O3 (?)
237	2980.774	CH4
238	2981.098	CH4 + HCL + (H2O)
239	2981.447	CH4

Table 1 (concluded)

CODE NO.	ν(OBSERVED) (CM^{-1})	IDENTIFICATION
240	2982.045	O3 (?) + SOLAR
241	2982.620	CH4
242	2983.018	O3 (?)
243	2983.392	O3
244	2983.729	O3
245	2984.212	H2O + (O3)
246	2984.919	?
247	2985.189	O3 (?)
248	2985.514	O3
249	2985.927	O3
250	2986.691	O3
251	2986.938	O3
252	2987.233	CH4 + (O3)
253	2987.534	H2O + O3 + (CH4)
254	2987.884	CH4 + O3
255	2988.213	CH4 + (O3)
256	2988.942	CH4
257	2989.398	CH4 + (O3)
258	2989.668	O3 + CH4

Table 2

Line Positions and Identifications within the HF Channel

CODE NO.	ν(OBSERVED) (CM⁻¹)	IDENTIFICATION
1	4000.250	O3 + H2O + SOLAR CO
2	4000.694	O3
3	4001.042	HF + O3 (?) + SOLAR CO
4	4001.270	O3 + H2O + SOLAR CO
5	4001.544	O3 + CH4 + SOLAR CO
6	4002.097	O3 + CH4
7	4002.584	O3 + SOLAR CO
8	4002.851	O3
9	4003.485	O3 + ATOMIC SOLAR + SOLAR CO
10	4003.879	O3
11	4004.152	O3
12	4004.741	O3 + SOLAR CO
13	4005.433	O3 + H2O + SOLAR CO
14	4006.097	O3
15	4006.549	O3
16	4006.730	O3
17	4007.341	O3
18	4007.598	H2O + O3 + SOLAR CO
19	4007.937	O3
20	4008.178	O3 + SOLAR CO + ATOMIC SOLAR
21	4008.578	H2O + O3 + (SOLAR CO)
22	4009.007	O3 + SOLAR CO
23	4009.786	O3
24	4010.146	O3
25	4010.383	O3
26	4010.754	O3
27	4011.129	O3 + H2O + ATOMIC SOLAR
28	4011.378	O3 + SOLAR CO
29	4011.644	O3
30	4012.093	O3
31	4012.370	O3 + SOLAR CO
32	4012.689	H2O + O3
33	4013.138	O3 + SOLAR CO
34	4013.370	O3 + SOLAR CO
35	4013.843	O3 + SOLAR CO
36	4014.257	O3 + SOLAR CO
37	4014.497	O3 + SOLAR CO
38	4014.818	O3
39	4015.141	O3

Table 2 (continued)

CODE NO.	ν (OBSERVED) (CM⁻¹)	IDENTIFICATION
40	4015.371	O3
41	4015.890	O3 + SOLAR CO
42	4016.047	O3 + SOLAR CO
43	4016.346	O3
44	4016.973	O3 + SOLAR CO
45	4017.443	O3 + SOLAR CO
46	4018.490	H2O + O3 + SOLAR CO
47	4018.885	CH4 + (O3?) + SOLAR CO
48	4019.160	SOLAR CO
49	4019.473	H2O + O3
50	4020.037	O3 + SOLAR CO
51	4020.562	O3 + SOLAR CO
52	4021.026	H2O + O3
53	4021.306	ATOMIC SOLAR
54	4021.827	O3 + SOLAR CO
55	4022.637	O3 + SOLAR CO
56	4023.258	O3
57	4023.602	O3
58	4023.827	O3 + SOLAR CO
59	4024.226	O3
60	4024.373	O3 + SOLAR CO
61	4024.647	O3
62	4025.044	O3 + CH4
63	4025.359	H2O
64	4025.954	O3 + (CH4)
65	4026.402	O3 + (CH4)
66	4026.942	O3 + SOLAR CO
67	4027.538	O3 + SOLAR CO
68	4028.021	O3 + ATOMIC SOLAR
69	4028.819	O3 + SOLAR CO
70	4029.249	O3
71	4029.548	O3 + SOLAR CO
72	4029.750	O3 + H2O + SOLAR CO
73	4030.060	O3 + SOLAR CO
74	4030.535	O3 + SOLAR CO
75	4030.808	O3 + ATOMIC SOLAR
76	4031.073	O3 + SOLAR CO
77	4031.375	O3 + H2O + ATOMIC SOLAR
78	4031.822	O3 + SOLAR CO
79	4032.121	O3

Table 2 (continued)

CODE NO.	ν(OBSERVED) (CM^{-1})	IDENTIFICATION
80	4032.598	O3 + SOLAR CO
81	4033.271	SOLAR CO
82	4033.619	SOLAR CO
83	4033.926	SOLAR CO
84	4034.189	SOLAR CO
85	4035.093	SOLAR CO
86	4035.456	SOLAR CO
87	4036.424	H2O
88	4038.333	SOLAR CO
89	4038.961	HF
90	4039.325	(H2O) + SOLAR CO
91	4040.055	SOLAR CO
92	4040.842	CH4 + SOLAR CO
93	4042.696	ATOMIC SOLAR
94	4043.090	SOLAR CO
95	4043.194	SOLAR CO
96	4043.480	H2O + SOLAR CO
97	4043.780	H2O + CH4 (?)
98	4044.344	?
99	4044.876	H2O + SOLAR CO
100	4045.346	SOLAR CO
101	4046.044	SOLAR CO
102	4046.656	SOLAR CO
103	4047.728	SOLAR CO
104	4048.485	CH4 (?) + SOLAR CO
105	4049.414	CH4
106	4049.864	CH4
107	4050.163	SOLAR CO
108	4050.583	CH4
109	4050.914	SOLAR CO
110	4051.278	SOLAR CO
111	4052.200	H2O + SOLAR CO
112	4053.191	SOLAR CO
113	4055.416	SOLAR CO
114	4055.927	ATOMIC SOLAR + SOLAR CO
115	4056.562	CH4 (?)
116	4056.790	SOLAR CO
117	4057.217	SOLAR CO
118	4057.699	H2O + SOLAR CO
119	4058.076	CH4 (?) + SOLAR CO

Table 2 (continued)

CODE NO.	ν(OBSERVED) (CM⁻¹)	IDENTIFICATION
120	4058.640	CH4
121	4059.053	CH4 (?)
122	4059.685	SOLAR CO
123	4060.035	CH4 (?) + ATOMIC SOLAR
124	4060.391	H2O + SOLAR CO
125	4060.610	H2O + SOLAR CO
126	4060.930	SOLAR CO
127	4061.212	SOLAR CO
128	4061.538	?
129	4061.733	SOLAR CO
130	4062.108	CH4 (?)
131	4062.361	CH4 (?) + SOLAR CO
132	4062.642	CH4 (?)
133	4063.055	CH4 (?) + SOLAR CO
134	4063.683	SOLAR CO
135	4064.338	SOLAR CO
136	4064.929	CH4
137	4065.587	SOLAR CO
138	4065.778	SOLAR CO
139	4066.100	SOLAR CO
140	4067.356	SOLAR CO
141	4068.146	(CH4) + ATOMIC SOLAR + SOLAR CO
142	4068.642	CH4
143	4068.830	SOLAR CO
144	4069.138	SOLAR CO
145	4069.493	SOLAR MN
146	4069.945	SOLAR CO
147	4070.532	CH4 (?)
148	4070.811	SOLAR CO
149	4071.106	CH4 + SOLAR FE
150	4071.476	SOLAR CO
151	4071.877	ATOMIC SOLAR
152	4072.306	CH4 (?) + SOLAR CO
153	4072.512	ATOMIC SOLAR
154	4073.123	SOLAR CO
155	4073.276	CH4 (?) + SOLAR CO
156	4073.844	H2O + (CH4) + SOLAR CO
157	4074.199	CH4 + SOLAR CO
158	4074.540	CH4 (?) + SOLAR CO
159	4074.962	SOLAR CO

Table 2 (continued)

CODE NO.	ν(OBSERVED) (CM^{-1})	IDENTIFICATION
160	4075.276	H2O + HF + SOLAR CO
161	4075.873	SOLAR CO
162	4076.371	SOLAR CO
163	4076.618	CH4 (?) + SOLAR CO
164	4077.173	CH4
165	4077.394	SOLAR CO
166	4077.878	SOLAR CO
167	4078.290	CH4 + SOLAR CO
168	4078.619	SOLAR CO
169	4078.748	CH4 (?) + SOLAR CO
170	4079.115	SOLAR CO
171	4079.389	H2O + SOLAR CO
172	4079.864	SOLAR CO
173	4080.246	(H2O) + SOLAR CO
174	4080.783	CH4 + SOLAR CO
175	4081.261	H2O + SOLAR CO
176	4081.815	CH4 (?)
177	4081.930	SOLAR CO
178	4082.314	SOLAR CO
179	4082.522	SOLAR FE
180	4082.875	SOLAR CO
181	4083.198	CH4 (?) + SOLAR CO
182	4083.469	CH4 (?)
183	4083.783	SOLAR CO
184	4084.002	CH4 (?) + SOLAR CO
185	4084.526	CH4 (?) + SOLAR CO
186	4084.840	H2O + SOLAR CO
187	4085.098	CH4
188	4085.413	SOLAR CO
189	4085.673	CH4 + SOLAR CO + (ATOMIC SOLAR)
190	4086.150	H2O + SOLAR CO
191	4086.544	CH4 (?) +SOLAR CO
192	4087.020	SOLAR CO
193	4087.394	SOLAR CO
194	4087.588	CH4 + SOLAR CO
195	4088.116	H2O + (CH4) + SOLAR CO
196	4088.896	CH4
197	4089.654	CH4
198	4090.078	CH4 (?)
199	4090.466	CH4 + SOLAR CO

Table 2 (continued)

CODE NO.	ν(OBSERVED) (CM^{-1})	IDENTIFICATION
200	4090.998	SOLAR CO
201	4091.291	CH4 + SOLAR CO
202	4091.591	CH4
203	4092.066	CH4
204	4092.279	CH4
205	4092.947	CH4
206	4093.314	CH4 (?) + SOLAR CO
207	4093.522	H2O
208	4093.670	SOLAR CO
209	4094.045	CH4
210	4094.543	CH4 (?) + ATOMIC SOLAR
211	4095.195	CH4 + SOLAR CO
212	4095.749	CH4
213	4096.058	SOLAR CO
214	4096.375	SOLAR CO
215	4096.682	CH4 + SOLAR CO
216	4097.043	SOLAR CO
217	4097.282	CH4
218	4097.566	CH4
219	4097.875	CH4
220	4098.126	CH4
221	4098.674	SOLAR CO
222	4098.958	CH4 + SOLAR CO
223	4099.310	?
224	4099.871	SOLAR CO + ATOMIC SOLAR (?)
225	4100.455	CH4
226	4101.505	CH4 + SOLAR CO + ATOMIC SOLAR
227	4101.826	CH4 (?)
228	4102.107	CH4 + SOLAR CO
229	4102.416	CH4
230	4102.866	CH4
231	4103.208	CH4 + SOLAR CO
232	4103.618	CH4
233	4103.901	SOLAR CO
234	4104.124	H2O
235	4104.470	CH4 (?) + SOLAR CO
236	4104.741	H2O + (CH4)
237	4105.476	CH4
238	4105.721	H2O + SOLAR CO
239	4106.038	H2O

Table 2 (continued)

CODE NO.	ν(OBSERVED) (CM^{-1})	IDENTIFICATION
240	4106.346	CH4 + SOLAR CO
241	4106.604	CH4 (?)
242	4106.736	H2O + (CH4)
243	4107.077	H2O
244	4107.397	(CH4) + SOLAR CO
245	4107.834	CH4
246	4108.210	CH4
247	4108.442	SOLAR FE + SOLAR CO
248	4109.067	CH4 + SOLAR CO
249	4109.584	CH4 + H2O
250	4109.926	CH4 + HF
251	4110.263	CH4 (?)
252	4110.690	CH4 + SOLAR CO
253	4111.041	CH4 + SOLAR CO
254	4112.425	CH4
255	4112.698	CH4 + SOLAR CO + ATOMIC SOLAR
256	4113.141	CH4 + SOLAR CO
257	4113.457	CH4 + SOLAR CO
258	4114.327	?
259	4114.879	CH4 + SOLAR CO
260	4115.218	CH4 + SOLAR CO
261	4115.687	CH4
262	4115.998	CH4 + SOLAR CO
263	4116.531	CH4 + ATOMIC SOLAR
264	4116.845	SOLAR CO
265	4117.241	CH4 + SOLAR CO
266	4117.615	CH4
267	4117.869	(CH4) + ATOMIC SOLAR + SOLAR CO
268	4118.875	CH4 + SOLAR CO
269	4119.199	CH4
270	4119.399	CH4 + SOLAR CO
271	4119.720	CH4
272	4120.211	CH4 + ATOMIC SOLAR
273	4120.642	SOLAR CO
274	4120.999	CH4 + SOLAR CO
275	4121.363	H2O + SOLAR CO
276	4121.697	CH4
277	4121.938	CH4
278	4122.363	CH4 + SOLAR CO
279	4122.899	CH4 + SOLAR CO

Table 2 (continued)

CODE NO.	ν(OBSERVED) (CM^{-1})	IDENTIFICATION
280	4123.157	CH4 + SOLAR CO
281	4123.535	CH4 + (H2O) + SOLAR CO
282	4123.968	CH4 + SOLAR CO
283	4124.206	CH4 + SOLAR CO
284	4124.731	CH4 + (SOLAR CO)
285	4125.182	H2O + CH4
286	4125.493	CH4
287	4125.620	SOLAR CO
288	4125.988	SOLAR CO
289	4126.423	SOLAR CO
290	4126.656	CH4
291	4127.195	CH4 + SOLAR CO
292	4127.807	CH4 + SOLAR CO
293	4128.708	CH4 + (H2O) + SOLAR CO
294	4129.124	CH4 + SOLAR CO
295	4129.323	SOLAR CO
296	4129.922	CH4
297	4130.084	SOLAR CO
298	4130.618	CH4 + SOLAR CO
299	4131.401	SOLAR CO
300	4131.928	CH4 + SOLAR CO
301	4132.163	CH4 + SOLAR CO
302	4132.654	SOLAR CO
303	4133.031	(CH4) + H2O + SOLAR CO
304	4133.265	CH4 + SOLAR CO
305	4133.699	H2O
306	4133.906	CH4 + SOLAR CO
307	4134.367	SOLAR CO
308	4134.730	H2O
309	4134.866	CH4 + SOLAR CO
310	4135.306	CH4 + SOLAR CO
311	4135.490	SOLAR CO
312	4135.897	SOLAR CO
313	4136.237	CH4
314	4136.434	SOLAR CO
315	4136.834	CH4 + SOLAR CO
316	4137.244	CH4 + ATOMIC SOLAR
317	4137.366	SOLAR CO
318	4137.754	CH4 + SOLAR CO
319	4138.284	(CH4) + SOLAR CO

Table 2 (continued)

CODE NO.	ν(OBSERVED) (CM^{-1})	IDENTIFICATION
320	4138.505	SOLAR CO
321	4138.840	H2O + SOLAR CO
322	4139.200	CH4 + SOLAR CO
323	4139.361	CH4 + H2O + SOLAR CO
324	4139.896	SOLAR CO
325	4140.418	CH4 + SOLAR CO
326	4140.861	SOLAR CO
327	4141.229	SOLAR CO
328	4141.666	(CH4) + SOLAR CO
329	4141.934	H2O + SOLAR CO
330	4142.152	SOLAR CO
331	4142.673	CH4 + SOLAR CO
332	4142.928	HF + H2O + SOLAR CO
333	4143.259	CH4 (?) + SOLAR CO
334	4143.927	SOLAR CO
335	4144.700	CH4
336	4145.384	CH4 + (H2O)
337	4145.925	SOLAR CO
338	4146.343	H2O
339	4146.702	CH4 (?) + SOLAR CO
340	4147.496	SOLAR CO
341	4147.844	CH4
342	4148.546	CH4
343	4148.853	CH4 + (H2O) + SOLAR CO
344	4149.378	CH4 + SOLAR CO
345	4149.499	H2O + CH4
346	4150.053	CH4
347	4150.562	CH4
348	4151.031	CH4 + SOLAR ATOMIC
349	4151.402	CH4
350	4151.522	SOLAR CO
351	4152.030	? + SOLAR CO
352	4152.257	SOLAR CO
353	4152.608	CH4
354	4153.311	H2O + CH4
355	4153.646	CH4 + (SOLAR CO)
356	4154.112	CH4 + SOLAR CO
357	4154.550	H2O + SOLAR CO
358	4155.399	CH4
359	4155.904	CH4 + (H2O)

Table 2 (concluded)

CODE NO.	ν(OBSERVED) (CM^{-1})	IDENTIFICATION
360	4156.898	CH4 + SOLAR CO
361	4157.250	CH4
362	4157.530	CH4
363	4158.022	?
364	4158.297	CH4
365	4158.541	CH4
366	4159.061	CH4 + H2O + SOLAR CO
367	4159.460	CH4 + H2O + SOLAR CO

Table 3

Comparison of Line Intensities (cm^{-2} atm^{-1} at 296 K)
in the R-Branch of the (1-0) Band of HCℓ

Line	Cℓ Isotope	1980 AFGL	Toth et al. (1970)	Benedict et al. (1956)	Lin et al. (1978)	Varanasi et al. (1972)
R0	35	5.58	5.03	4.84	4.35	5.21
	37	1.81	1.65	1.65	1.41	1.71
R1	35	9.89		8.74	7.23	8.92
	37	3.20	3.04	3.03	2.34	2.88
R2	35	11.87		9.83	8.56	10.14
	37	3.87	3.50	3.20	2.77	3.07
R3	35	11.45		9.61	7.98	9.95
	37	3.72	3.31	3.52	2.58	3.38
R4	35	9.37		7.75	6.42	7.89
	37	3.05	2.75	2.50	2.08	2.60
R5	35	6.67		6.02	4.81	6.59
	37	2.17	1.99	2.04	1.56	2.20
R6	35	4.16	3.73	3.68	2.88	4.24
	37	1.36	1.25	1.40	0.933	1.40
R7	35	2.30	2.10	2.09	1.58	2.11
	37	0.751	0.693	0.654	0.513	0.68
R8	35	1.14	1.07	1.05	0.813	1.08
	37	0.369	0.351	0.409	0.263	0.44
R9	35	0.501	0.460			0.48
	37	0.164	0.151			0.17
R10	35	0.198	0.188			0.20
	37	0.0649	0.0624			0.068

Table 4

Comparison of Nitrogen-broadened HCℓ (1-0) Band Halfwidths (cm^{-1} atm^{-1} at 296 K)

m	Toth and Darnton* (1974)	Houdeau et al. (1980)	Babrov et al. (1960)	Benedict* et al. (1956)	Rank et al. (1963)	Lin et al. (1978)	Miziolek (1977)
-11	0.0172						
-10	0.0204						
- 9	0.0247					0.0220	0.0307
- 8	0.0337		0.0269	0.031		0.0325	0.0349
- 7	0.0412		0.0365	0.040		0.0420	0.0443
- 6	0.0543		0.0437	0.054		0.0585	
- 5	0.0642	0.0579	0.0597	0.062		0.0731	
- 4	0.0795	0.0681	0.0646	0.069	0.0900	0.0775	
- 3	0.0920	0.0770	0.0728	0.089	0.0985	0.0900	
- 2	0.0952	0.0837	0.0857	0.088	0.0960	0.0973	
- 1	0.0967	0.0928	0.0932	0.092	0.1035	0.0997	
1	0.0967	0.0885		0.092	0.1105	0.1060	
2	0.0952	0.0811		0.088	0.0980	0.1011	
3	0.0920	0.0739		0.089	0.0955	0.0959	
4	0.0795	0.0681		0.069	0.0845	0.0885	
5	0.0642	0.0584		0.062	0.0665	0.0722	
6	0.0543	0.0460		0.054	0.0565	0.0550	
7	0.0412	0.0353		0.040	0.0395	0.0435	
8	0.0337	0.0259		0.031	0.0305	0.0312	
9	0.0247				0.0270	0.0216	
10	0.0204				0.0180		
11	0.0172						

*Individual measurements of P and R branch widths not presented. We list the same values for the corresponding lines of both branches.

Table 5

Comparison of Line Intensities (cm^{-2} atm^{-1} at 296 K) of the (1,0) Band of HF*

Line	1980 AFGL	Lovell and Herget (1962)	Kuipers (1958)	Hinchen and Hobbs (1979)
P12	1.52(-4)			1.58(-4)
P11	1.38(-3)			1.43(-3)
P10	1.04(-2)			1.08(-2)
P9	6.44(-2)			6.57(-2)
P8	3.25(-1)			3.22(-1)
P7	1.33(+0)		1.55(+0)	1.34(+0)
P6	4.41(+0)	4.44(+0)	4.29(+0)	4.39(+0)
P5	1.16(+1)	1.16(+1)	1.31(+1)	1.16(+1)
P4	2.43(+1)	2.42(+1)	2.80(+1)	2.45(+1)
P3	3.89(+1)	3.74(+1)	4.71(+1)	
P2	4.54(+1)	4.56(+1)	5.16(+1)	
P1	3.25(+1)	3.32(+1)	3.87(+1)	
R0	3.67(+1)	3.72(+1)	3.97(+1)	
R1	5.78(+1)	5.55(+1)	6.49(+1)	
R2	5.60(+1)	5.85(+1)	6.07(+1)	
R3	3.94(+1)	4.06(+1)	4.06(+1)	
R4	2.13(+1)	2.18(+1)	1.97(+1)	
R5	9.12(+0)	9.15(+0)	8.87(+0)	
R6	3.12(+0)	2.95(+0)	2.58(+0)	
R7	8.60(-1)	6.94(-1)	6.34(+0)	
R8	1.93(-1)		1.34(-1)	
R9	3.54(-2)			
R10	5.33(-3)			
R11	6.62(-4)			
R12	6.79(-5)			

*Note: numbers in parentheses are powers of 10.

Table 6

HALOE HCℓ and HF Cell Conditions
and Line Parameter Requirements

	HCℓ	HF
Nominal Fill Conditions		
• Instrument Cell		
- Pressure	0.1 atm	0.2 atm
- Mixing Ratio	0.1	0.5
• Calibration Cell 1		
- Pressure	0.07 atm	0.07 atm
- Mixing Ratio	0.021	0.021
• Calibration Cell 2		
- Pressure	0.01 atm	0.01 atm
- Mixing ratio	0.064	0.008
Gas Cell Stability Requirements		
- Pressure	3%	10%
- Mixing Ratio	3%	10%
Line-parameter Accuracy Requirements		
• Absorbing Gas		
- Position	± 0.003 cm^{-1}	± 0.003 cm^{-1}
- Strength	3%	3%
- Self-broadened Halfwidth	3%	3%
- N_2-broadened Halfwidth	3%	3%
- Air-broadened Halfwidth	5%	5%
• Interfering Gases		
- Position	± 0.003 cm^{-1}	± 0.003 cm^{-1}
- Strength (see text)	3 to 5%	3 to 5%
- Air-broadened Halfwidth (see text)	5 to 10%	5 to 10%

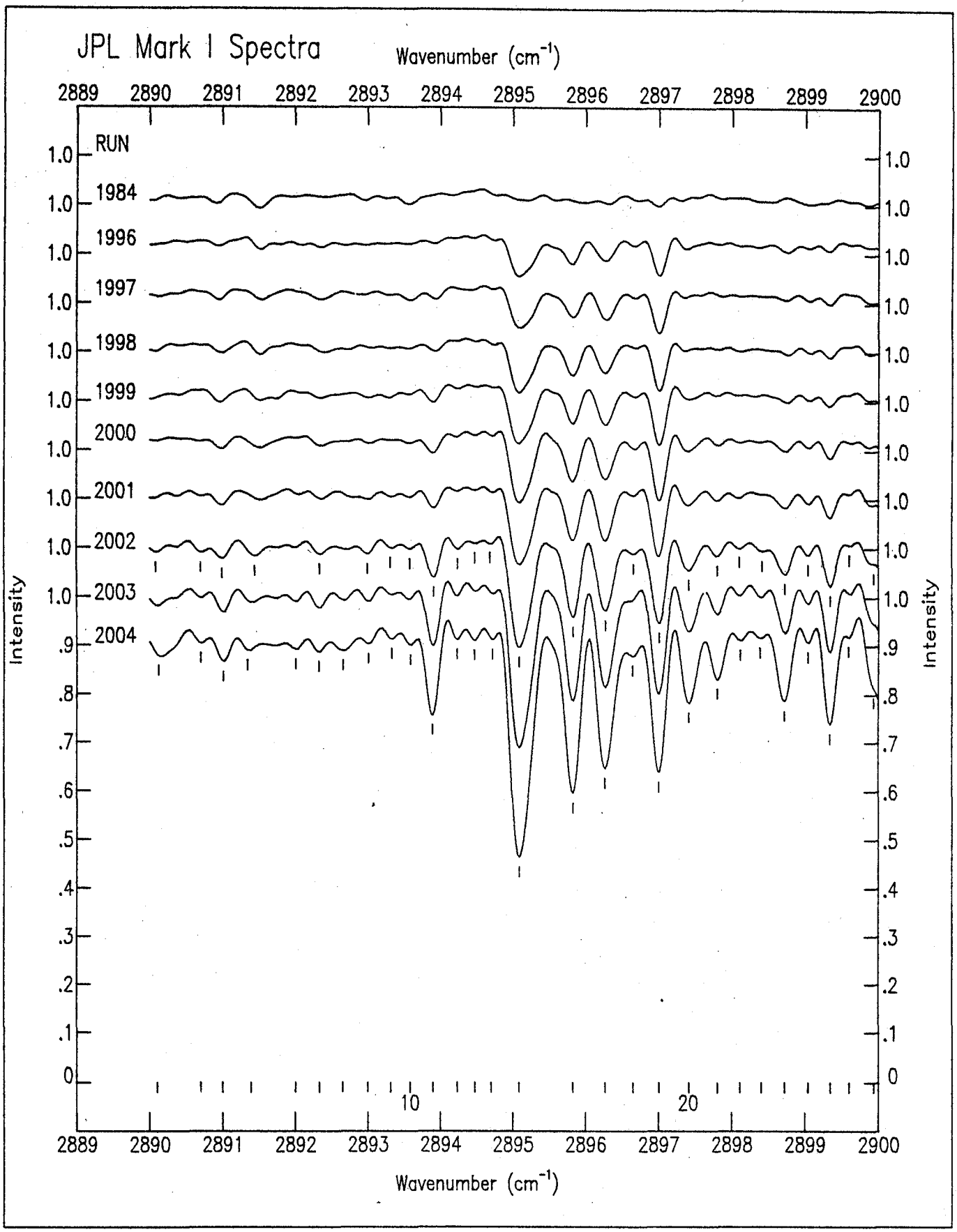

Figure 1.-JPL stratospheric spectra in the region 2890-2900 cm^{-1}.

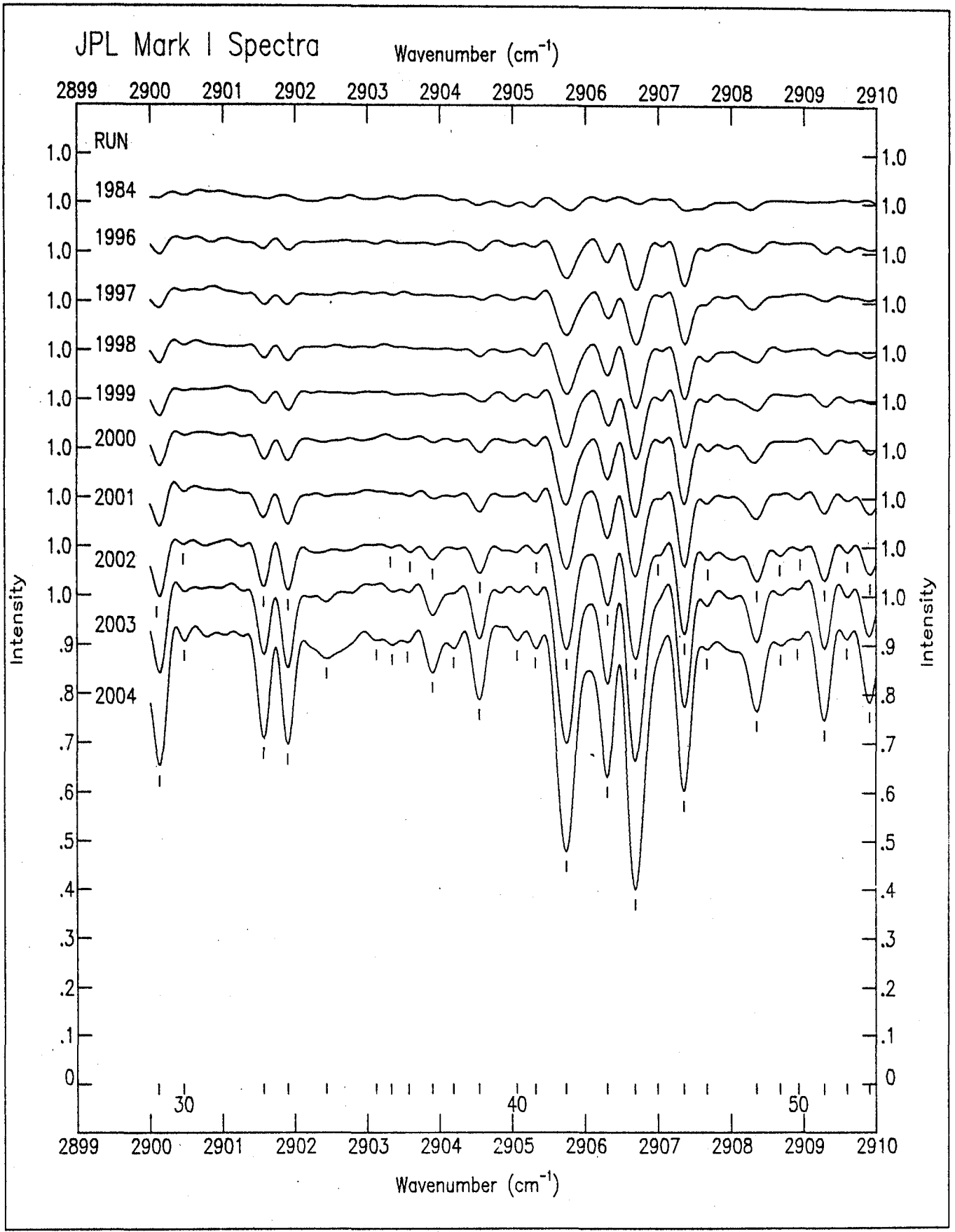

Figure 2.-JPL stratospheric spectra in the region 2900-2910 cm^{-1}.

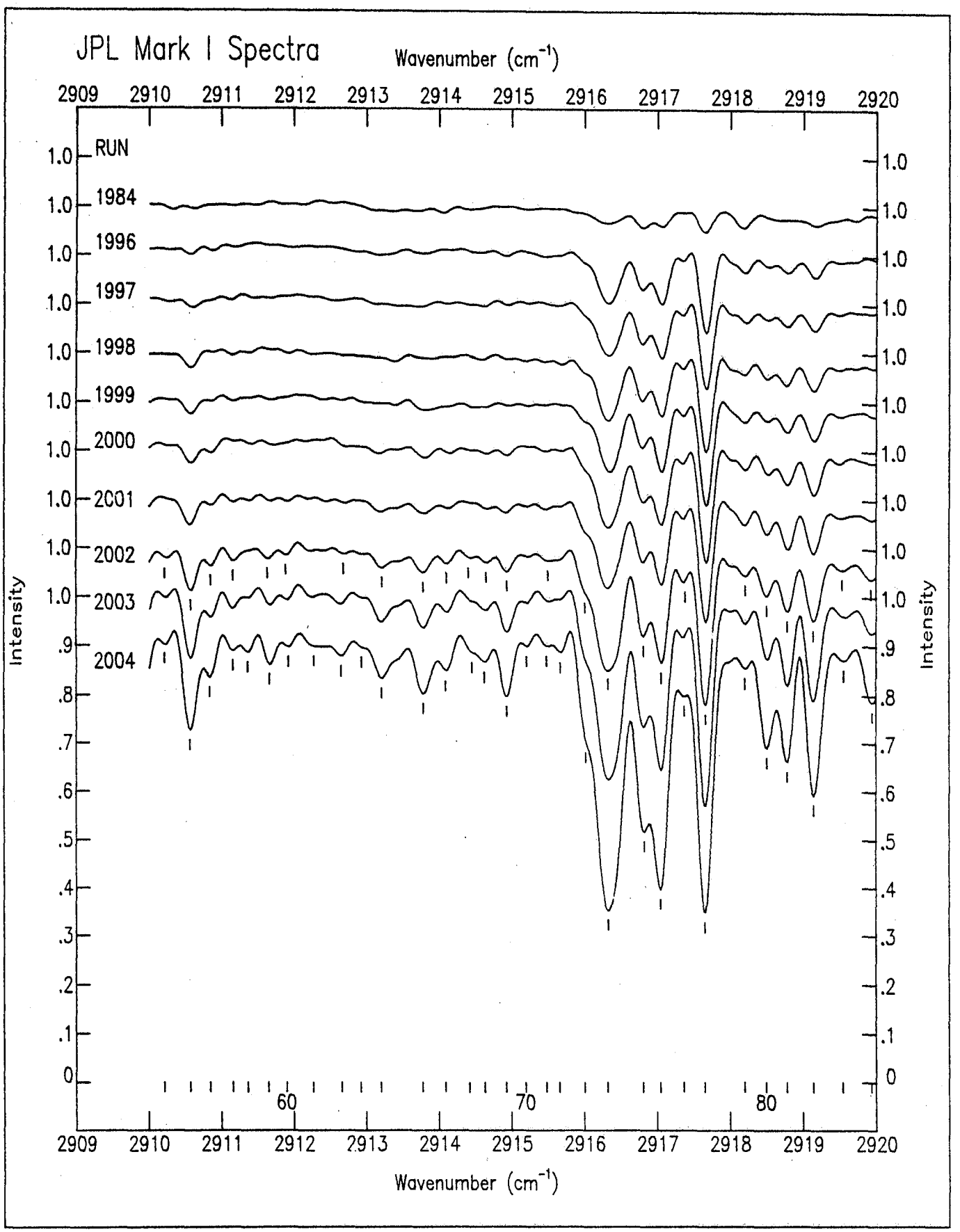

Figure 3.-JPL stratospheric spectra in the region 2910-2920 cm^{-1}.

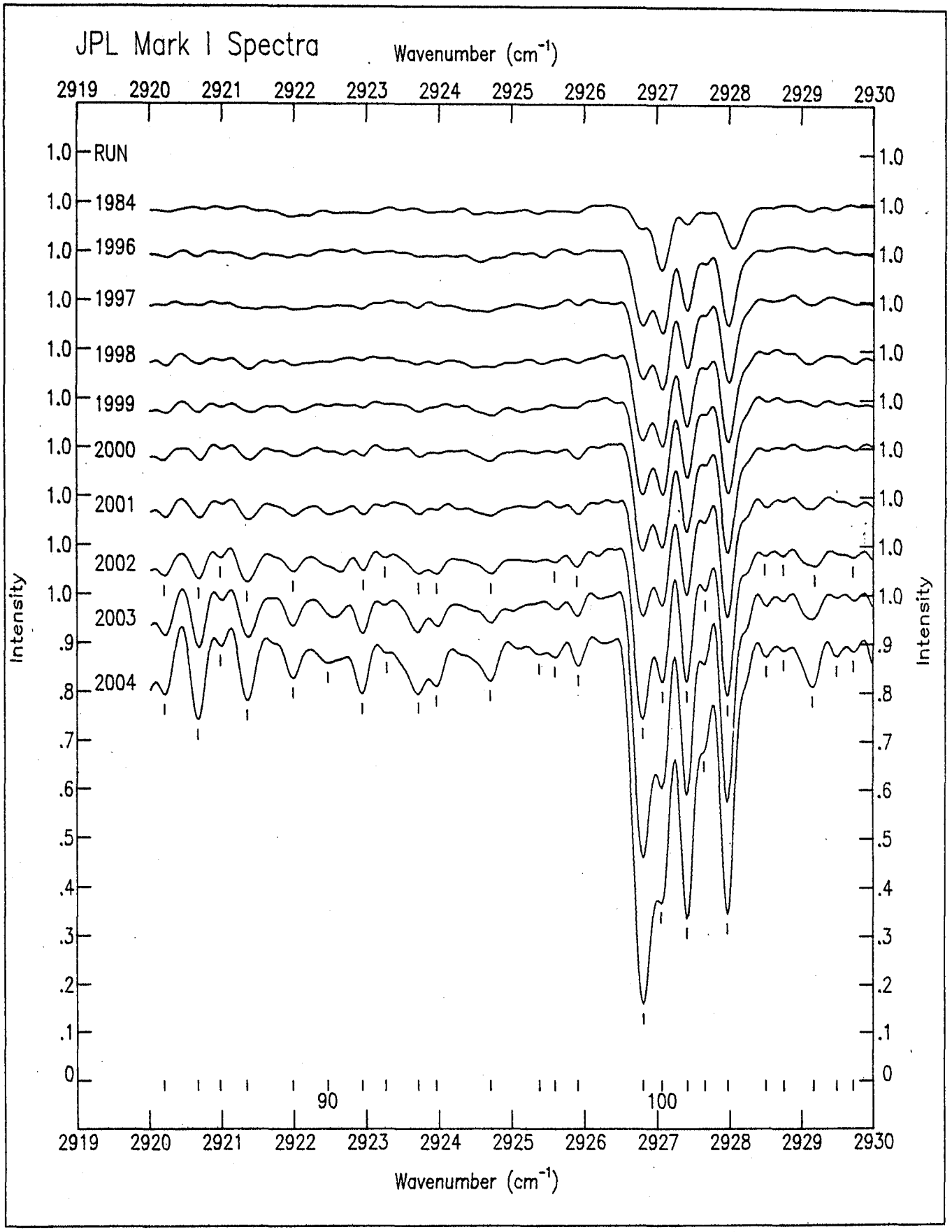

Figure 4.-JPL stratospheric spectra in the region 2920-2930 cm^{-1}.

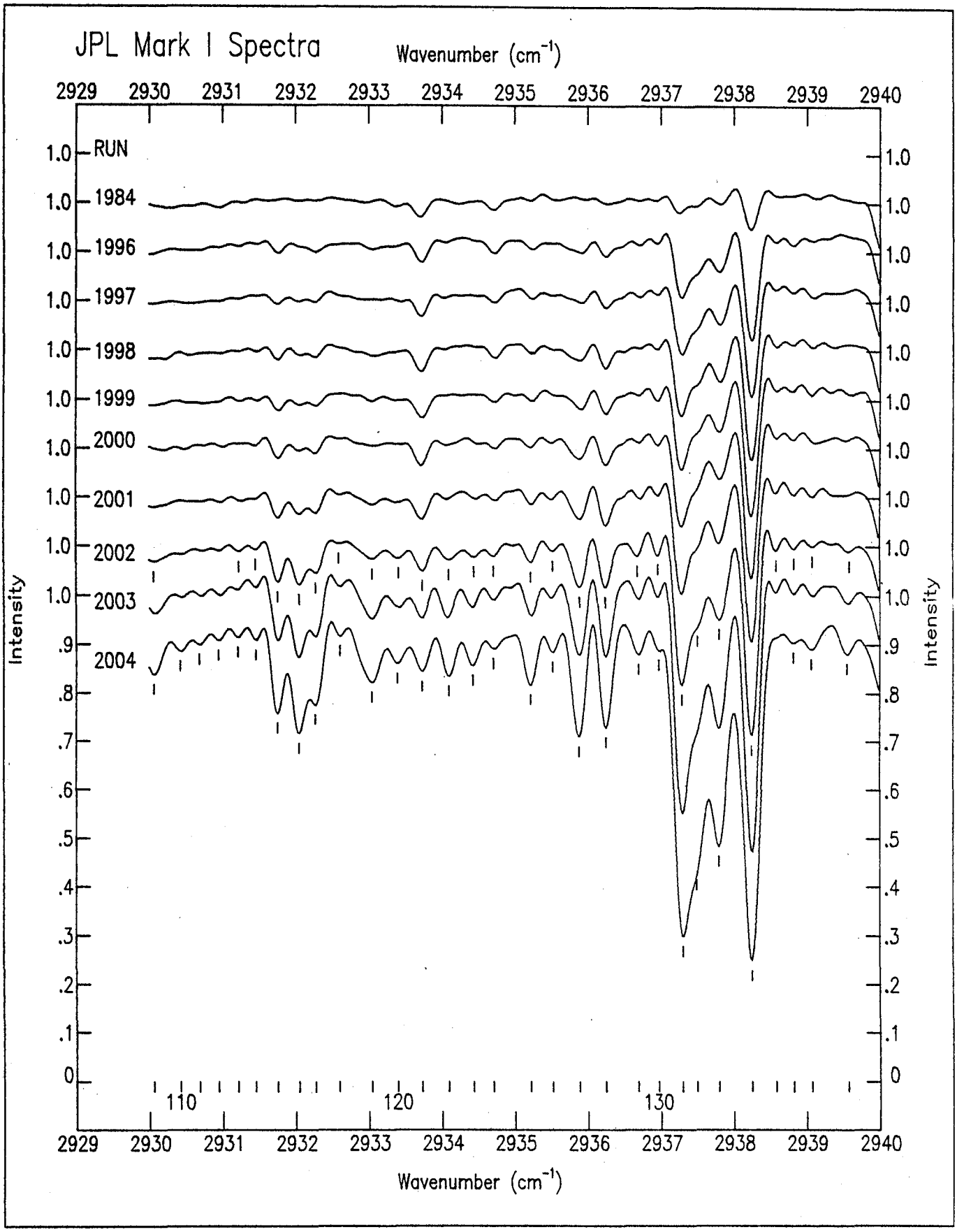

Figure 5.-JPL stratospheric spectra in the region 2930-2940 cm^{-1}.

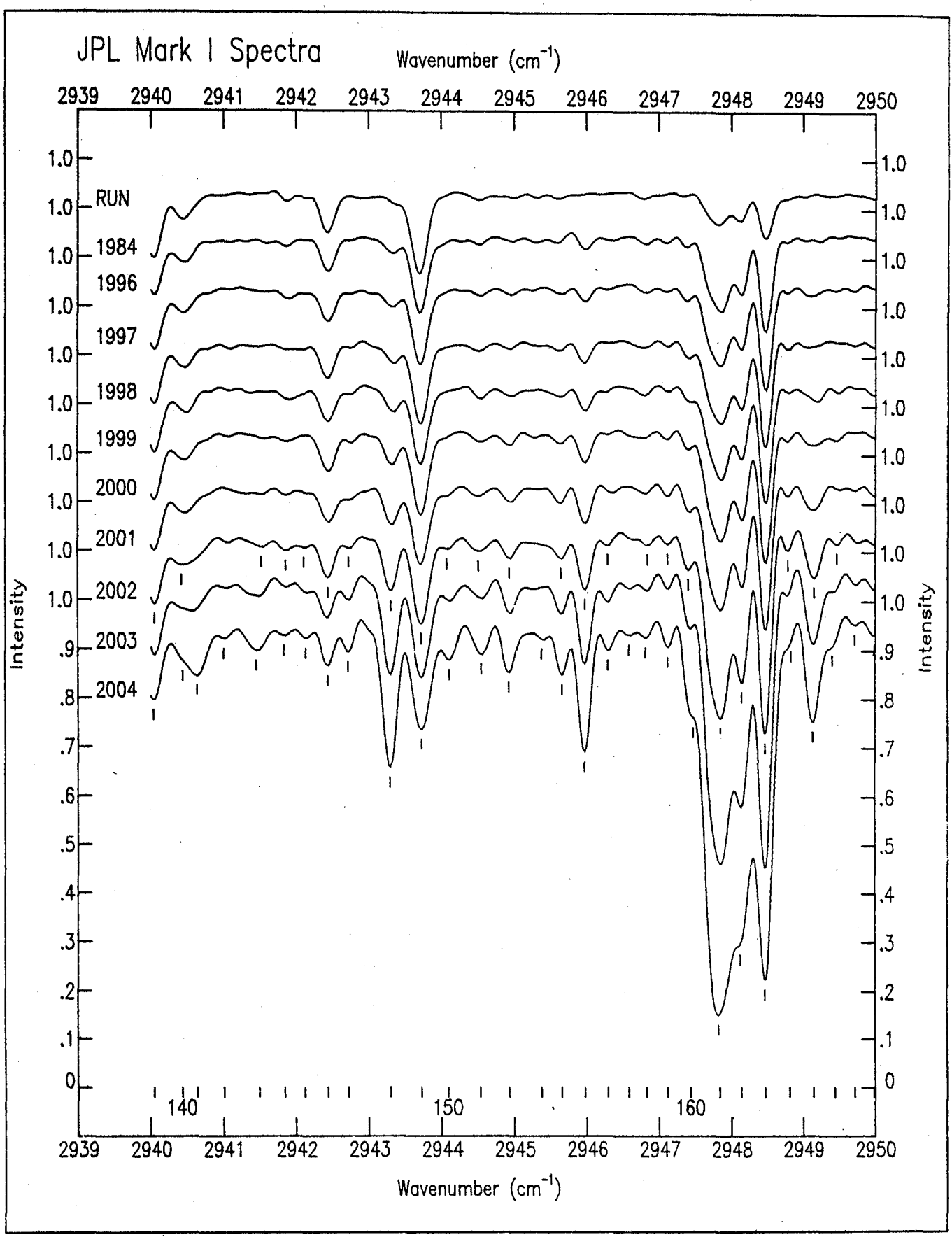

Figure 6.-JPL stratospheric spectra in the region 2940-2950 cm^{-1}.

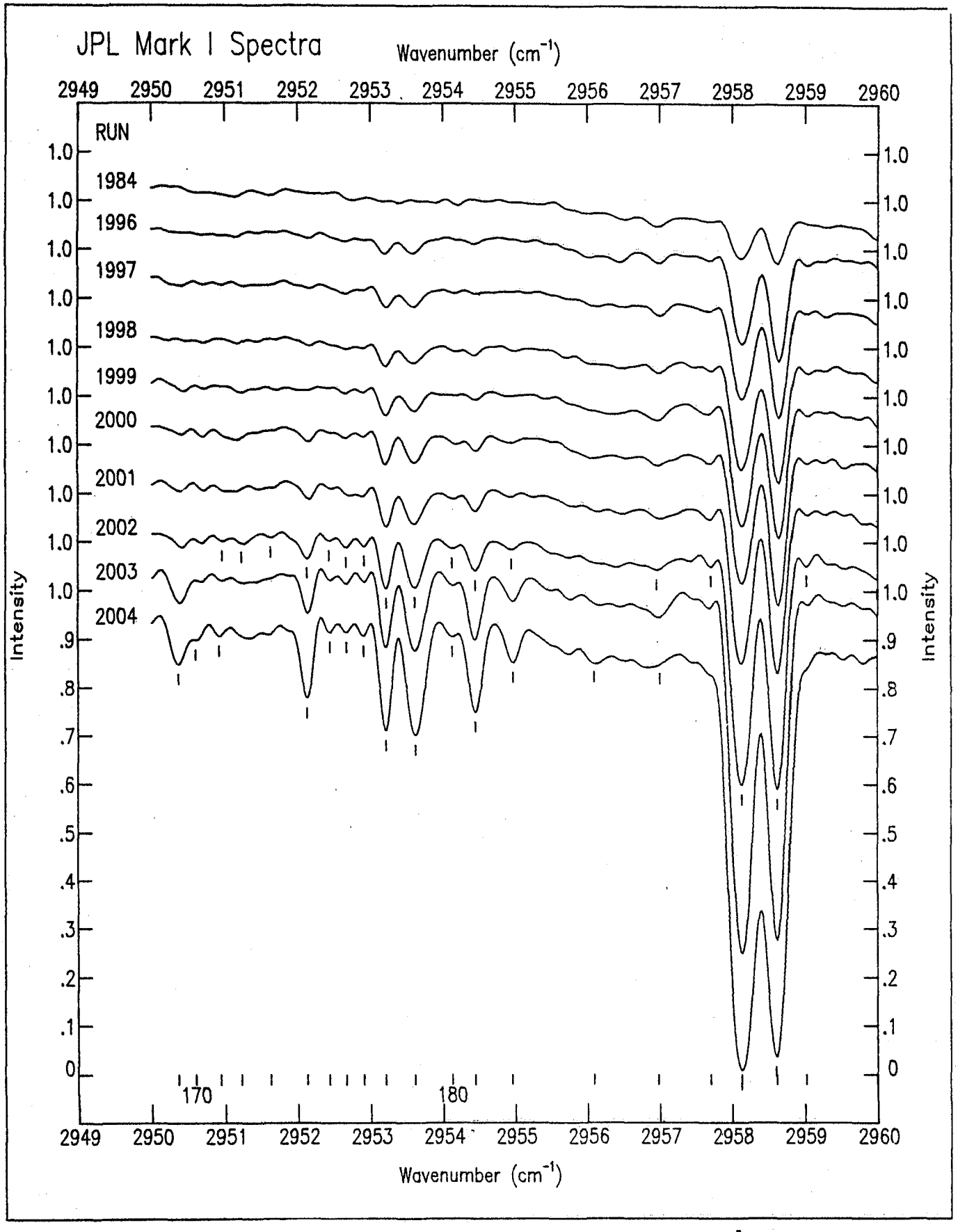

Figure 7.-JPL stratospheric spectra in the region 2950-2960 cm^{-1}.

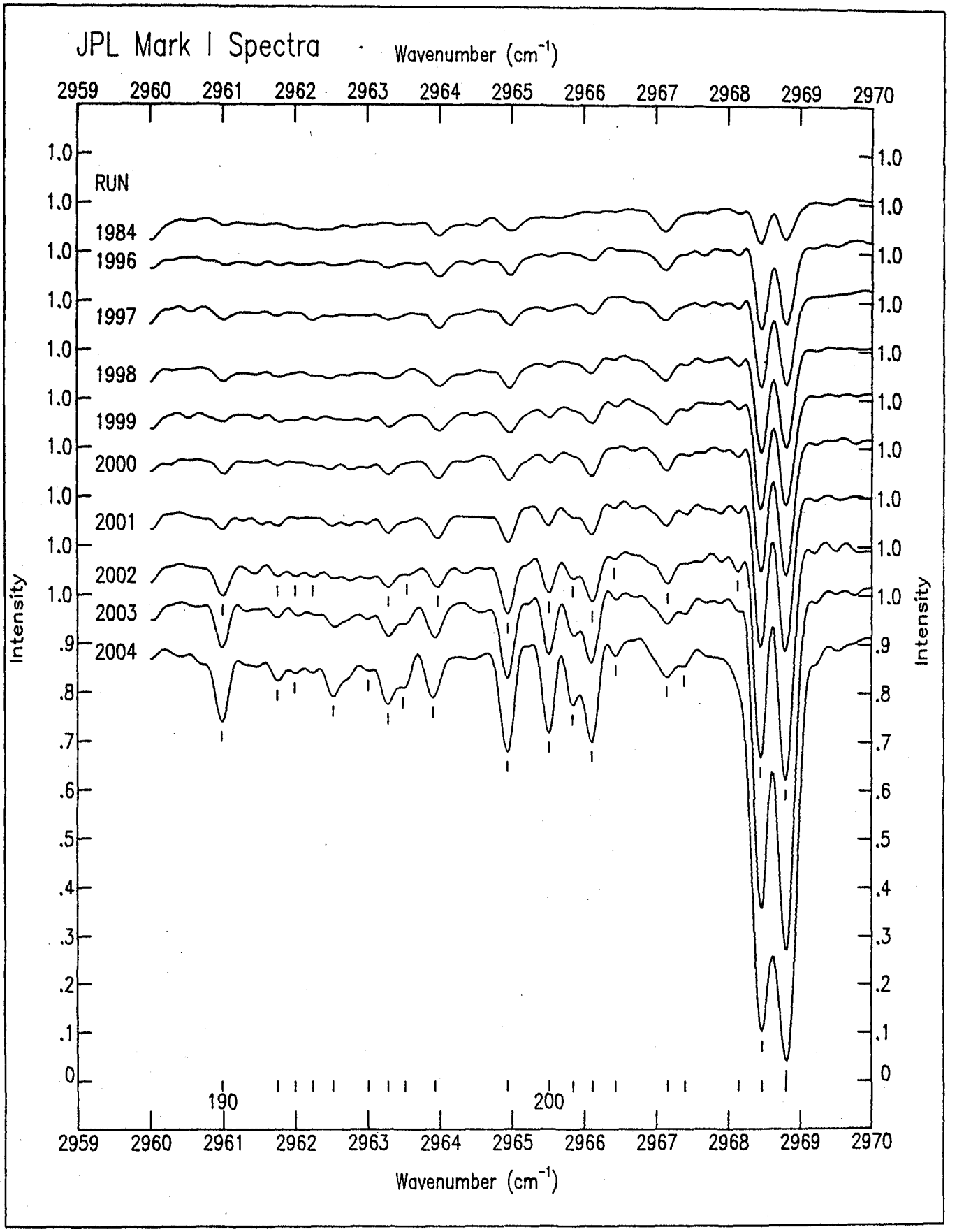

Figure 8.-JPL stratospheric spectra in the region 2960-2970 cm^{-1}.

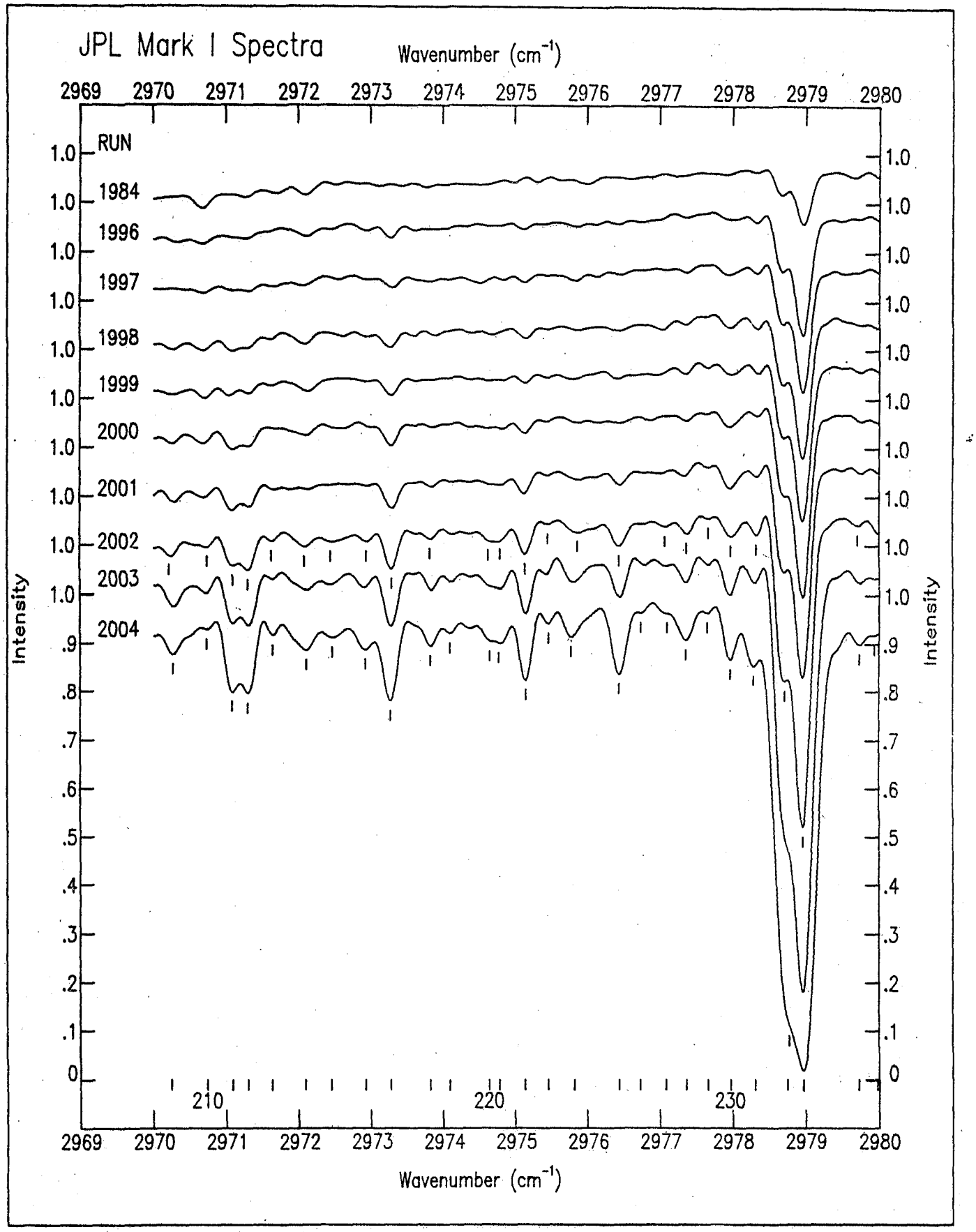

Figure 9.-JPL stratospheric spectra in the region 2970-2980 cm^{-1}.

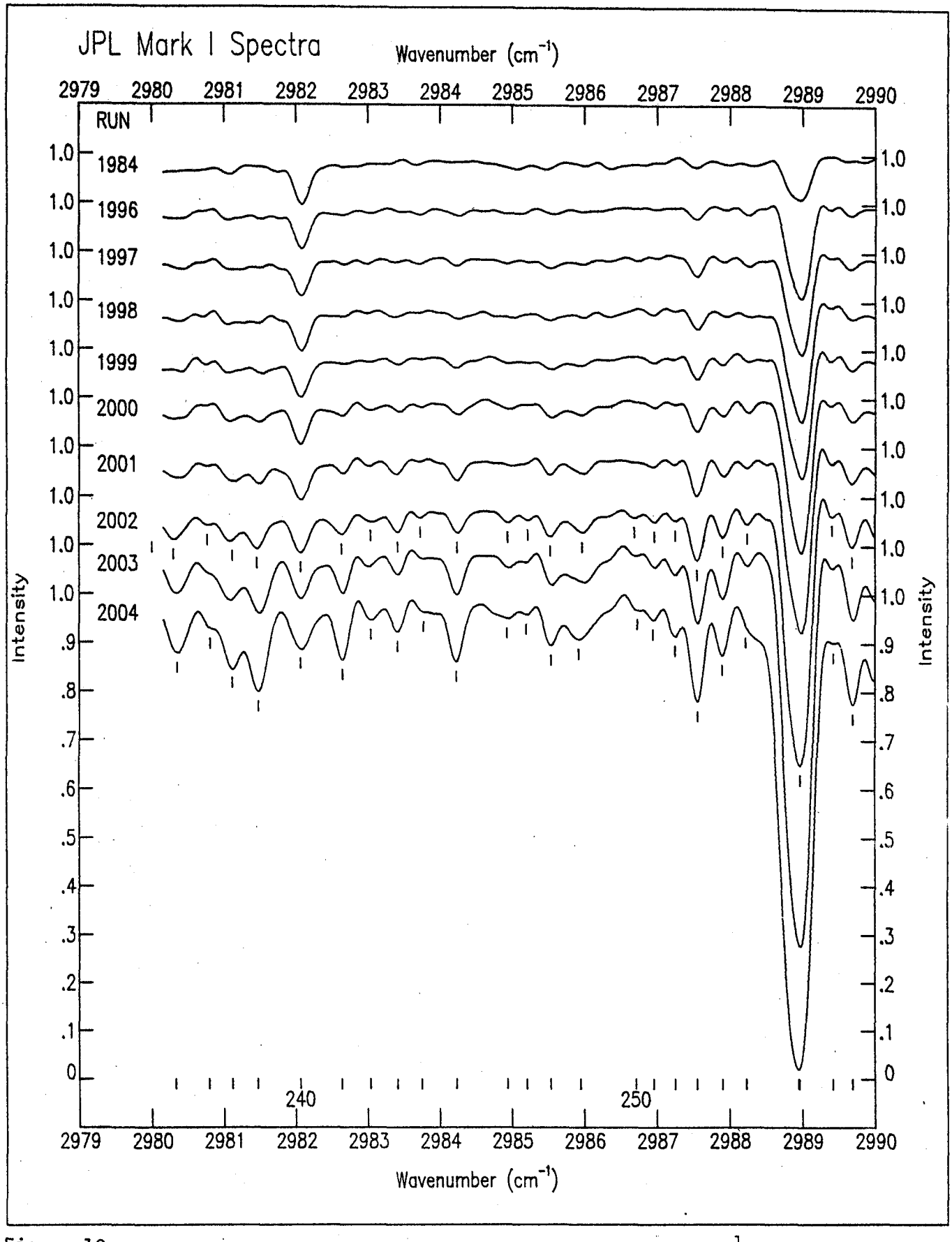

Figure 10.-JPL stratospheric spectra in the region 2980-2990 cm^{-1}.

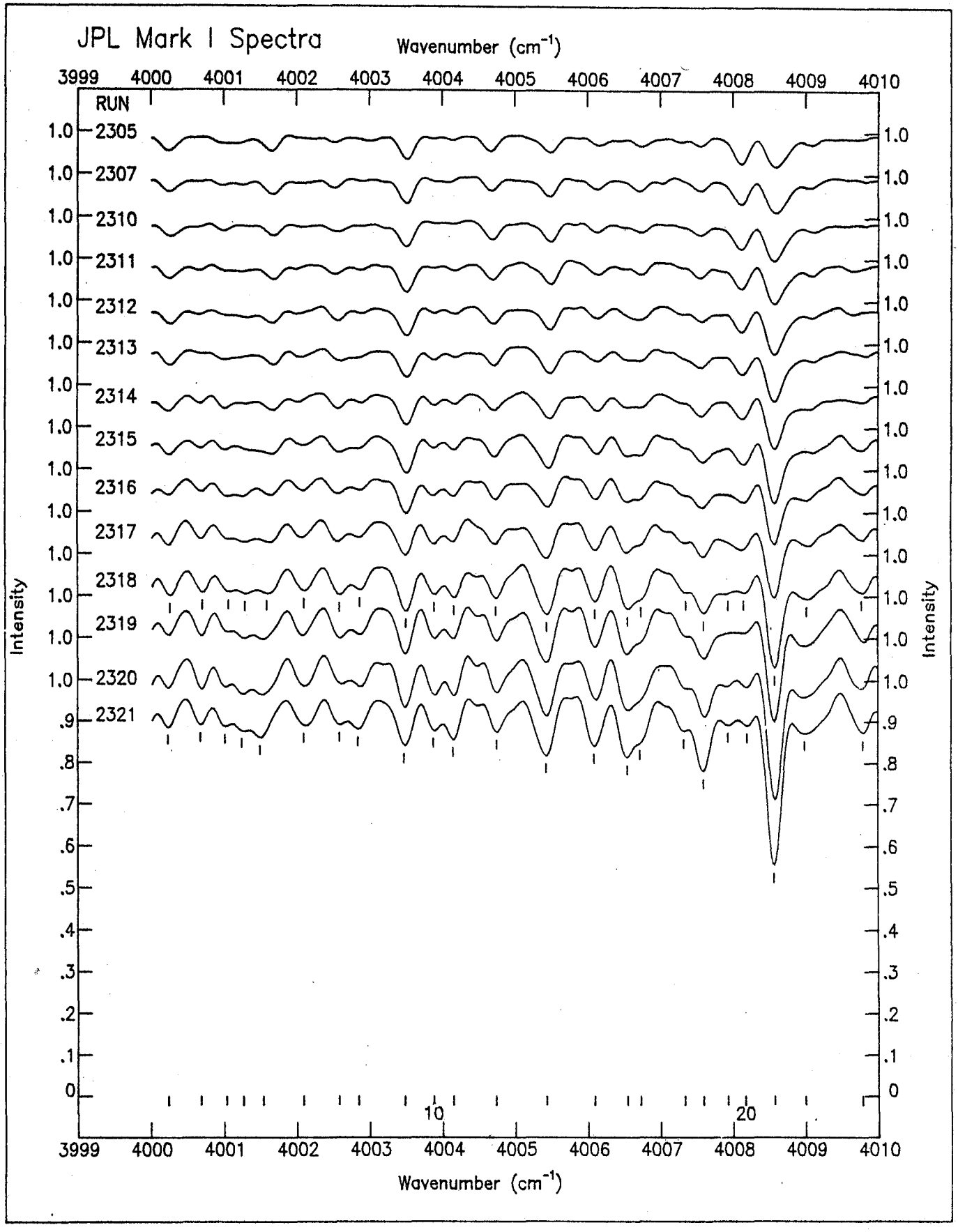

Figure 11.-JPL stratospheric spectra in the region 4000-4010 cm^{-1}.

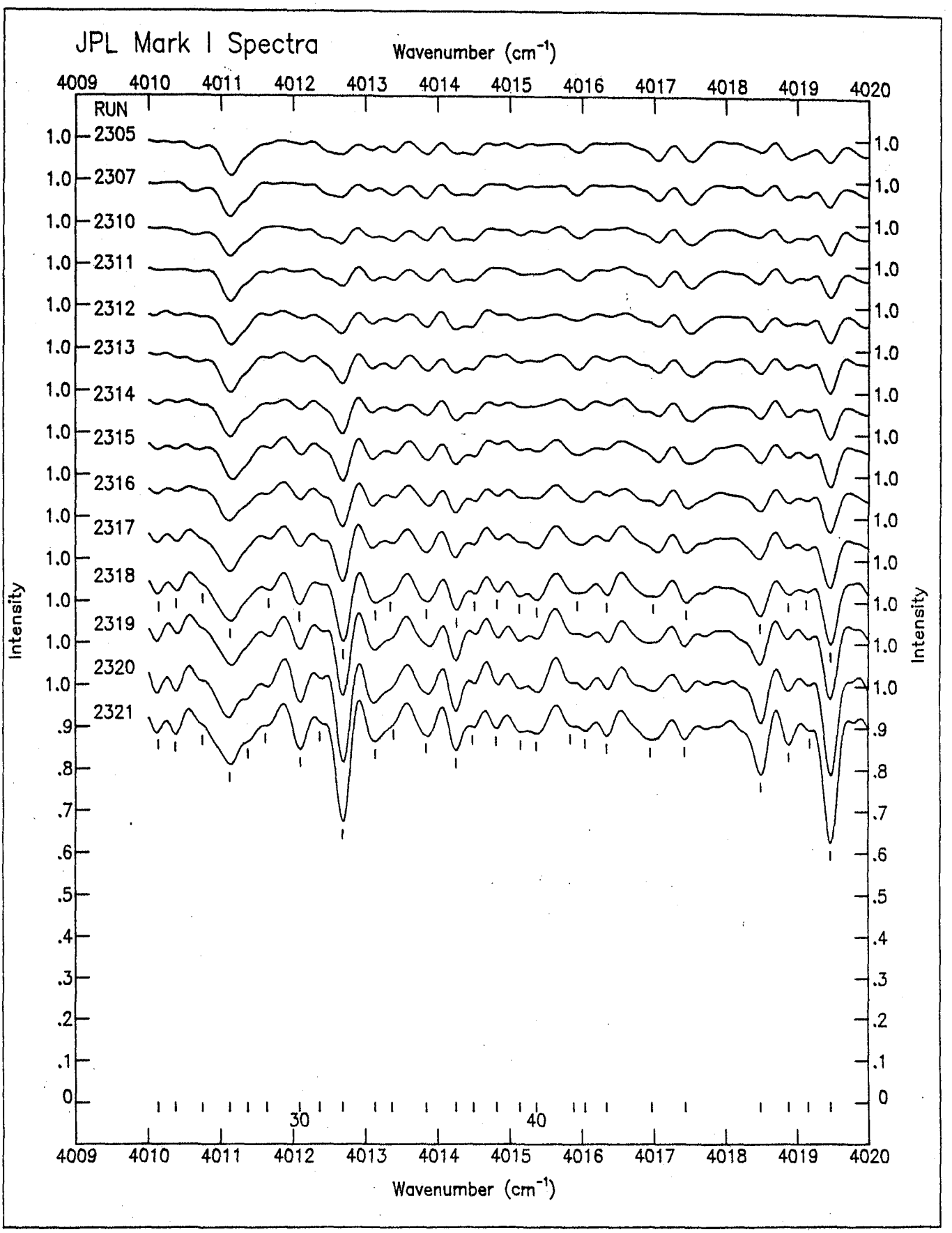

Figure 12.-JPL stratospheric spectra in the region 4010-4020 cm^{-1}.

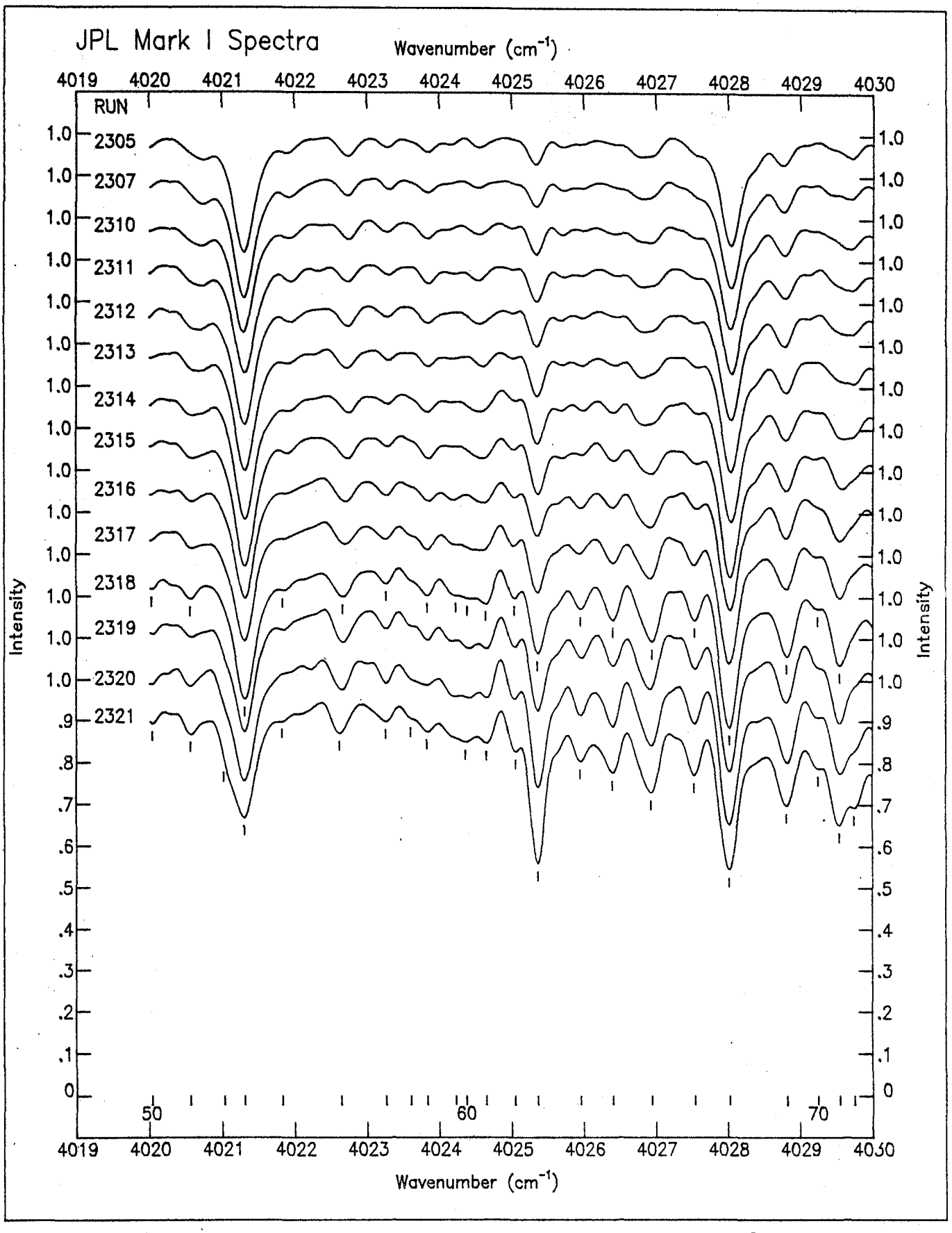

Figure 13.-JPL stratospheric spectra in the region 4020-4030 cm^{-1}.

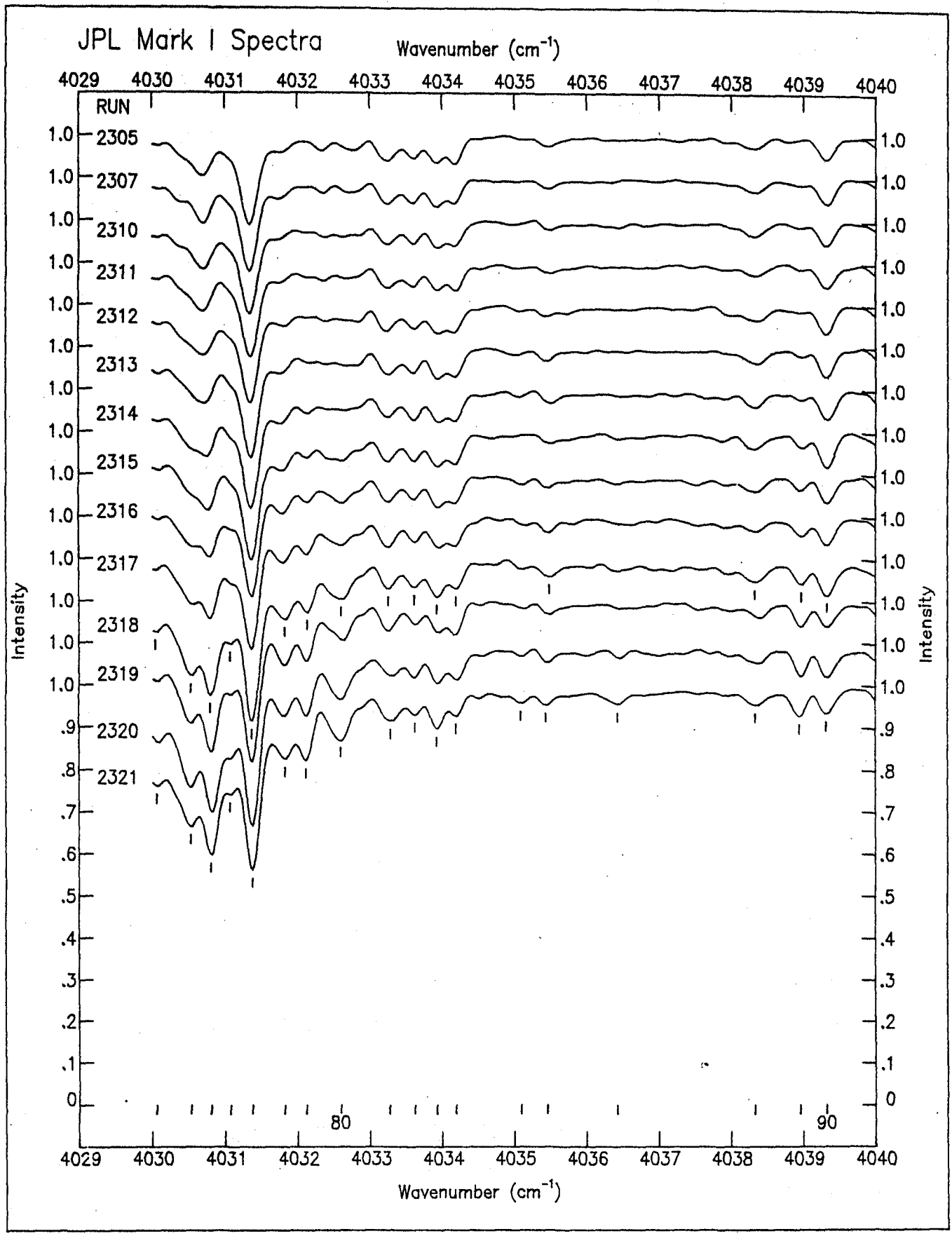

Figure 14.-JPL stratospheric spectra in the region 4030-4040 cm^{-1}.

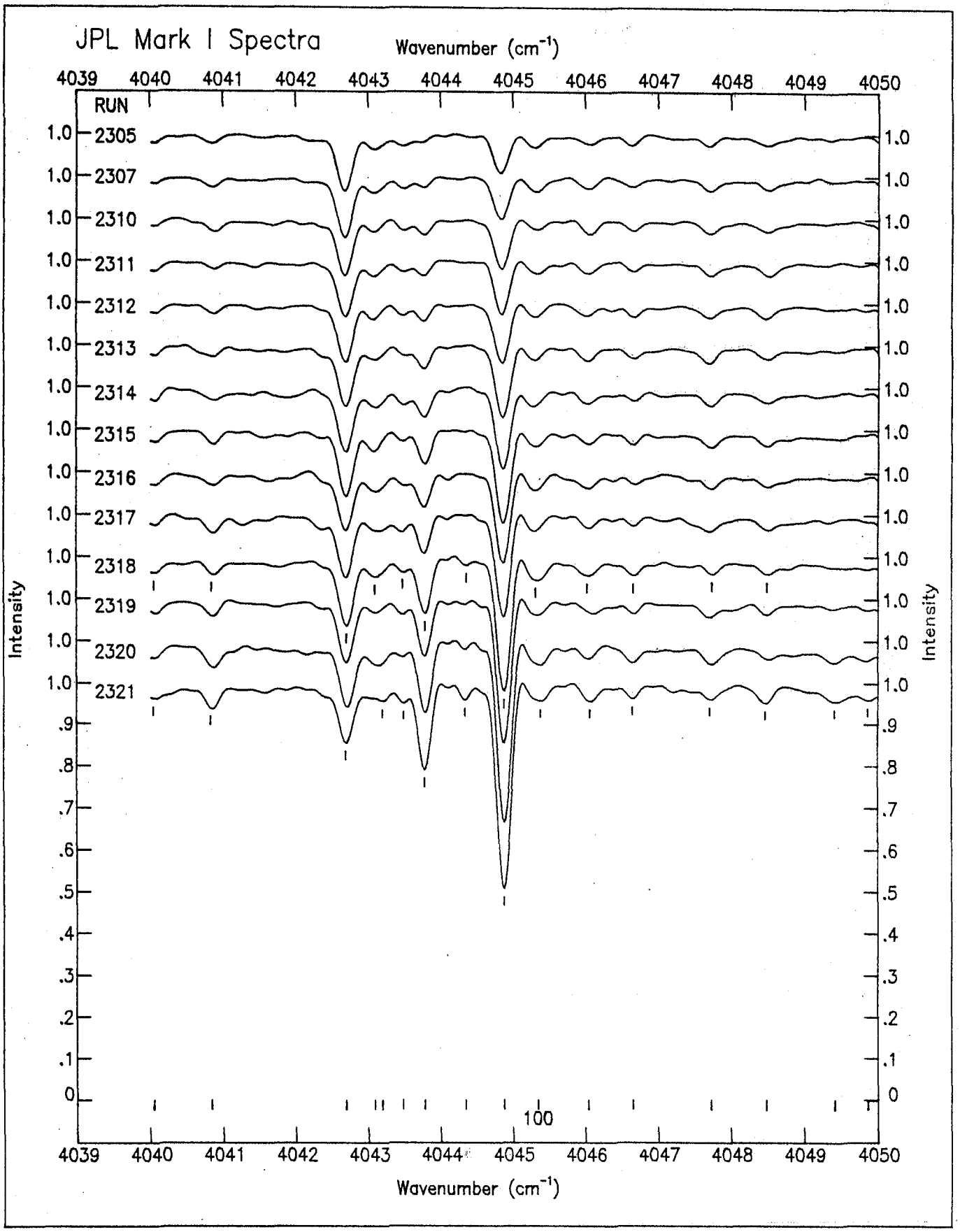

Figure 15.-JPL stratospheric spectra in the region 4040-4050 cm^{-1}.

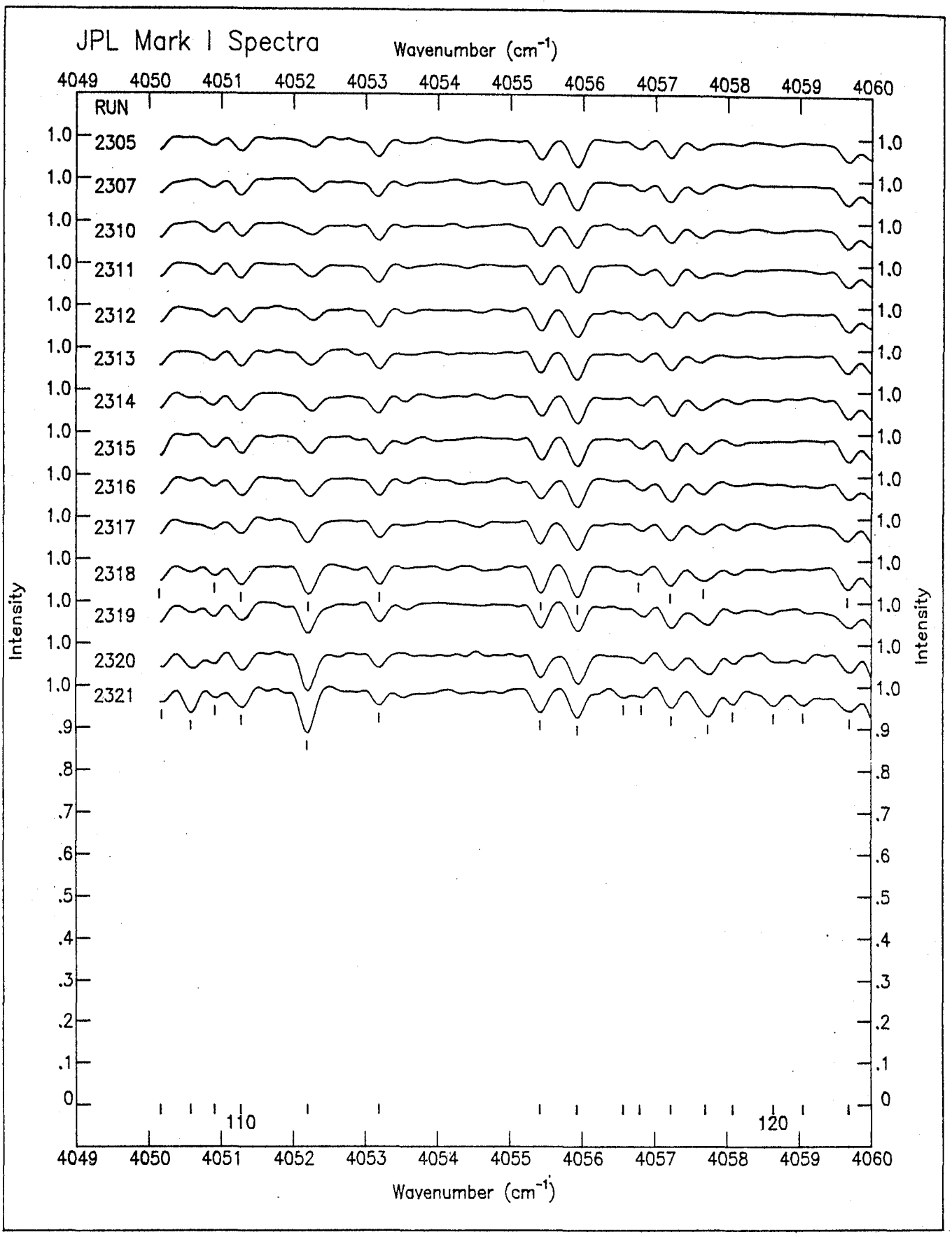

Figure 16.-JPL stratospheric spectra in the region 4050-4060 cm^{-1}.

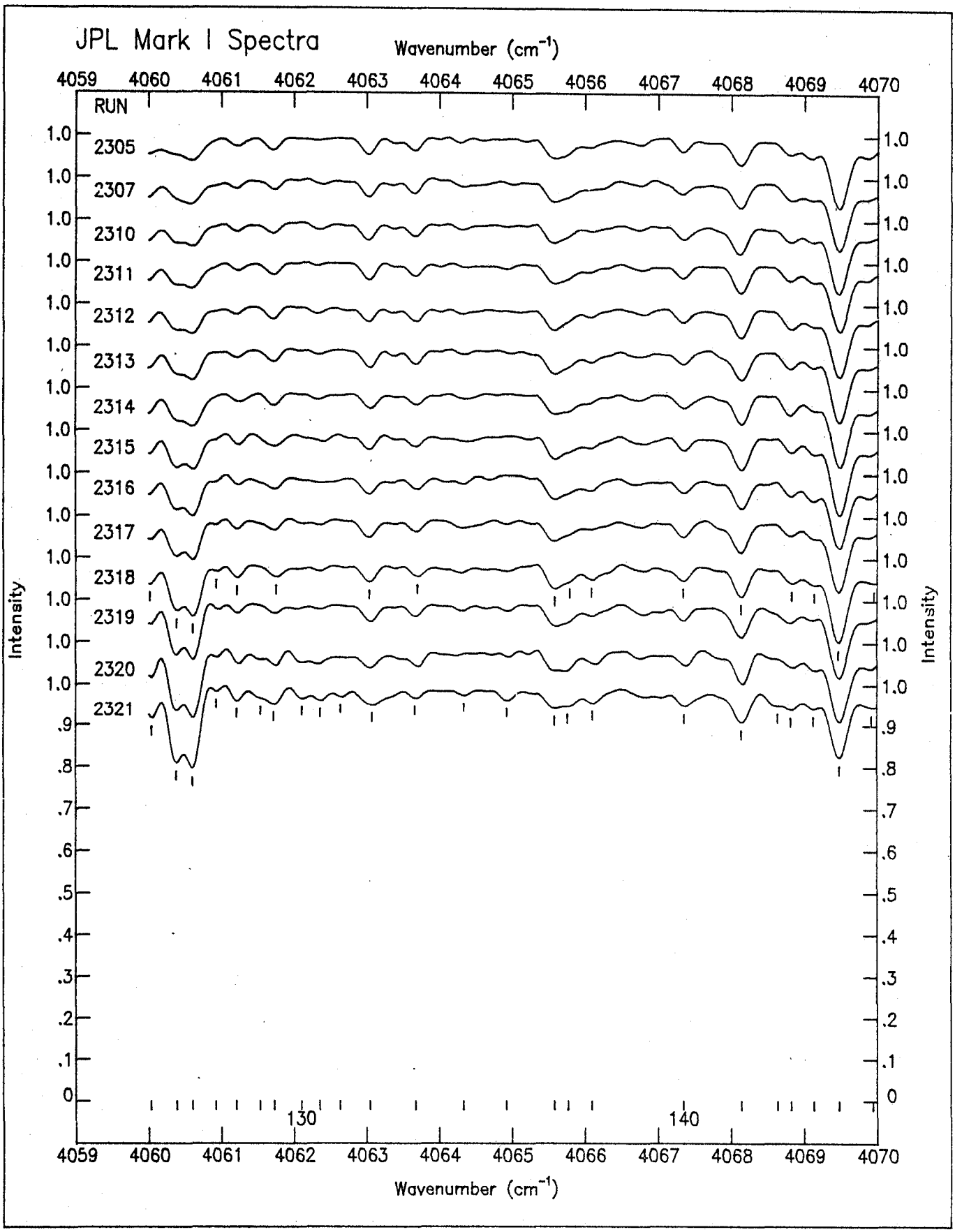

Figure 17.-JPL stratospheric spectra in the region 4060-4070 cm^{-1}.

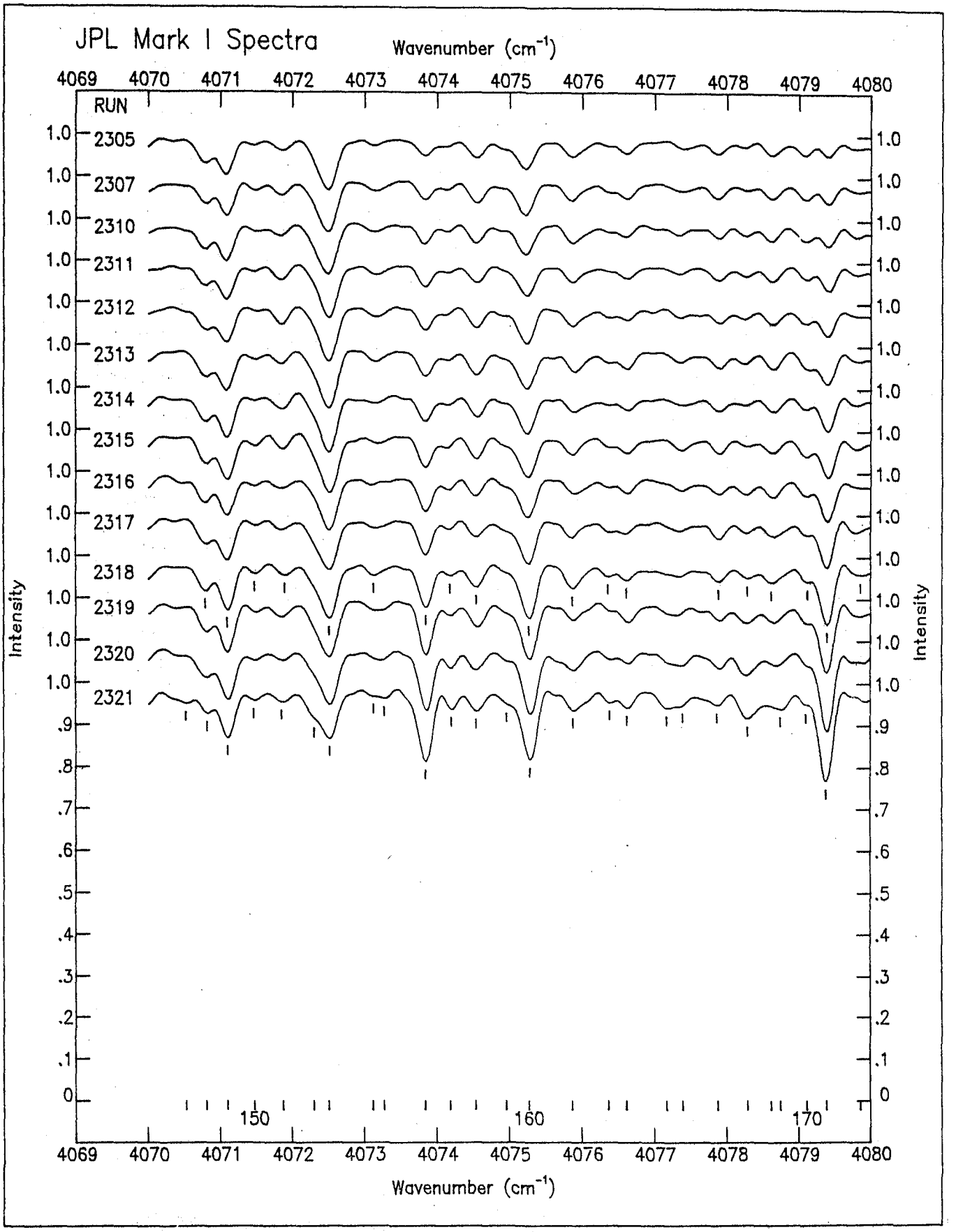

Figure 18.-JPL stratospheric spectra in the region 4070-4080 cm^{-1}.

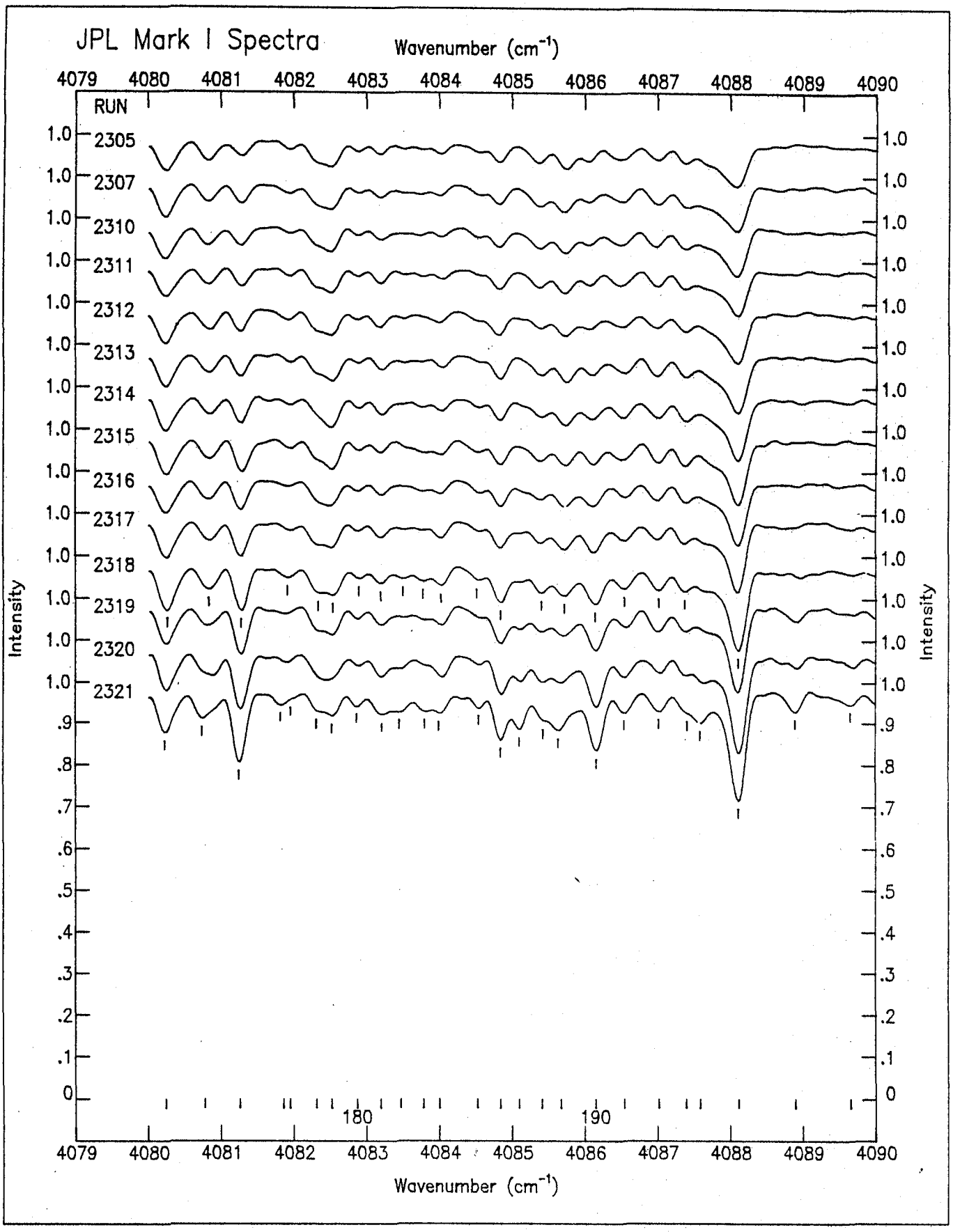

Figure 19.-JPL stratospheric spectra in the region 4080-4090 cm^{-1}.

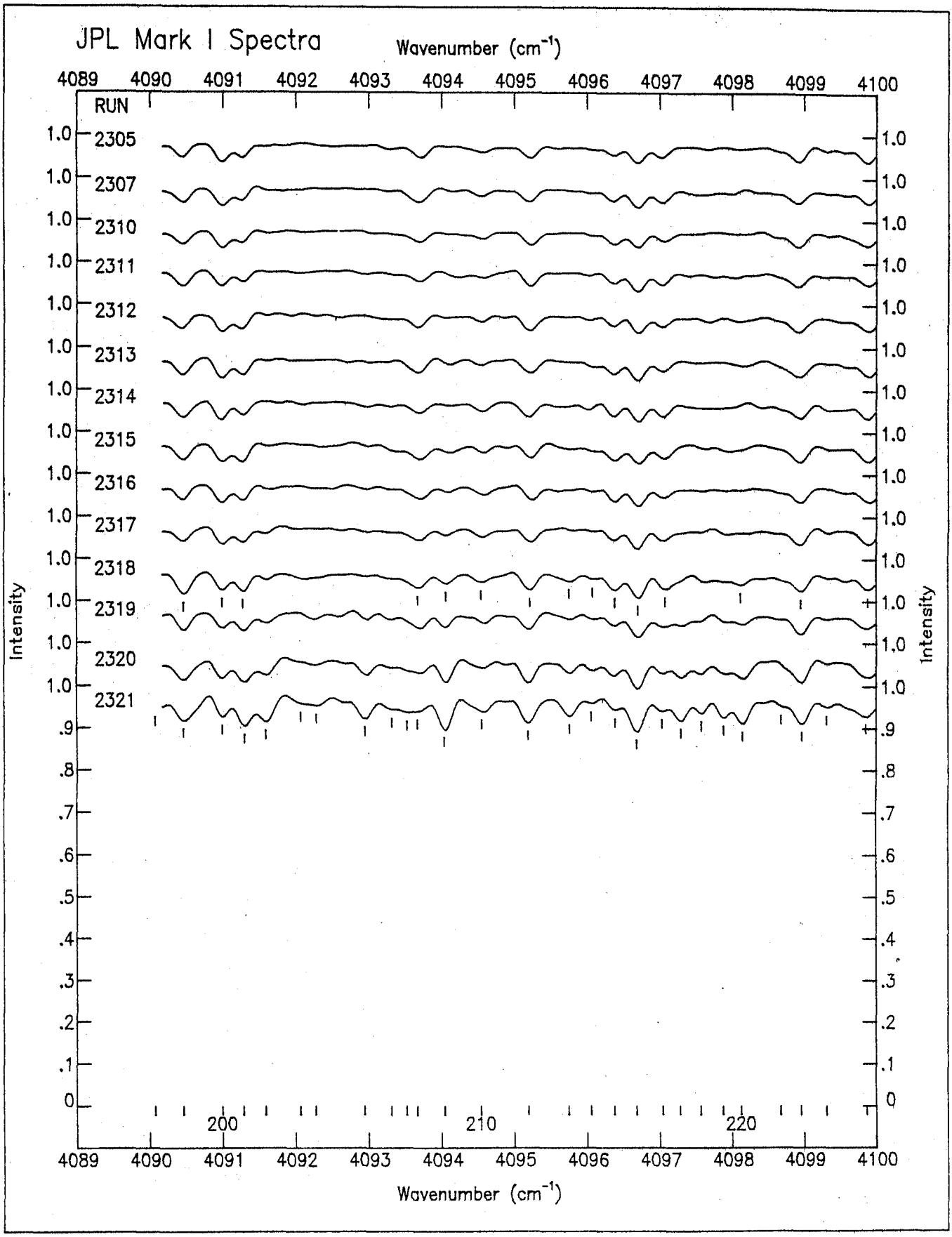

Figure 20.-JPL stratospheric spectra in the region 4090-4100 cm^{-1}.

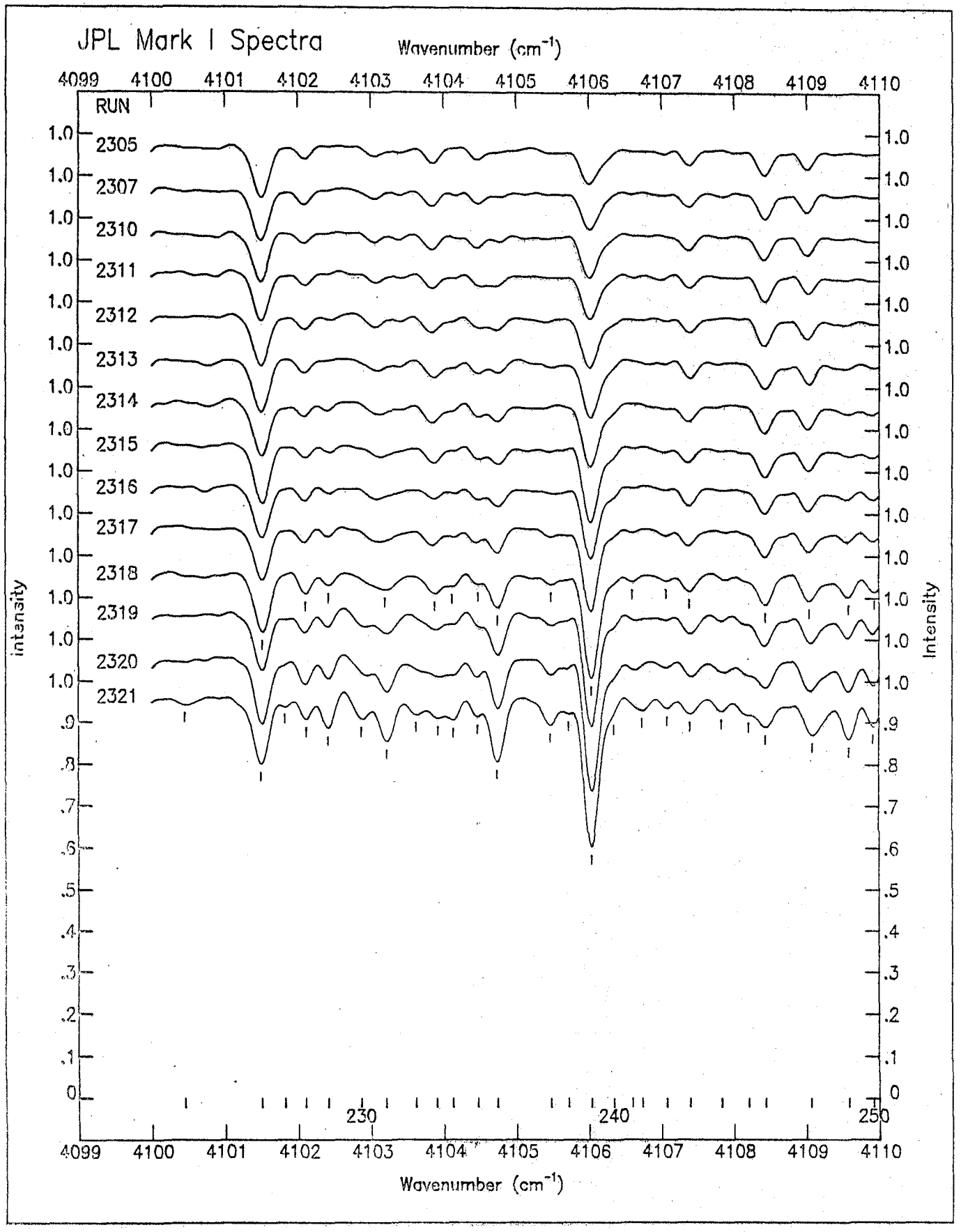

Figure 21.-JPL stratospheric spectra in the region 4100-4110 cm^{-1}.

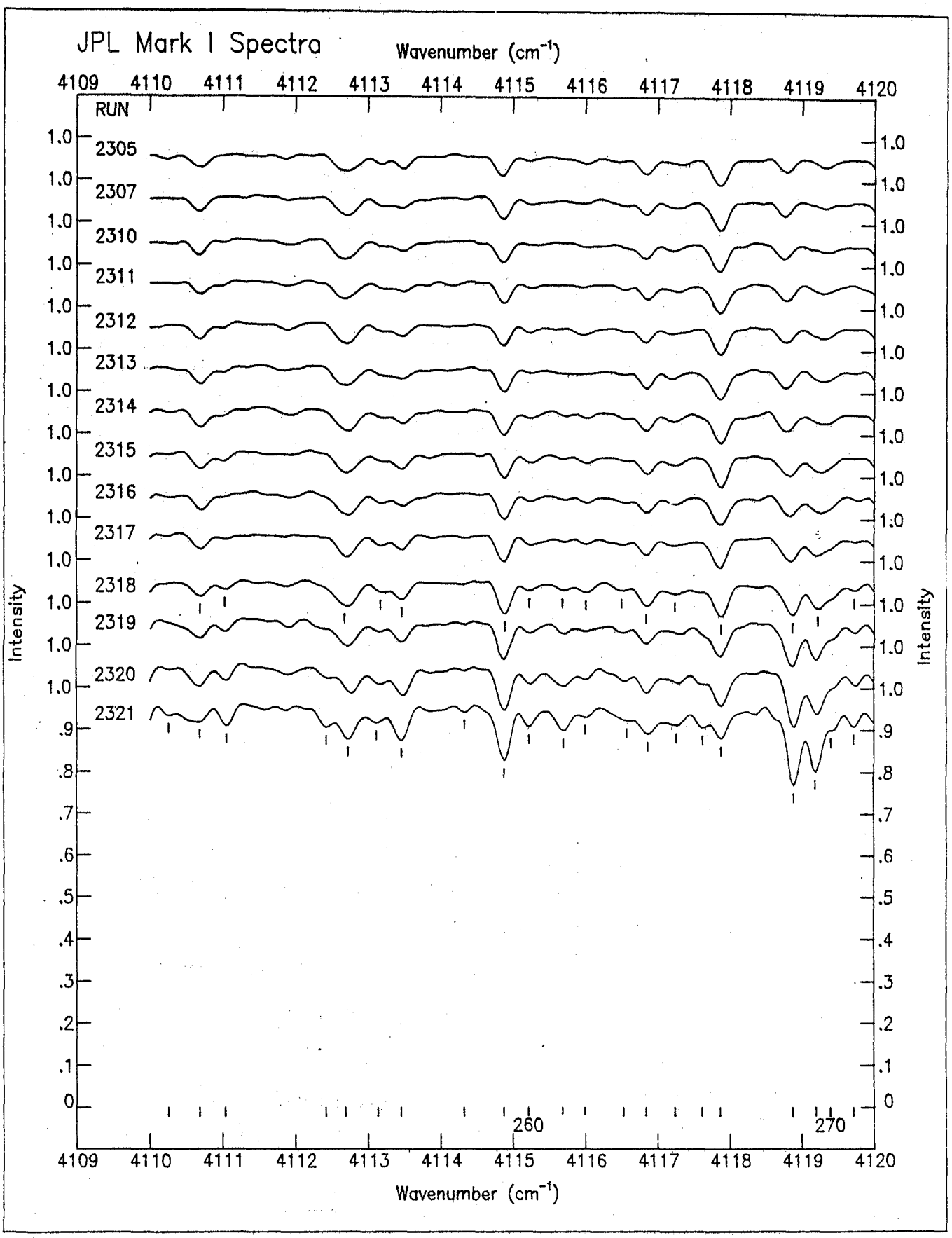

Figure 22.-JPL stratospheric spectra in the region 4110-4120 cm^{-1}.

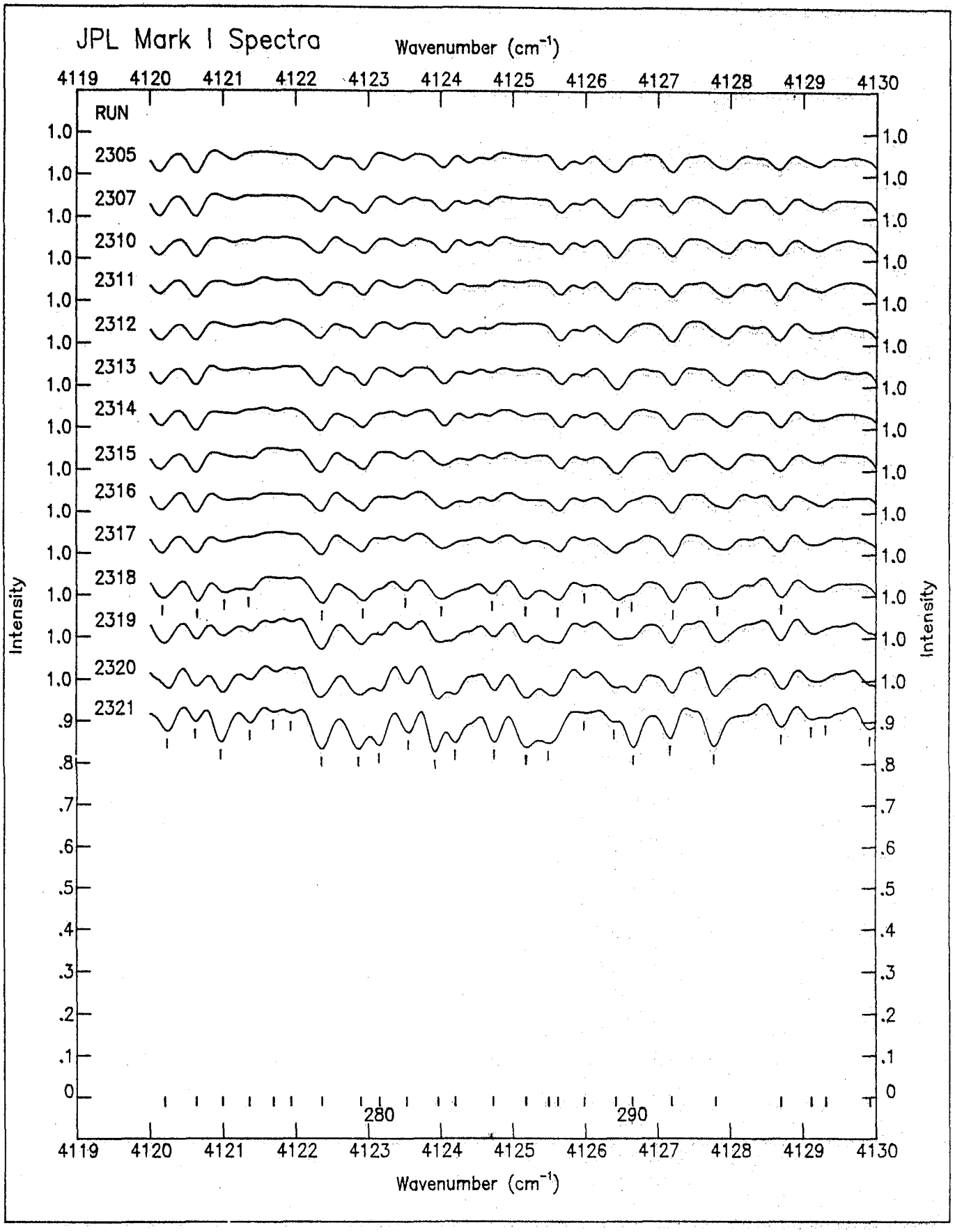

Figure 23.-JPL stratospheric spectra in the region 4120-4130 cm^{-1}.

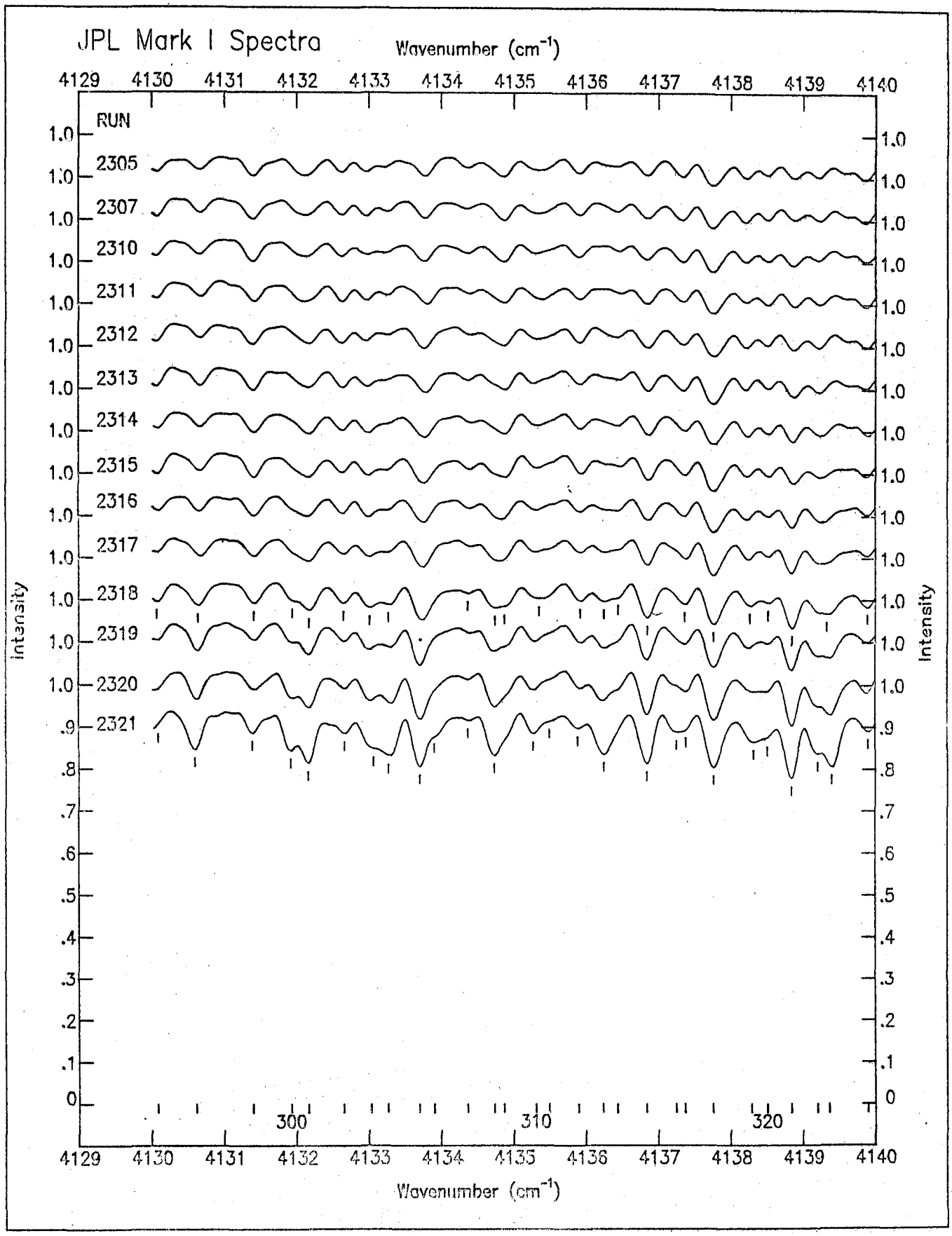

Figure 24.-JPL stratospheric spectra in the region 4130-4140 cm^{-1}.

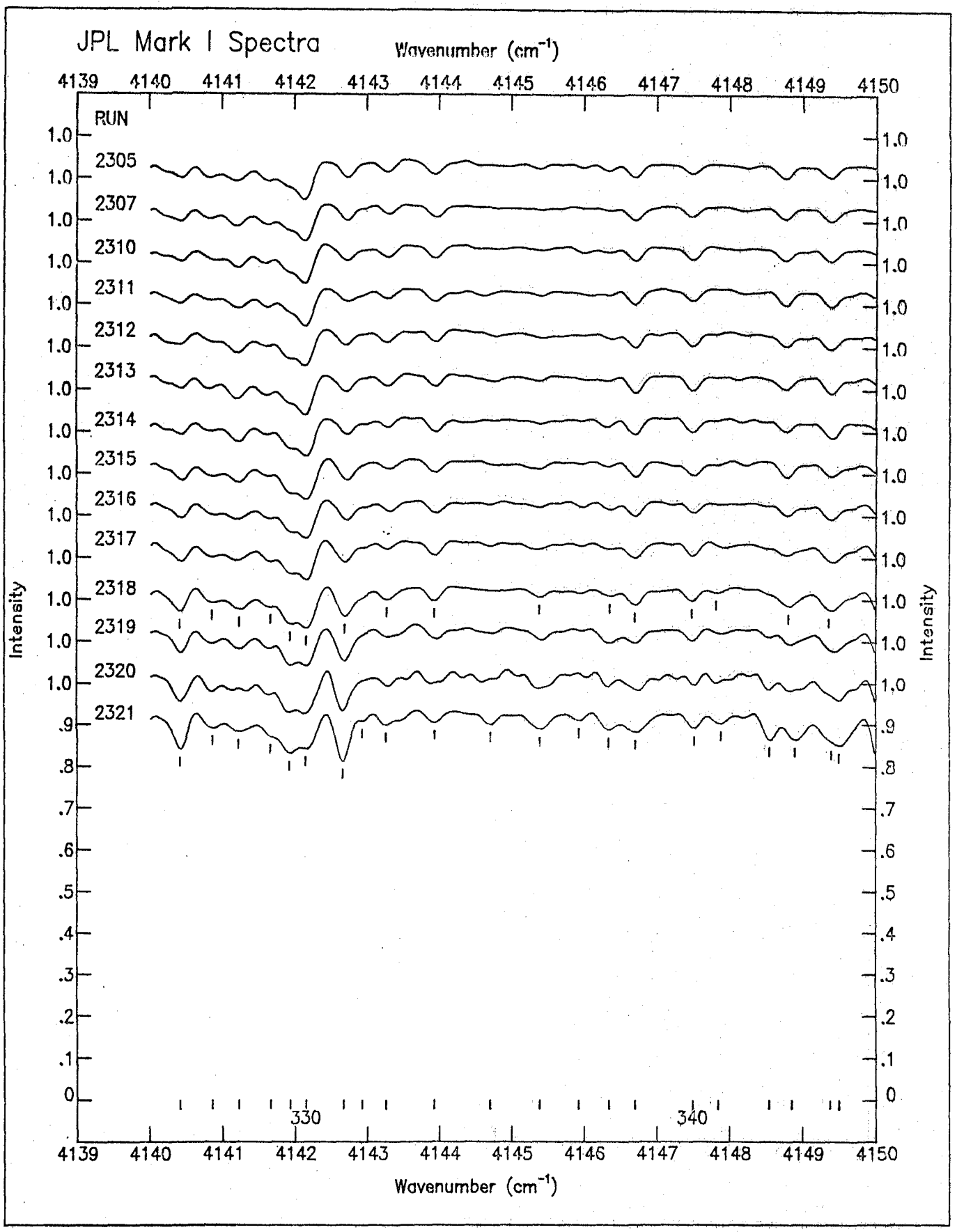

Figure 25.-JPL stratospheric spectra in the region 4140-4150 cm^{-1}.

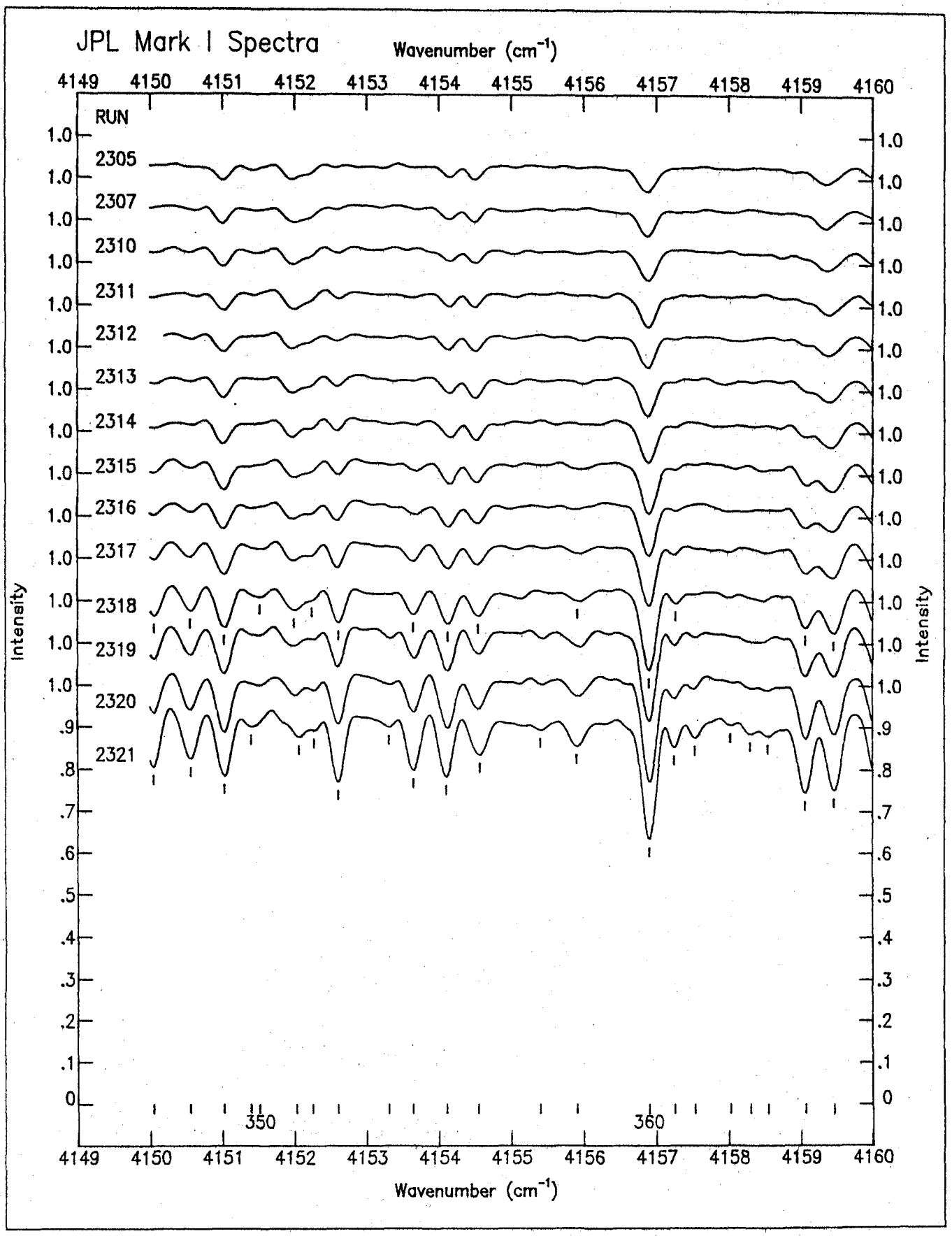

Figure 26.-JPL stratospheric spectra in the region 4150-4160 cm^{-1}.

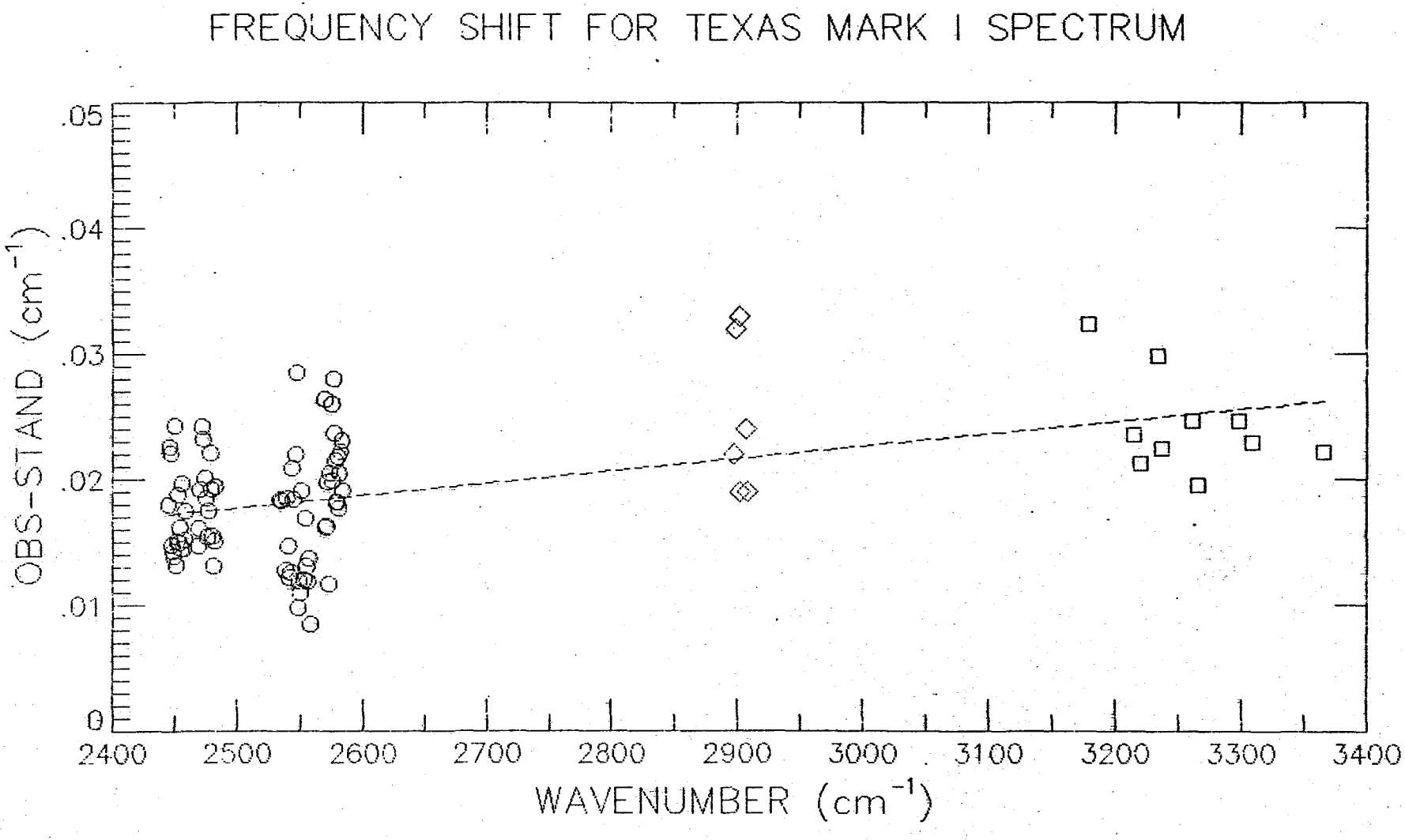

Figure 27.-Observed minus calculated positions for standard lines of N_2O (O), CH_4 (◇), and H_2O (□)

Figure 28.-Comparison between observed and simulated stratospheric spectra.

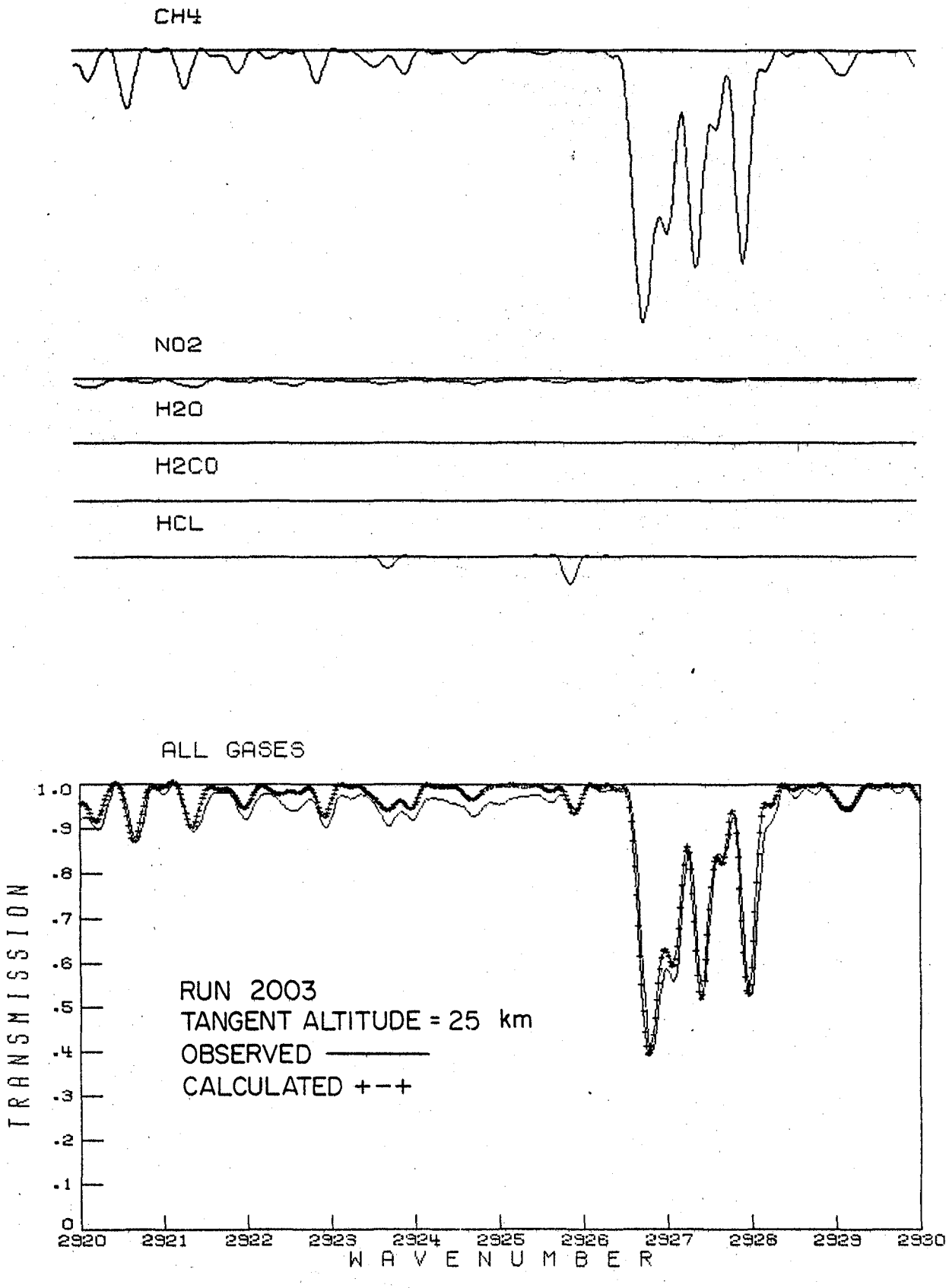

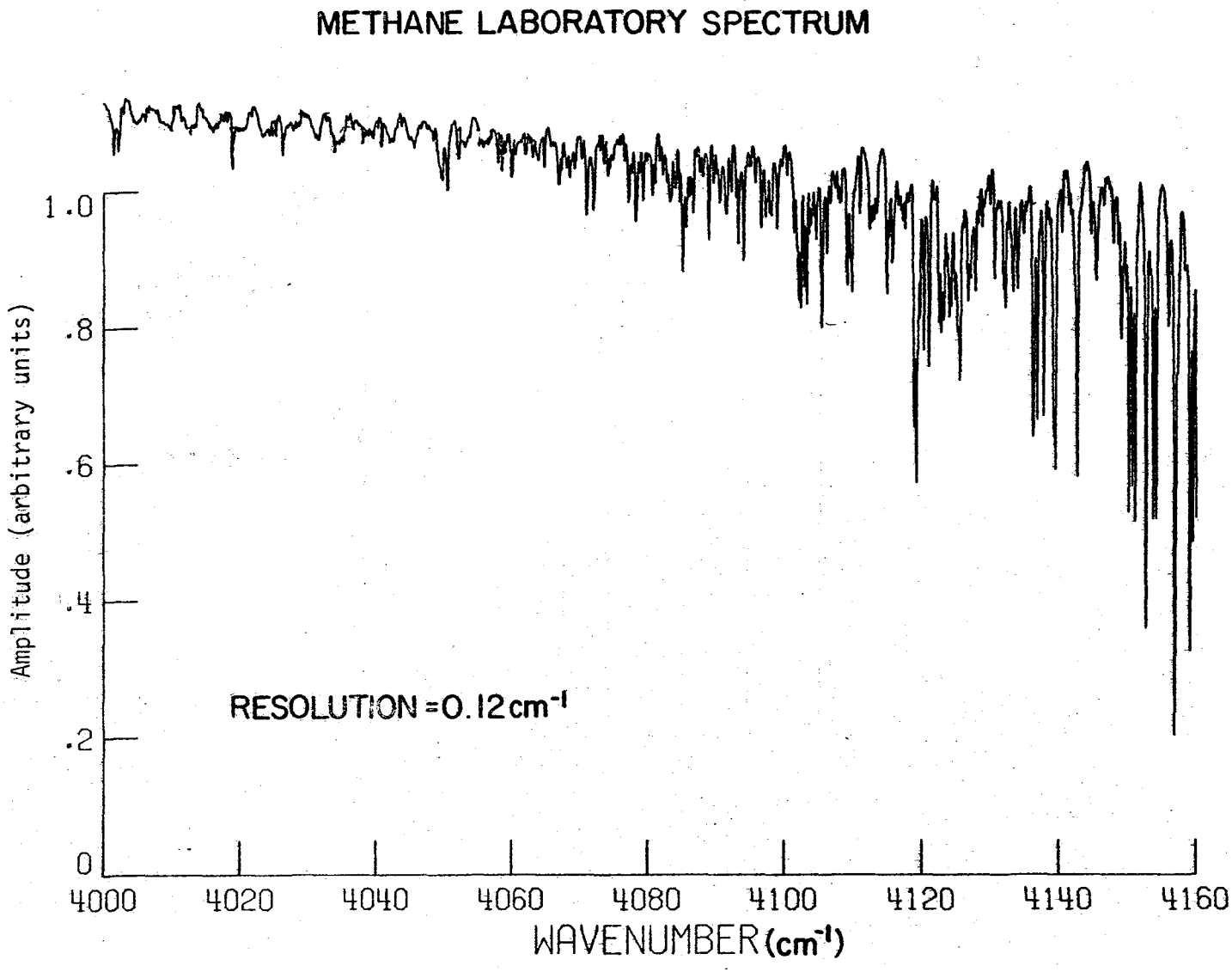

Figure 29.-Room-temperature laboratory spectrum of methane recorded with 0.8 atm of pure CH_4 in a 10 cm path length HALOE test cell.

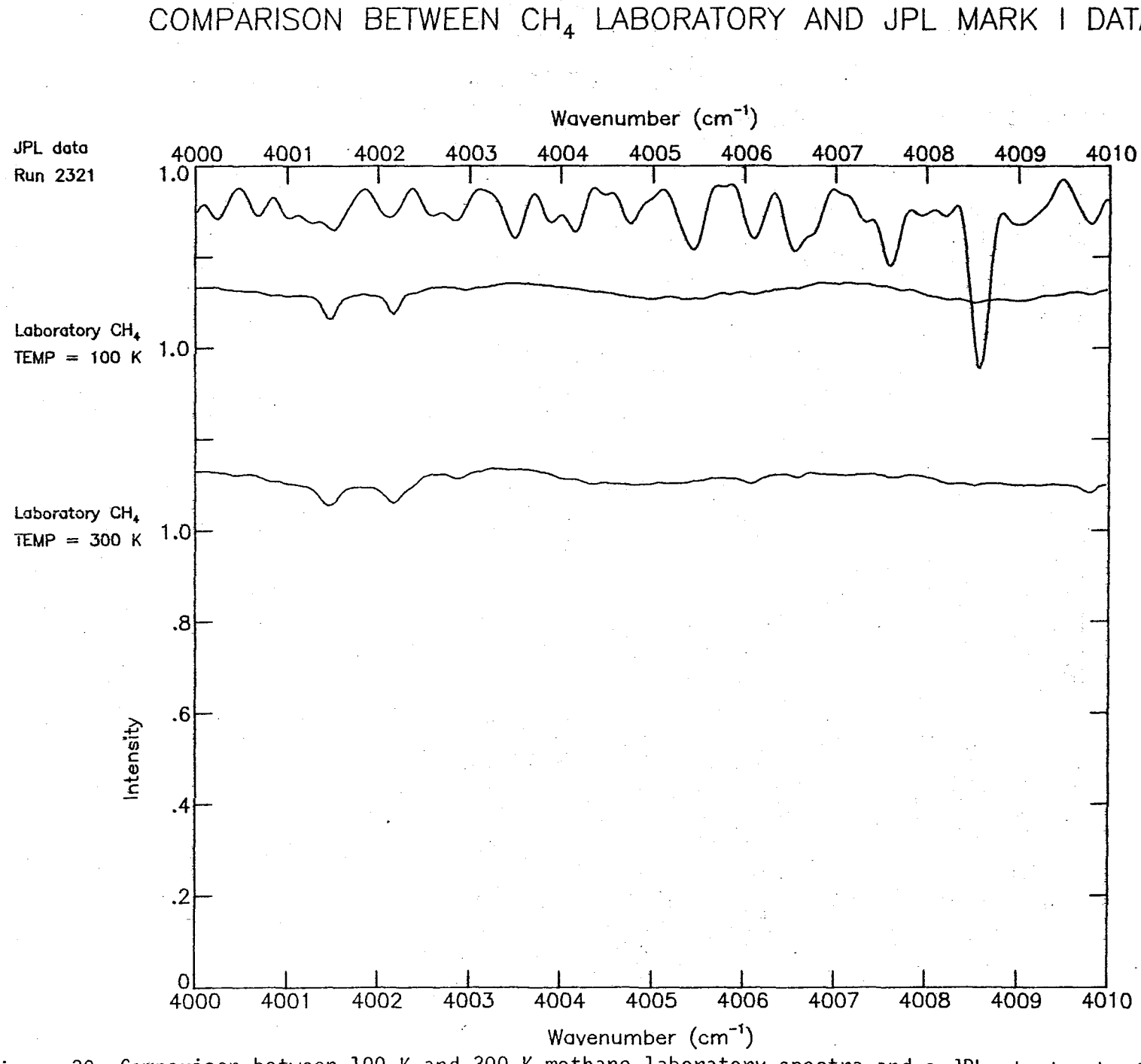

Figure 30.-Comparison between 100 K and 300 K methane laboratory spectra and a JPL stratospheric spectrum (tangent altitude=18.5 km) in the region 4000-4010 cm^{-1}.

COMPARISON BETWEEN CH_4 LABORATORY AND JPL MARK I DATA

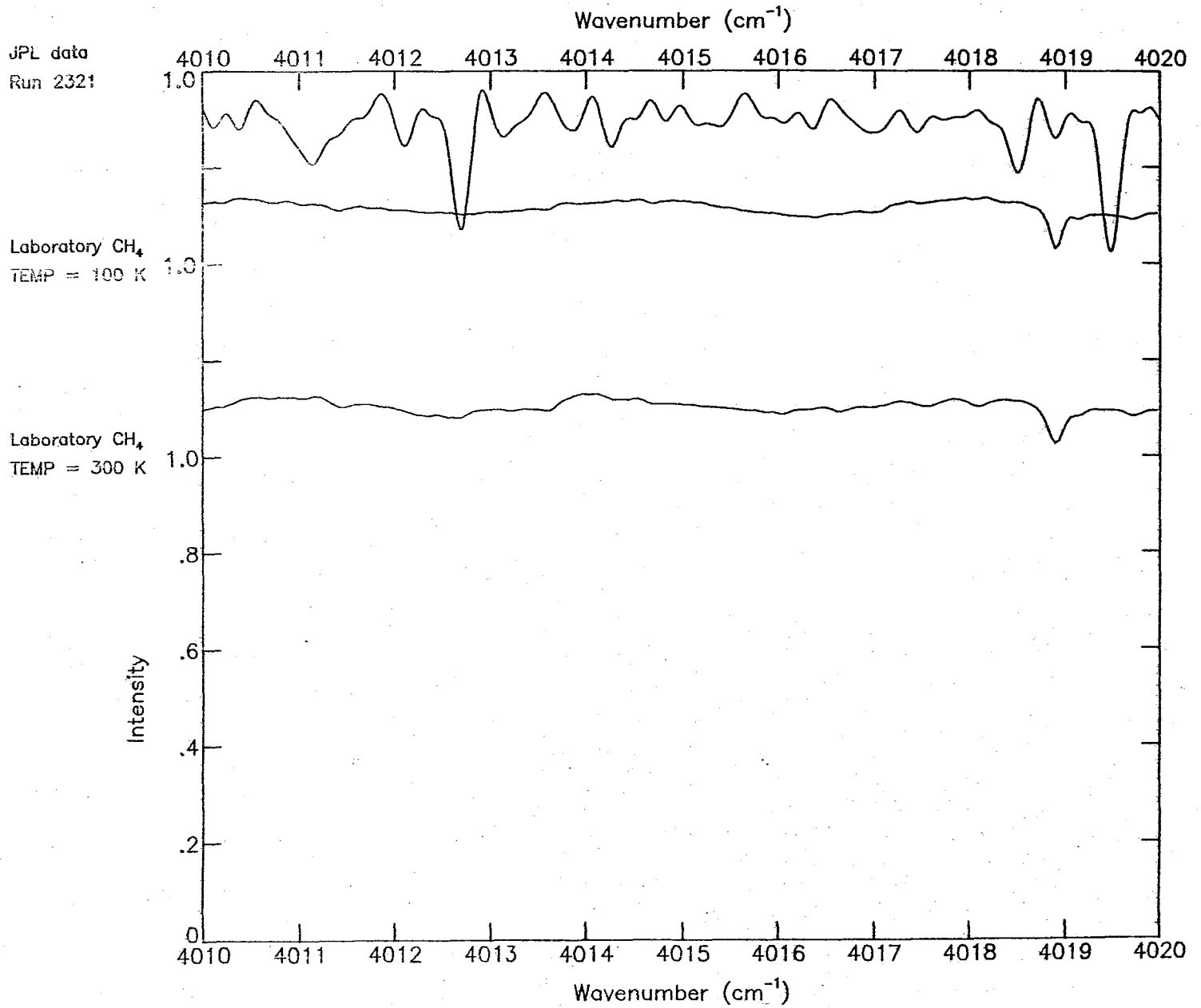

Figure 31.-Comparison between 100 K and 300 K methane laboratory spectra and a JPL stratospheric spectrum (tangent altitude=18.5 km) in the region 4010-4020 cm^{-1}.

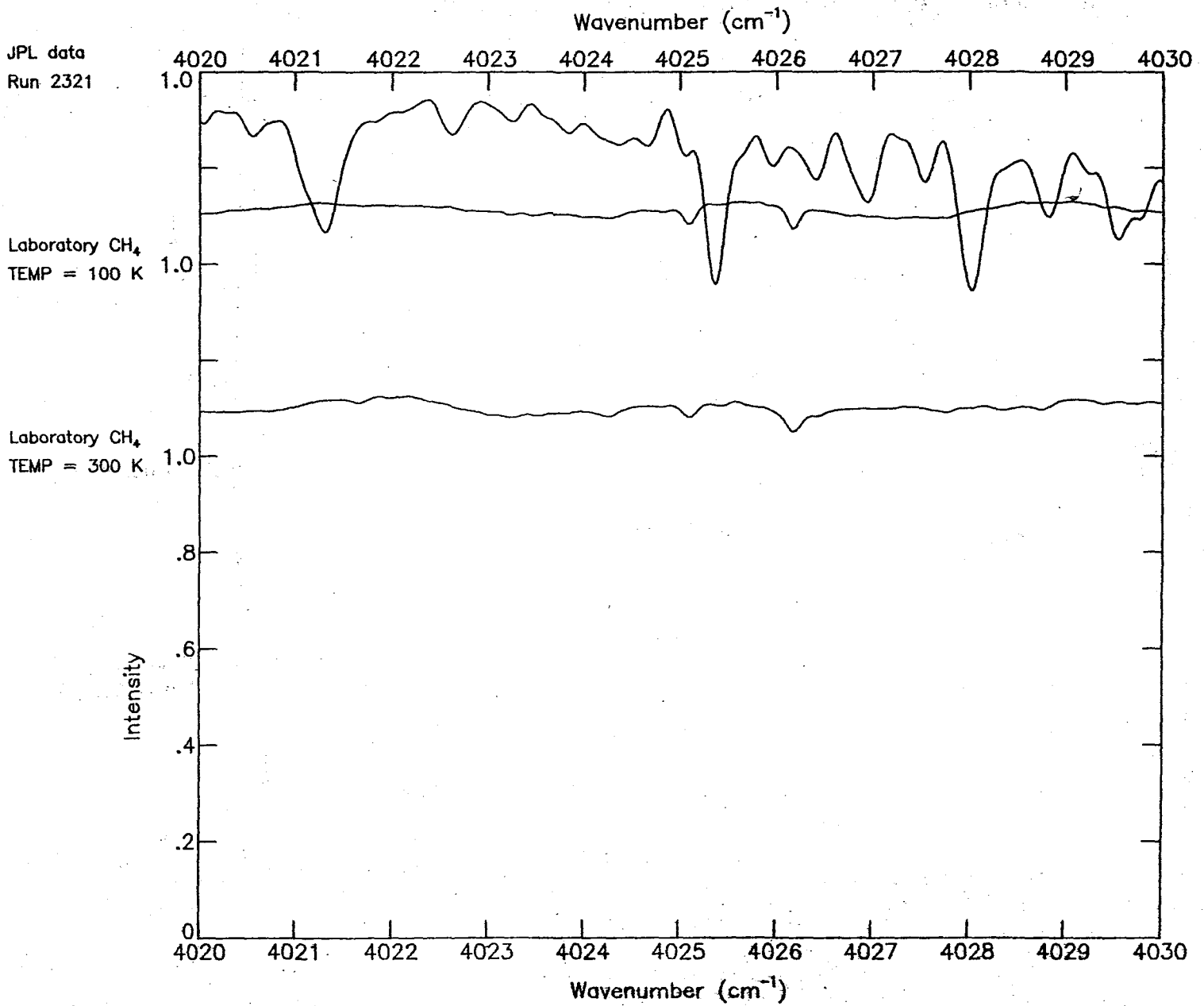

Figure 32.-Comparison between 100 K and 300 K methane laboratory spectra and a JPL stratospheric spectrum (tangent altitude=18.5 km) in the region 4020-4030 cm^{-1}.

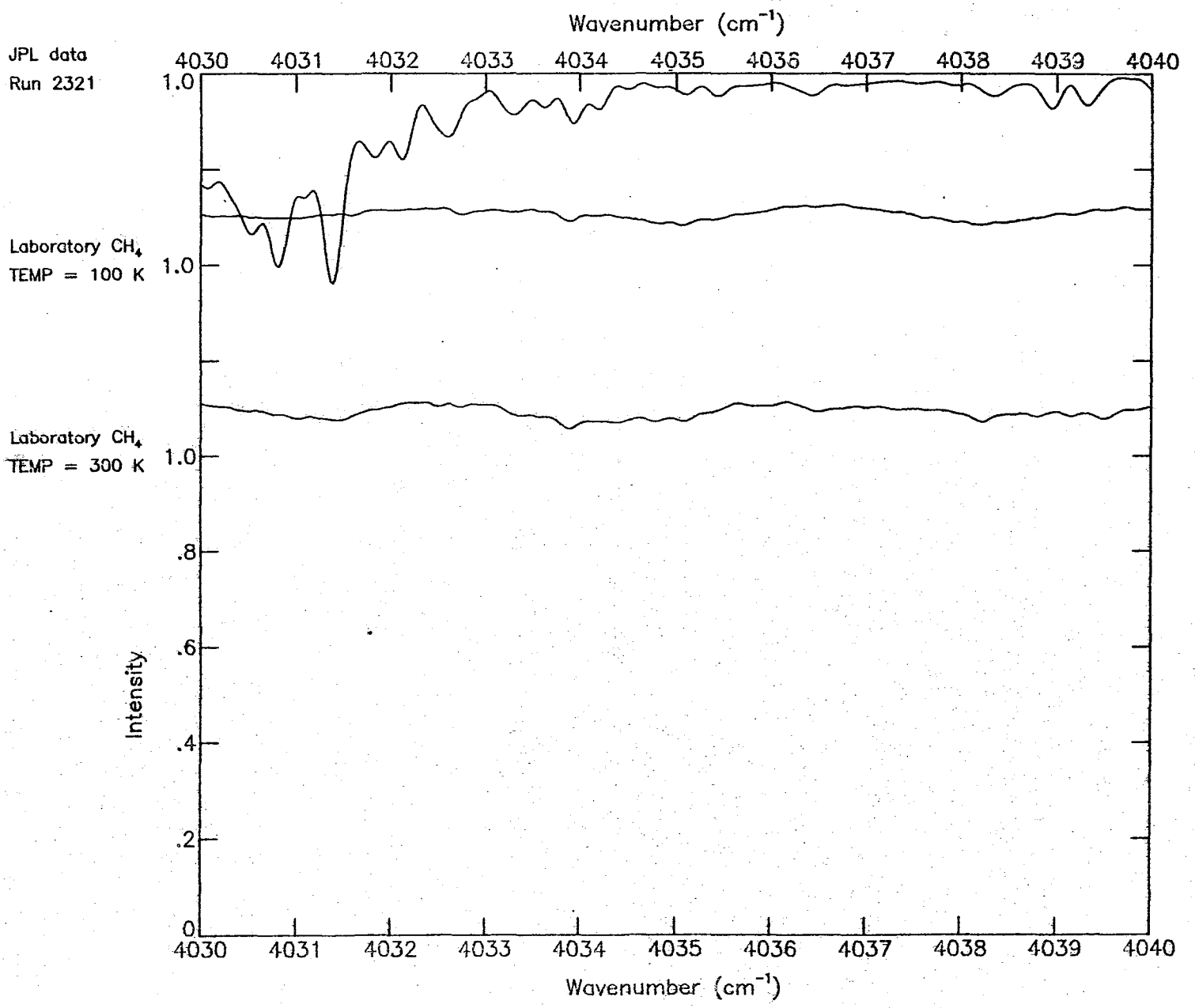

Figure 33.-Comparison between 100 K and 300 K methane laboratory spectra and a JPL stratospheric spectrum (tangent altitude=18.5 km) in the region 4030-4040 cm^{-1}.

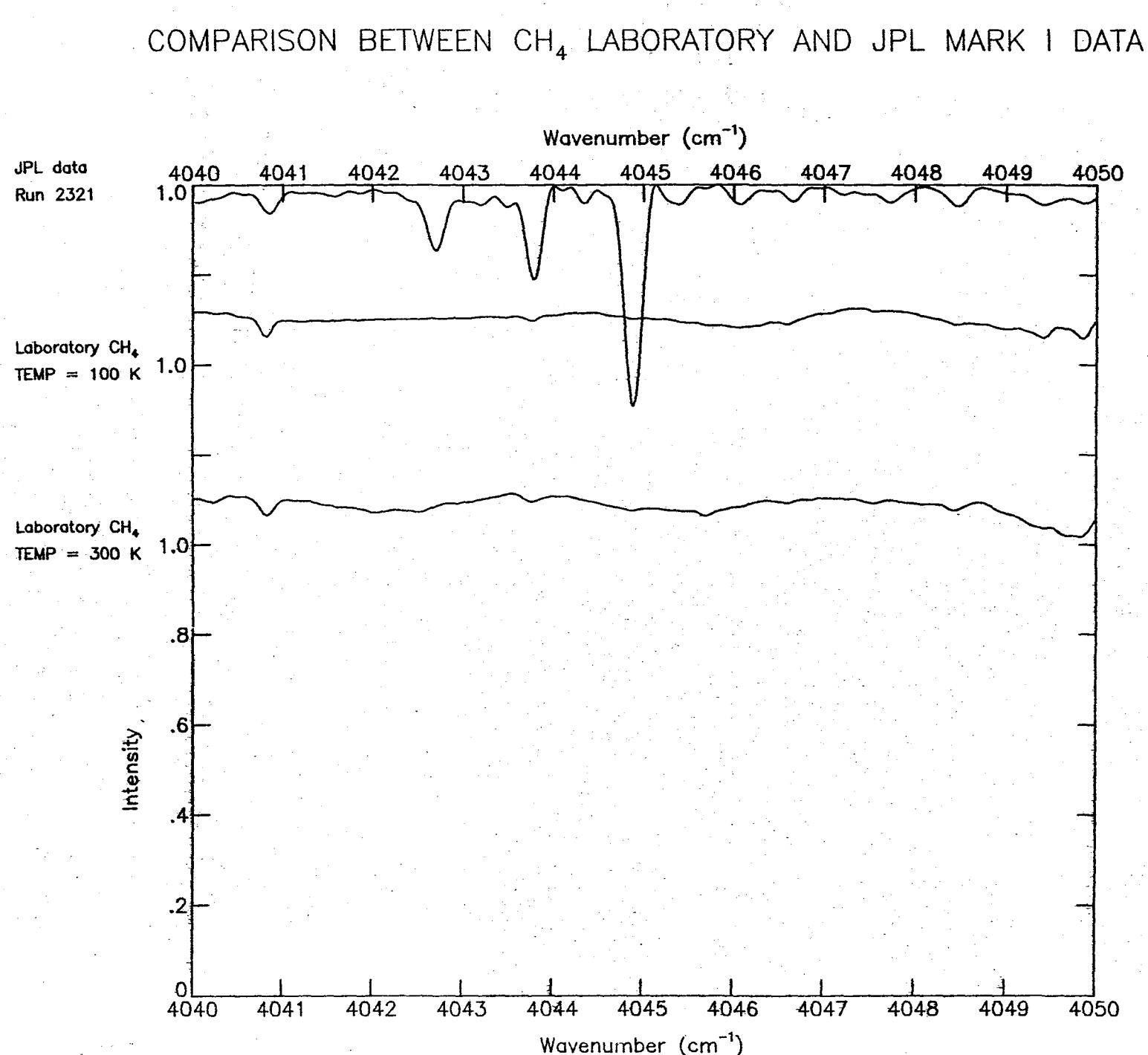

Figure 34.-Comparison between 100 K and 300 K methane laboratory spectra and a JPL stratospheric spectrum (tangent altitude=18.5 km) in the region 4040-4050 cm^{-1}.

COMPARISON BETWEEN CH_4 LABORATORY AND JPL MARK I DATA

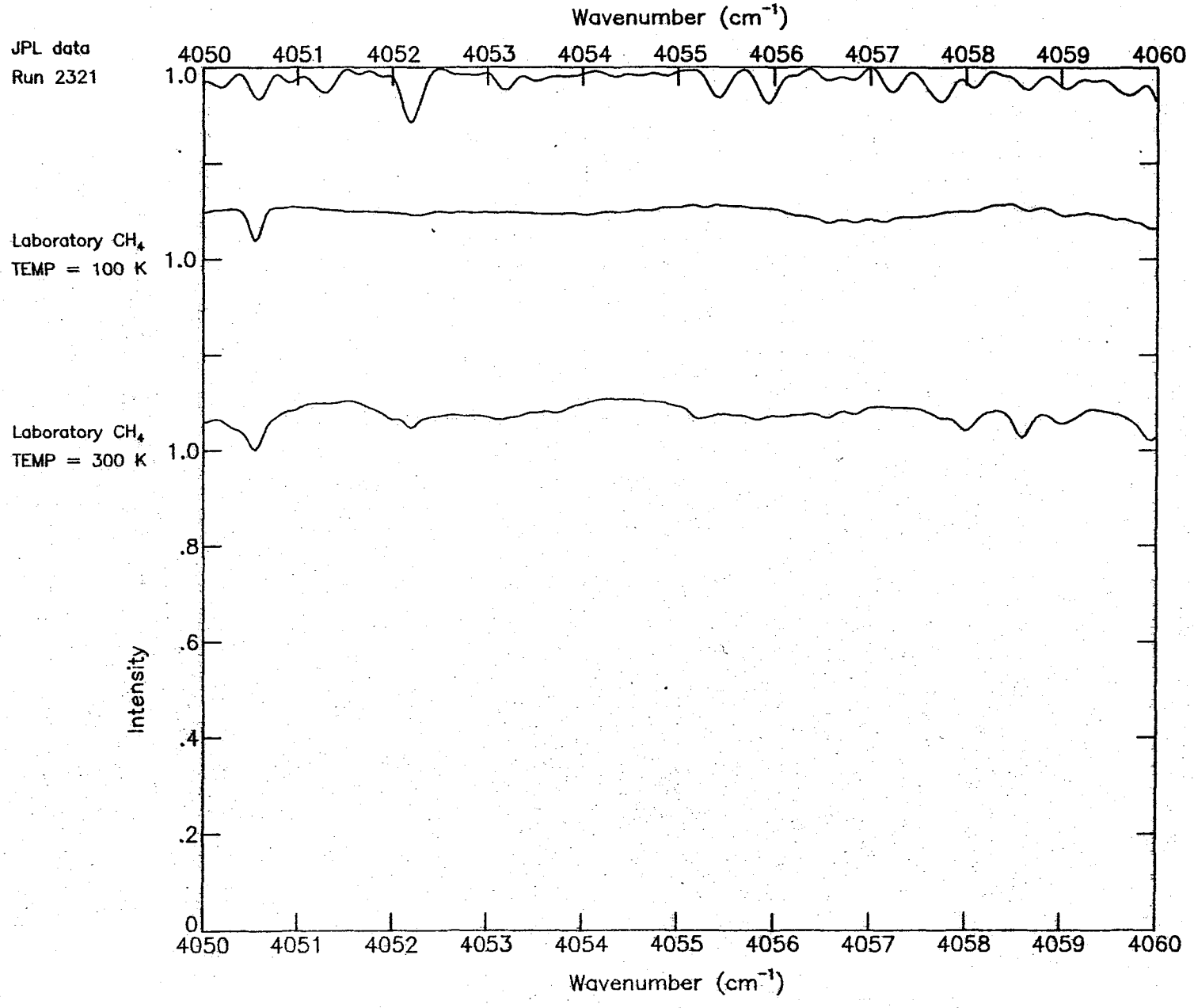

Figure 35.-Comparison between 100 K and 300 K methane laboratory spectra and a JPL stratospheric spectrum (tangent altitude=18.5 km) in the region 4050-4060 cm^{-1}.

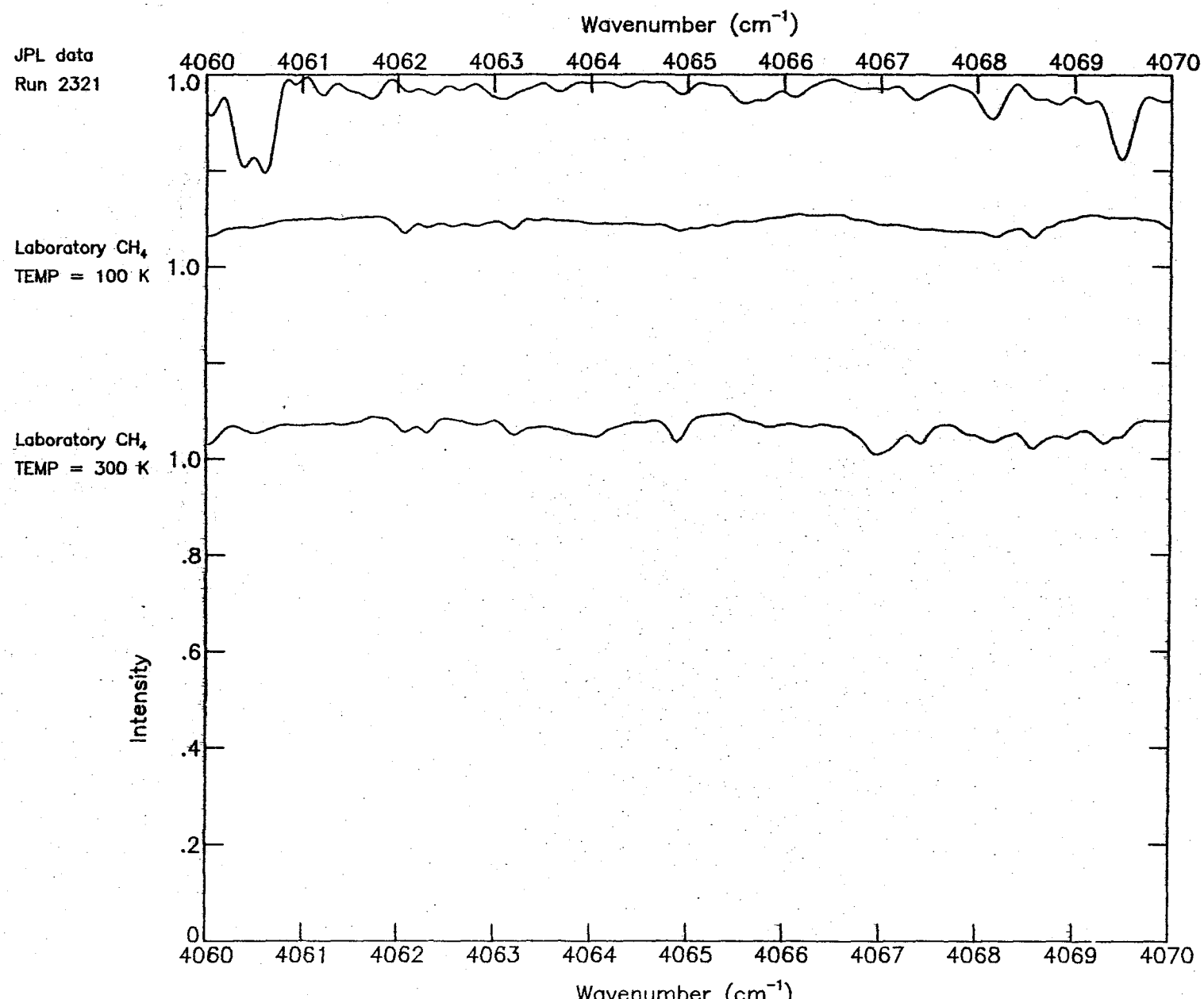

Figure 36.-Comparison between 100 K and 300 K methane laboratory spectra and a JPL stratospheric spectrum (tangent altitude=18.5 km) in the region 4060-4070 cm^{-1}.

COMPARISON BETWEEN CH_4 LABORATORY AND JPL MARK I DATA

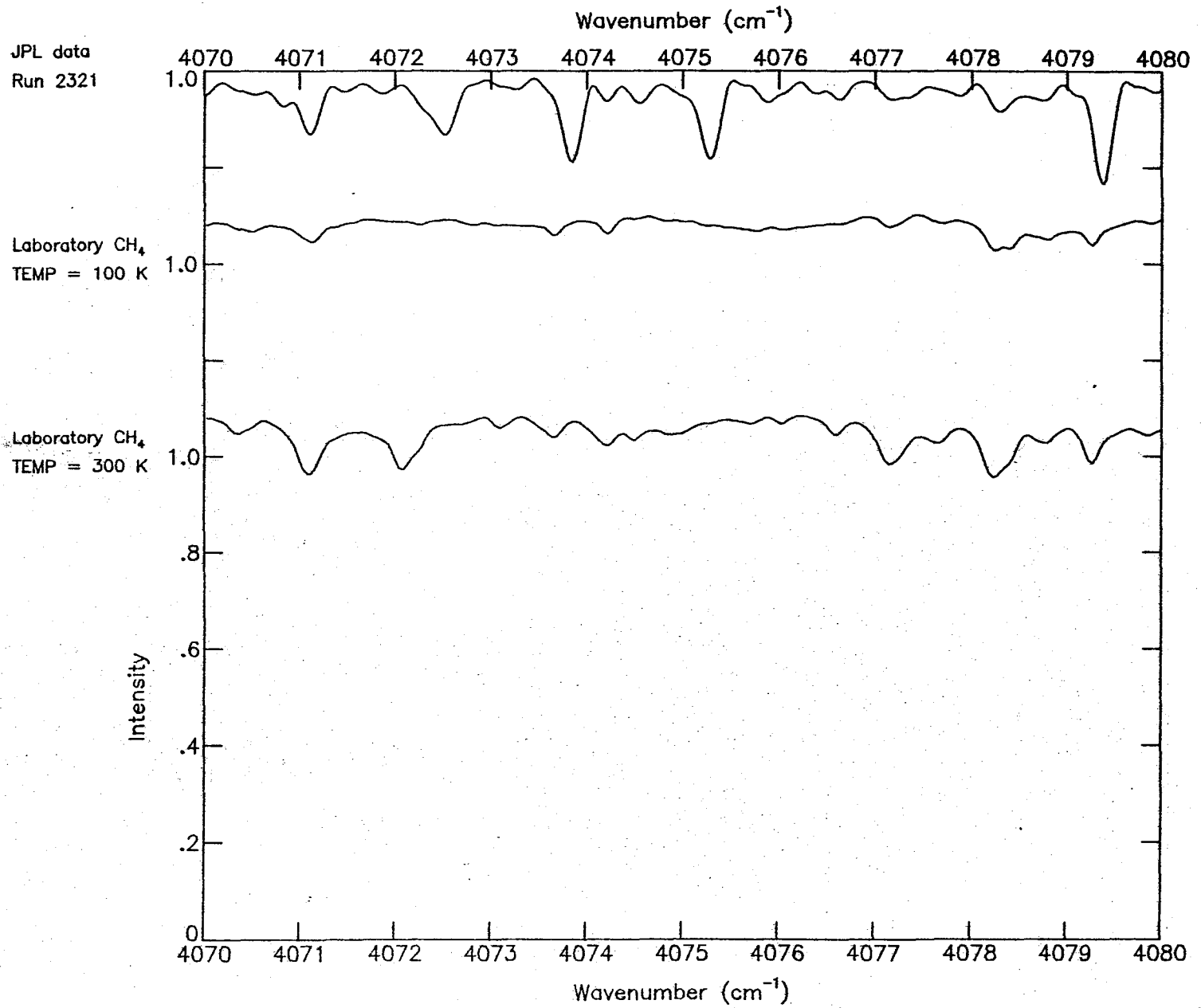

Figure 37.-Comparison between 100 K and 300 K methane laboratory spectra and a JPL stratospheric spectrum (tangent altitude=18.5 km) in the region 4070-4080 cm^{-1}.

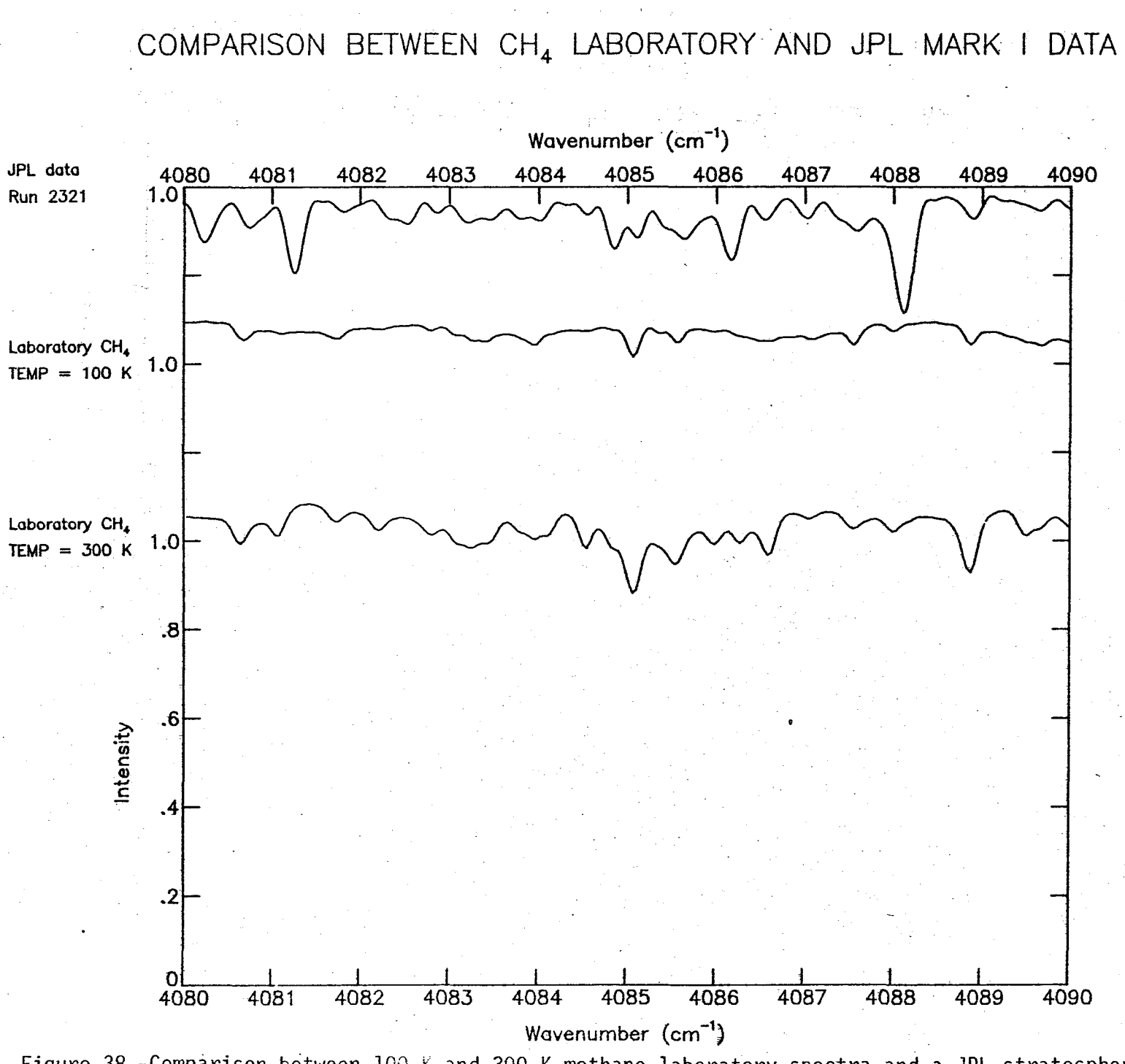

Figure 38.-Comparison between 100 K and 300 K methane laboratory spectra and a JPL stratospheric spectrum (tangent altitude=18.5 km) in the region 4080-4090 cm^{-1}.

COMPARISON BETWEEN CH_4 LABORATORY AND JPL MARK I DATA

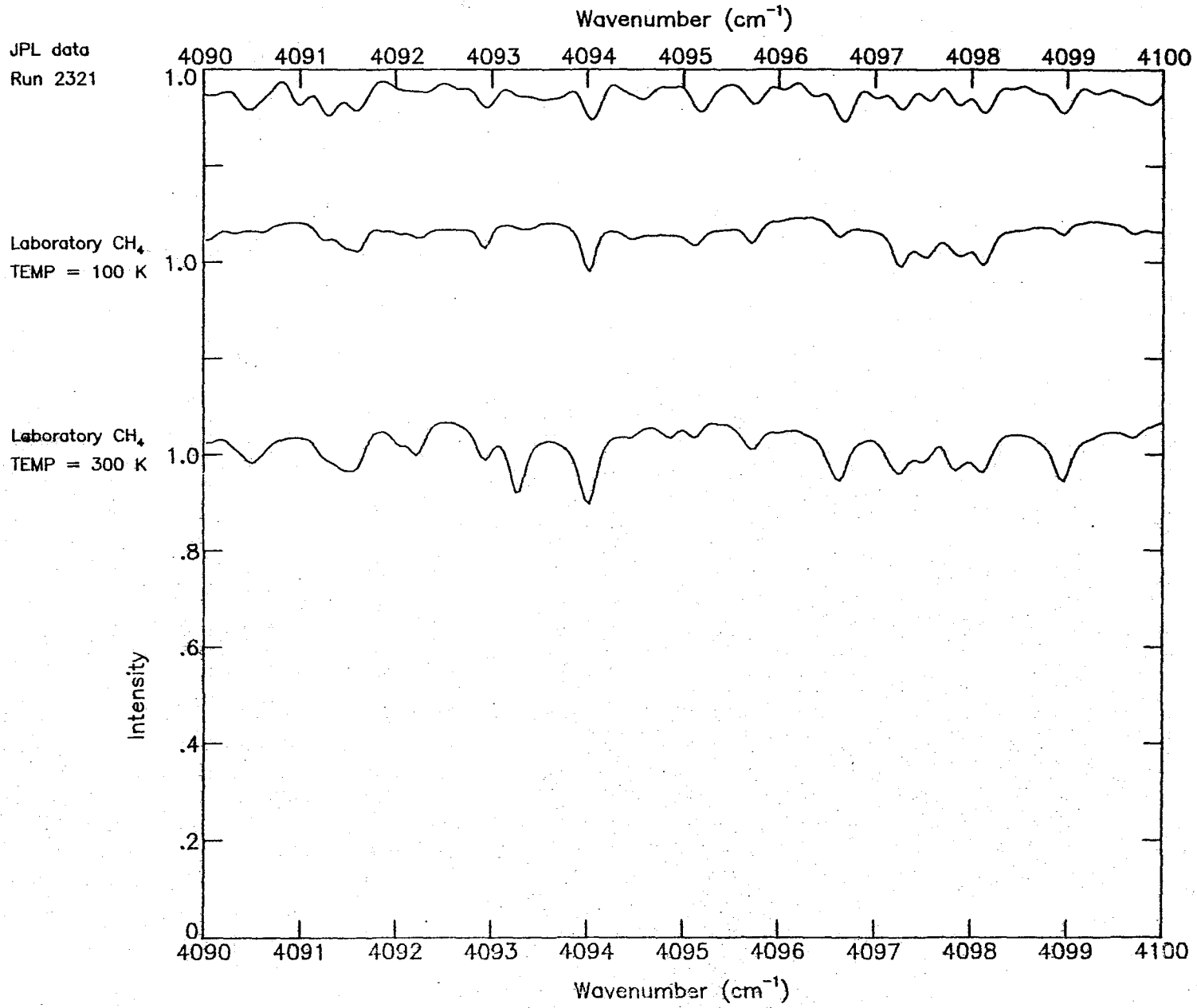

Figure 39.-Comparison between 100 K and 300 K methane laboratory spectra and a JPL stratospheric spectrum (tangent altitude=18.5 km) in the region 4090-4100 cm^{-1}.

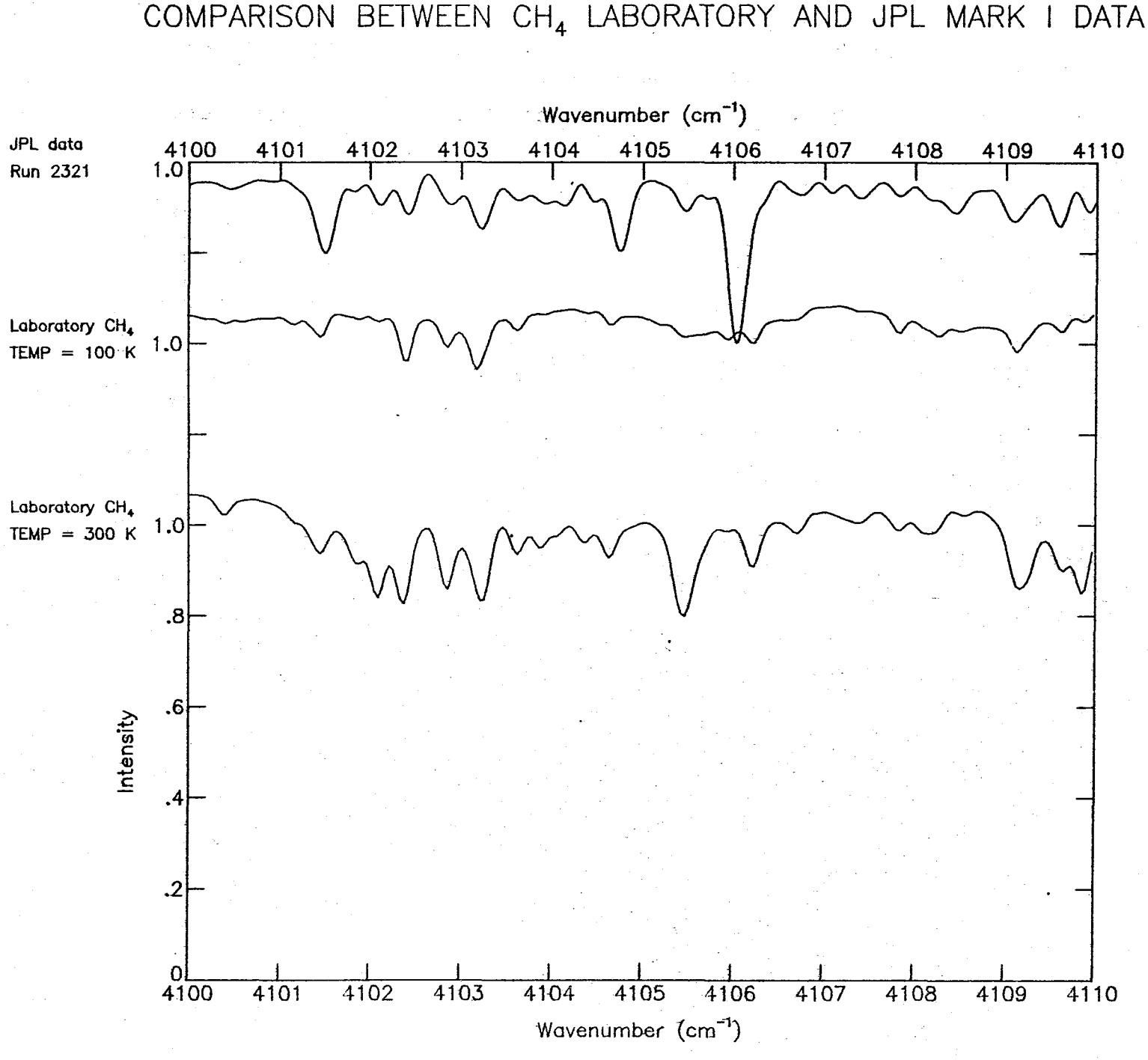

Figure 40.-Comparison between 100 K and 300 K methane laboratory spectra and a JPL stratospheric spectrum (tangent altitude=18.5 km) in the region 4100-4110 cm^{-1}.

COMPARISON BETWEEN CH_4 LABORATORY AND JPL MARK I DATA

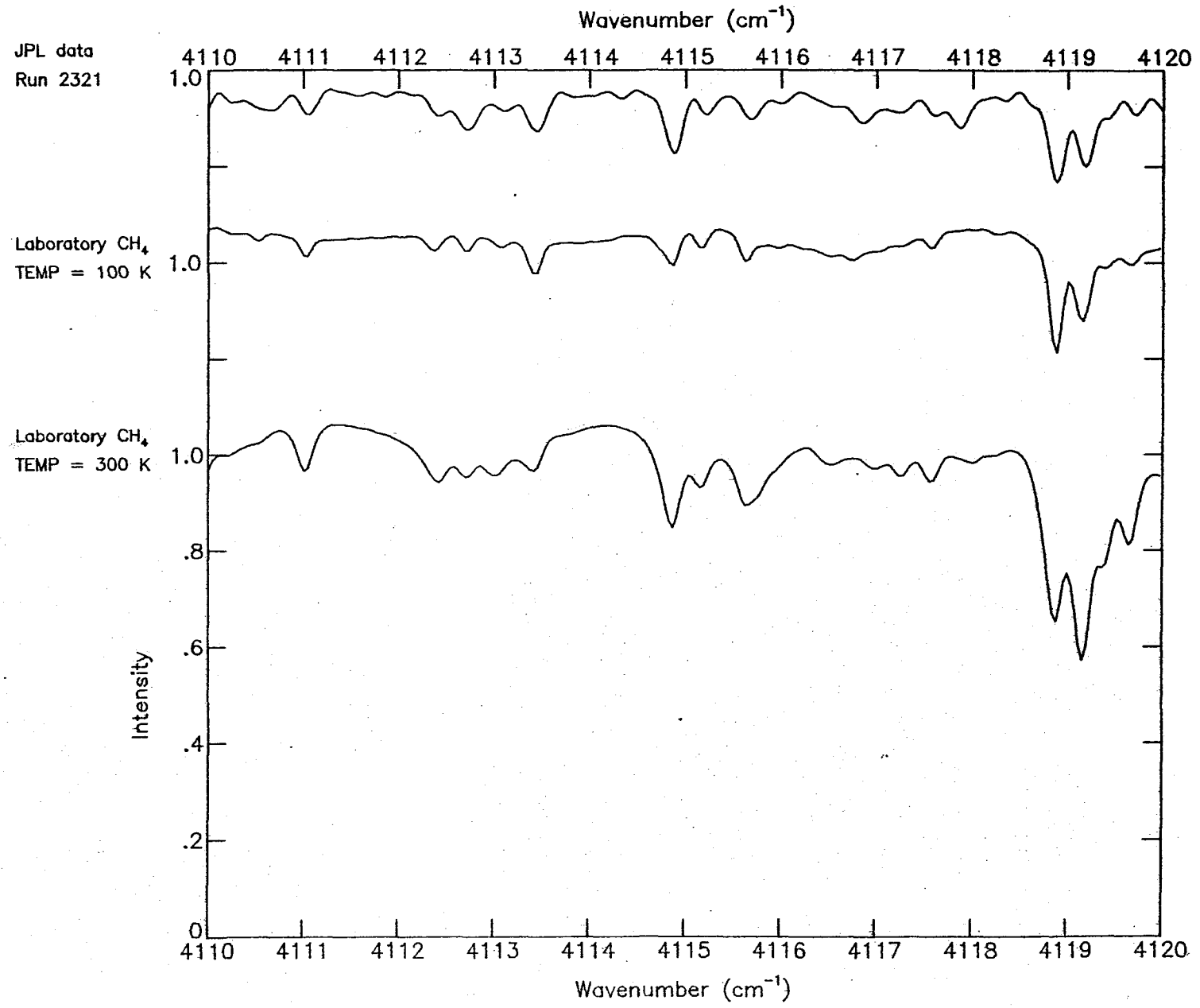

Figure 41.-Comparison between 100 K and 300 K methane laboratory spectra and a JPL stratospheric spectrum (tangent altitude=18.5 km) in the region 4110-4120 cm^{-1}.

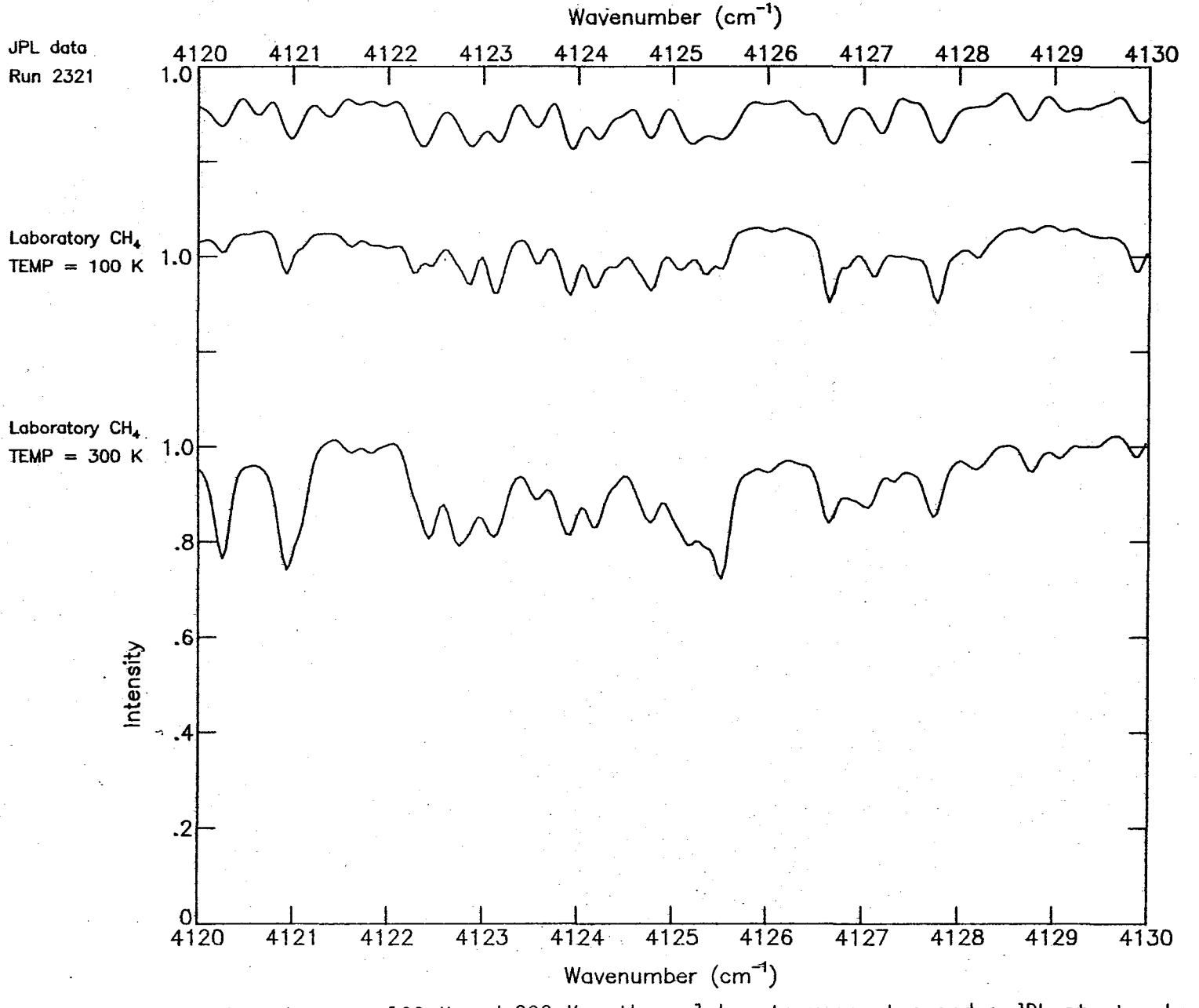

Figure 42.-Comparison between 100 K and 300 K methane laboratory spectra and a JPL stratospheric spectrum (tangent altitude=18.5 km) in the region 4120-4130 cm^{-1}.

COMPARISON BETWEEN CH_4 LABORATORY AND JPL MARK I DATA

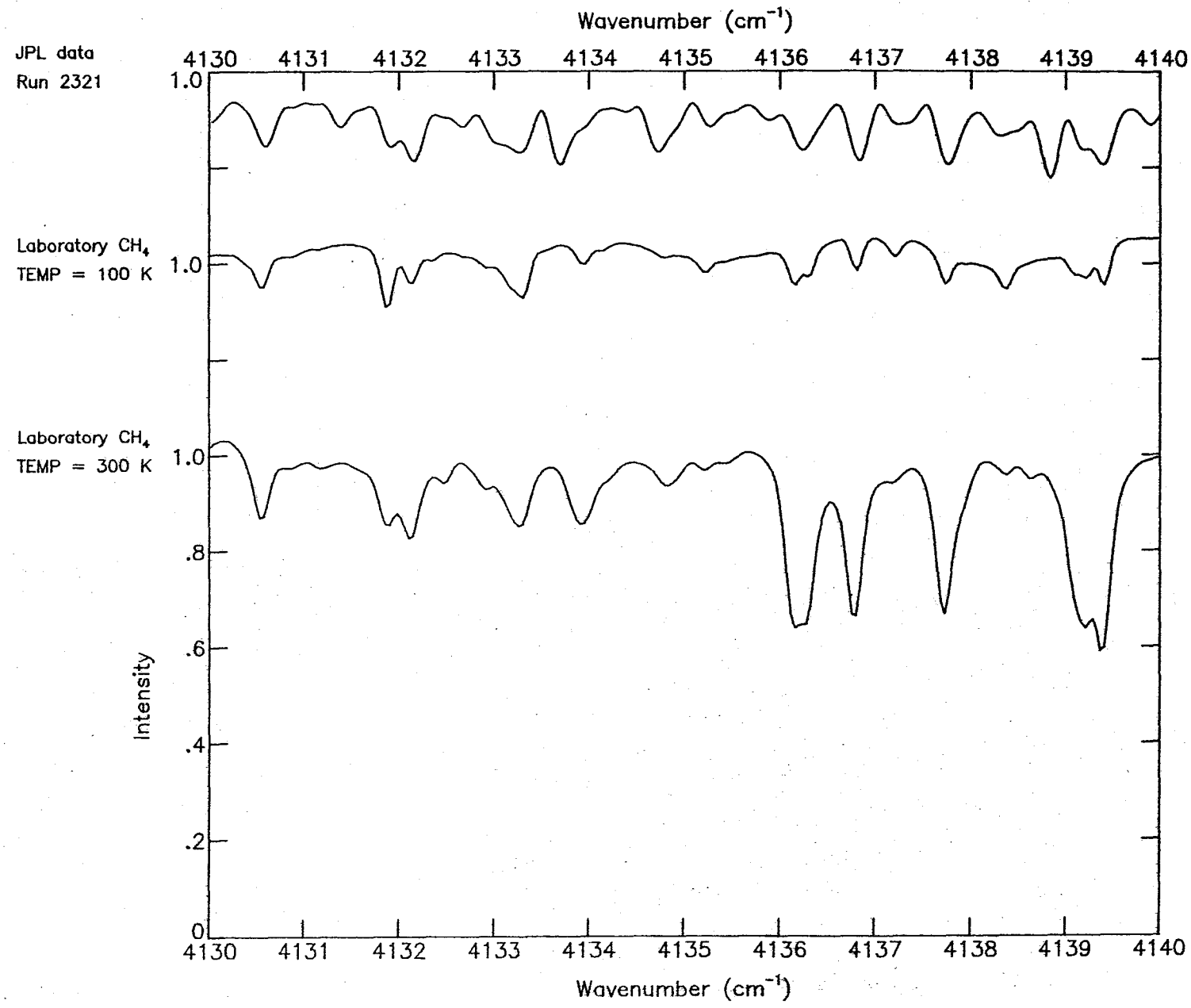

Figure 43.-Comparison between 100 K and 300 K methane laboratory spectra and a JPL stratospheric spectrum (tangent altitude=18.5 km) in the region 4130-4140 cm^{-1}.

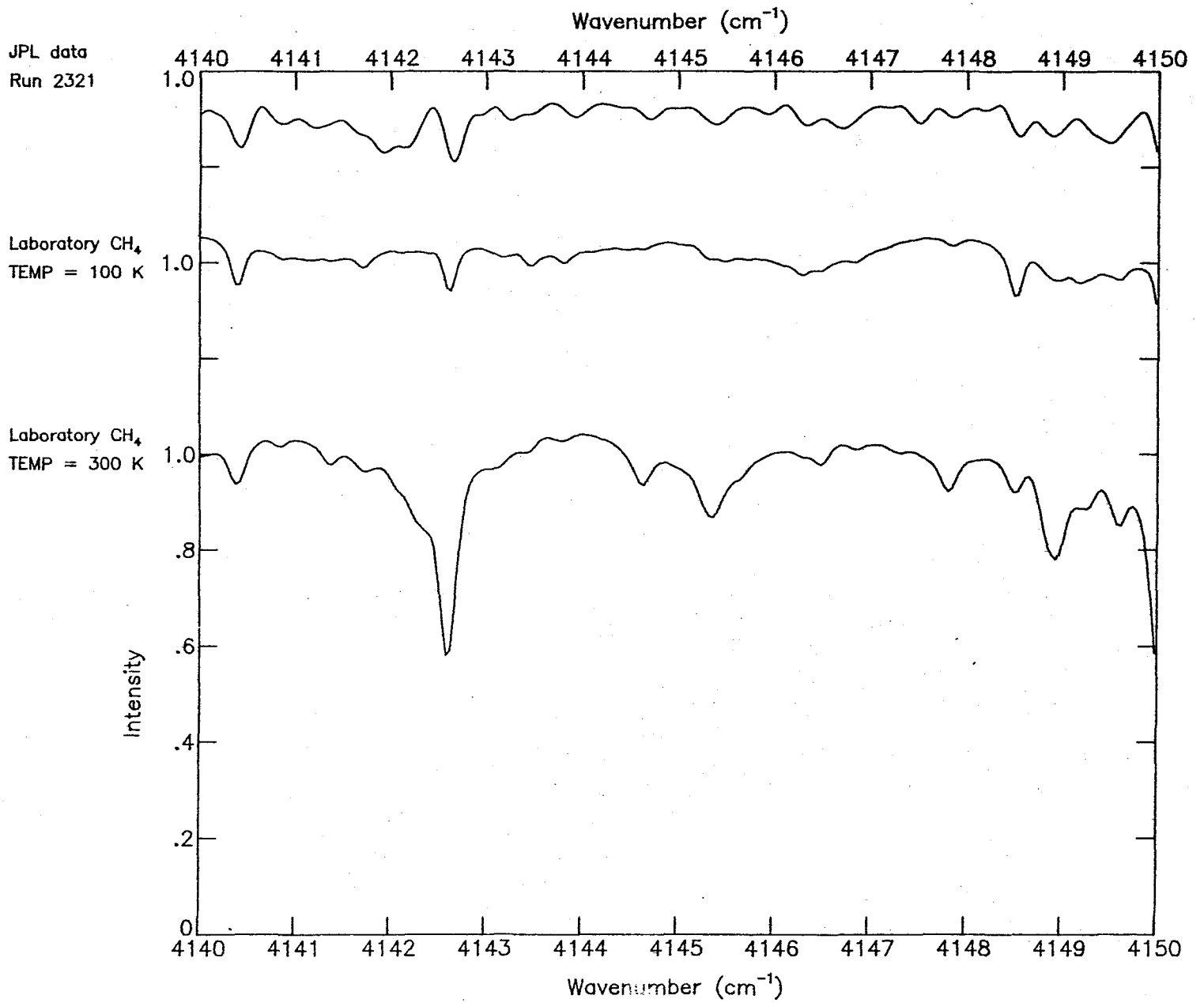

Figure 44.-Comparison between 100 K and 300 K methane laboratory spectra and a JPL stratospheric spectrum (tangent altitude 18.5 km) in the region 4140-4150 cm^{-1}.

COMPARISON BETWEEN CH_4 LABORATORY AND JPL MARK I DATA

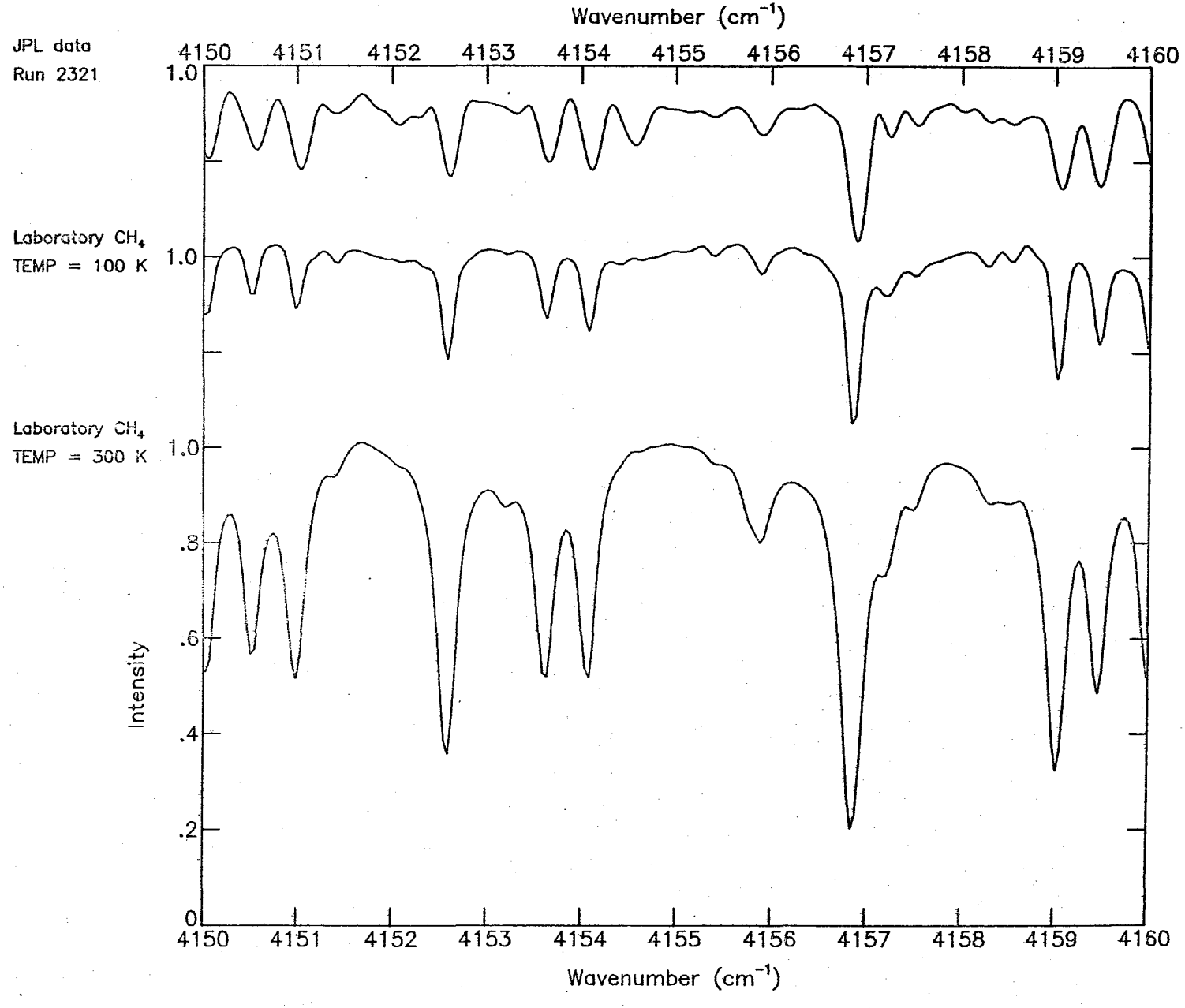

Figure 45.-Comparison between 100 K and 300 K methane laboratory spectra and a JPL stratospheric spectrum (tangent altitude=18.5 km) in the region 4150-4160 cm^{-1}.

1. Report No.	2. Government Accession No.	3. Recipient's Catalog No.
NASA TM-83232		

4. Title and Subtitle	5. Report Date
Spectroscopic Requirements for HALOE: An Analysis of the HCℓ and HF Channels	March 1982
	6. Performing Organization Code

7. Author(s)	8. Performing Organization Report No.
C. P. Rinsland*, M. A. H. Smith, J. H. Park, G. A. Harvey, J. M. Russell III, D. J. Richardson**	618-14-00-01
	10. Work Unit No.

9. Performing Organization Name and Address	11. Contract or Grant No.
NASA Langley Research Center Hampton, VA 23665	
	13. Type of Report and Period Covered
12. Sponsoring Agency Name and Address	Technical Memorandum
National Aeronautics and Space Administration Washington, DC 20546	14. Sponsoring Agency Code

15. Supplementary Notes

*College of William and Mary
Williamsburg, VA

** Systems and Applied Sciences Corp.
Hampton, VA

16. Abstract

This report presents an evaluation of the current state of knowledge of the spectral line parameters that have absorption features within the HCℓ and HF channels of the Halogen Occultation Experiment (HALOE). Line positions and identifications of stratospheric and solar absorption features in both channels are presented based on an analysis of high-resolution, balloon-borne solar occultation spectra. For the relevant HCℓ and HF lines and for transitions of the interfering species, the accuracy of the following spectral parameters was assessed: line positions, line strengths, lower state energies, air-broadened collisional half-widths, and temperature dependence of the air-broadened half-widths. In addition, since the HALOE instrument and calibration cells are filled with mixtures of HCℓ in N_2 and HF in N_2, the self-broadened and N_2-broadened HF and HCℓ half-widths were also considered. HALOE instrument requirements are presented along with recommendations for future spectroscopic investigations that would enhance the accuracy of HALOE results.

17. Key Words (Suggested by Author(s))	18. Distribution Statement
Remote sensing Stratospheric gases Gas correlation technique	Unclassified - Unlimited Subject Category 46

19. Security Classif. (of this report)	20. Security Classif. (of this page)	21. No. of Pages	22. Price
Unclassified	Unclassified	102	

For sale by the National Technical Information Service, Springfield, Virginia 22161